# Gene Expression Within the Fluctuating Life Cycle Stages of Trypanosome Parasites

A Thesis Submitted to the Faculty of the
University of Minnesota by

**Emily Kay Susa**

In Partial Fulfillment of the Requirements for the
Degree of Master of Science

**Dr. Sara Zimmer, Ph.D.**

May 2019

## Abstract

*Trypanosoma cruzi* and *Trypanosoma brucei are* vector-borne protozoan parasites that cause devastating disease to humans and livestock in South America, North America and Africa. Both parasites have complex life cycles which involve a variety of different environments and nutrient sources within mammalian hosts and arthropod vectors. Transitioning between life cycle stages requires a transformation of morphology, replicative ability, and metabolism, which requires remodeling of mitochondrial and nuclear gene expression. To better understand the complicated genetic factors involved in life stage differentiation in these organisms, we have investigated several aspects of the regulation of gene expression through life stage transitions. In *T. brucei,* we investigated the role of a putative endoribonuclease, EEP1, on the transition from the mammalian life stage to the insect life stage. Our results indicate that EEP1 does not play a role in the differentiation process, and may serve an entirely unique function. In *T. cruzi,* we examined the mitochondrial genome which plays a crucial role in metabolism and has been shown to exhibit life-stage specific remodeling in related species. Mitochondrial genome regulation must occur post-transcriptionally in the form of RNA editing, translational control, and stability. Significant changes were detected in mature mRNA abundance between several life stages, and these differences appeared to be correlated with nutrient availability and replication status. Overall, both of these studies provide further understanding of the regulatory processes that govern life cycle transitions in trypanosome parasites.

# Table of Contents

# List of Tables

**Table Description** **Page**

# List of Figures

**Figure Description** **Page**

# List of Abbreviations

| Abbreviation | Definition |
|---|---|
| VSG | Variant-specific surface glycoprotein |
| HAT | Human African Trypanosomiasis |
| UTR | Untranslated region |
| rRNA | Ribosomal RNA |
| gRNA | Guide RNA |
| mtRNA | Mitochondrial RNA |
| RECC | RNA editing core complex |
| RESC | RNA editing substrate binding complex |
| MURF | Maxicircle unidentified reading frames |
| CLB | CL Brener (strain of *T. cruzi*) |
| SYL-X10 | Sylvio X10 (strain of *T. cruzi*) |
| RPMI | Roswell Park Memorial Institute Medium (used for metacyclic trypomastigote generation) |
| FBS | Fetal bovine serum |
| MOI | Multiplicity of Infection |
| LIT | Liver infusion tryptose (used for *T. cruzi* epimastigote culture) |
| TAU | Nutrient deprivation medium |
| BF | Bloodstream form (*T. brucei)* |
| PF | Procyclic form (*T. brucei)* |
| EEP1 | (Exonuclease-endonuclease-phosphatase domain-containing 1) |
| EEP1-OE | EEP1 overexpressing plasmid: pLEW100EEP1-LSH |
| EEP1-RNAi | EEP1 silencing plasmid: p2T7-177EEP1 |
| +TET | Tetracycline induced to express plasmid |
| -TET | Uninduced plasmid |

# Chapter 1: Introduction

The genus Trypanosoma is comprised of parasitic unicellular protozoa, characterized by the presence of a flagellum that provides mobility and a kinetoplast, shown in Figure 1, that comprises the mitochondrial genome. Trypanosomes also possess several distinct biological characteristics, such as the utilization of a unique process of RNA editing and a glycosome, an organelle that serves as the location for glucose metabolism (Tielens and van Hellemond 2009). Although trypanosome species share many defining characteristics, they vary greatly in the mechanisms they utilize to carry out their life cycle in various hosts and invertebrate vectors. *Trypanosoma brucei (T. brucei)* and *Trypanosoma cruzi (T. cruzi),* which will be the focus of this thesis, are of clinical importance because they are responsible for diseases that affect millions of humans and livestock animals in rural communities around the globe (WHO 2016; CDC 2017). *T. brucei* and *T. cruzi* share several similarities in their parasitic life cycles. Both carry out life cycle stages within an insect vector before transmission to a host, and are able to maintain presence within a mammalian host for an extended period of time, evading the host immune system for years before instigating enough damage to cause death (Stijlemans et al. 2016; Cardoso, Reis-Cunha, and Bartholomeu 2015). These trypanosome species differ in their specific life cycle and differentiation stages, metabolism and energy utilization, and process of pathogenicity in a host.

### The *Trypanosoma cruzi* life cycle and pathogenicity

The life cycle of *T. cruzi* takes place within a hematophagous triatomine insect vector (various *Triatoma* species) and a mammalian host. The life cycle of this parasite

includes three main forms: epimastigotes, amastigotes and trypomastigotes, as well as a variety of intermediates (Tyler and Engman 2001) (Figure 2). Epimastigotes and amastigotes are replicating life stages, which are able to reproduce asexually via binary fission (CDC 2017). Trypomastigotes are the infective form of the parasite, and can be classified as either metacyclic trypomastigotes (insect vector stage) or bloodstream trypomastigotes (mammalian host stage). The life stages of *T. cruzi* are distinguished by their typical position in the parasitic life cycle and morphological characteristics. As *T. cruzi* proceeds through its life cycle, it experiences major changes in specific gene expression and control in the nuclear and mitochondrial genome, which dictate its morphology, behavior and metabolic activity in the parasitic process (Pastro et al. 2017; Shaw, Kalem, and Zimmer 2016; Li et al. 2016; Berná et al. 2017).

*T. cruzi* parasites replicating in the midgut of the insect vector are referred to as epimastigotes. Epimastigotes are elongated (reaching 30 μm or more in length, according to Tyler and Engman 2001) have a visible flagellum emerging from the anterior portion of the cell body (Gonçalves et al. 2018), and a kinetoplast located anterior to the nucleus (Ferreira et al. 2008). This life stage subsists on mainly carbohydrate and amino acid catabolism (Berná et al. 2017) as the parasites replicate and move through the insect's digestive tract. When epimastigotes reach the terminal portion of the digestive tract, they attach to the rectal wall before differentiating into metacyclic trypomastigotes (Kollien and Schaub 2000). Metacyclic trypomastigotes are a highly infective and non-replicative life stage of *T. cruzi* that will ultimately be released in the feces of the triatomine insect (CDC 2017).

The *T. cruzi* insect-stage differentiation process from the epimastigote to metacyclic trypomastigote is termed metacyclogenesis. This is an extreme event of

transformation, involving changes in morphology, metabolism, surface marker expression, and the cease of proliferation (Tyler and Engman 2001). Factors that trigger metacyclogenesis are still unclear, but previous studies support that the process may be initiated by nutrient deficiency, cyclic AMP, and adenylate cyclase (Gonzales-Perdomo, Romero, and Goldenberg 1988). Tyler and Engman 2001 suggests that the hydrophobic interaction of the epimastigote flagellum with the lining of the insect digestive tract may prompt a cAMP signal that triggers metacyclogenesis. A study by Regina C. B Q. et al. 2000 showed that adhesion itself may be initiated by nutritional stress, as both the adhesion and differentiation process was inhibited when nutrients were provided to starved *T. cruzi* cells in vitro.

Triatomine insects facilitate the transmission of *T. cruzi* by taking a blood meal from a mammal and defecating near the bite wound. Feces from an infected insect vector contain high levels of metacyclic trypomastigotes, which can infect the mammalian host when the human or animal rubs infected feces into the bite wound or transmits it into the eyes or other mucosal membranes (Hemmige, Tanowitz, and Sethi 2012). Metacyclic trypomastigotes are then able to attach to host cells via extracellular proteins, become internalized via a membrane-bound parasitophorous vacuole (Fernandes and Andrews 2012) and escape into the cytoplasm by secreting a porin-like molecule that facilitates lysis of the vacuole (Andrews 1993). This attachment and entry process requires a considerable amount of parasitic metabolic energy (Barrias, de Carvalho, and De Souza 2013). Within the parasitophorous vacuole, *T. cruzi* receives signals that initiate transformation into an amastigote (Li et al. 2016; Tomlinson et al. 1995) with a rounded cell body 3-5 μm in diameter (Tyler and Engman 2001) and a shortened and nearly invisible flagellum protruding from its anterior (Lentini, Dos Santos

Pacheco, and Burleigh 2018) (Figure 3).

Amastigotes proliferate in the cytoplasm for 3-5 days (Li et al. 2016) before differentiating once again to an elongated morphology with visible flagella, bursting through the host cell wall, and escaping into the bloodstream or interstitial fluid (Ley et al. 1988). A *T. cruzi* parasite in this non-replicating extracellular life stage is called a bloodstream trypomastigote, and is able to opportunistically invade other types of host cells, such as macrophage cells, muscle cells, nerve cells and others or be taken up with the blood by a triatomine insect (Van Overtvelt et al. 1999). Alternatively, replicating amastigotes can lead to host cell death, be released from the cell before differentiation and proceed to infect additional cells (Walker et al. 2014). The precise mechanism of infection by extracellular amastigotes remains unclear (Walker et al. 2014). *T. cruzi* amastigotes proliferate within the cell, and can enter a latent phase in which they may remain dormant for decades (Teixeira et al. 2011).

**Chagas disease symptoms and epidemiology**

*Trypanosoma cruzi* infection in humans can cause a variety of pathological symptoms. These manifestations comprise Chagas disease, also known as American trypanosomiasis. The disease has two distinct phases: the acute phase and the chronic phase (CDC 2017). Acute symptoms after becoming infected can be mild or asymptomatic, and can include a fever or inflammation around the bite wound or membrane that was exposed to the parasite (CDC 2017). If left untreated, 15 to 30% of infected patients will develop chronic Chagas disease, which most commonly affects the heart and gastrointestinal tract (Hemmige, Tanowitz, and Sethi 2012). Chagas cardiomyopathy manifests in a variety of conditions, such as arrhythmias, heart blocks,

heart failure, thromboembolism, and stroke (Biolo, Ribeiro, and Clausell 2010). In the GI tract, the disease can cause motor disorders that disrupt the digestive process, and can also cause dilation of the gastrointestinal tract at different loci (Matsuda, Miller, and Evora 2009). Chronic Chagas disease typically manifests 10 – 20 years after initial *T. cruzi* infection (Sabino et al. 2013).

Chagas disease is a neglected tropical disease that affects an estimated total of 10 million people in North and South America and has been dubbed by some researchers as "the new HIV/AIDS of the Americas" due to a lack of safe and effective treatments (Hotez et al. 2012). *T. cruzi* is most commonly known to be transmitted by its insect vector, but the parasite can also be transmitted through blood transfusion, organ transplantation, and from mother to child through vertical transmission (Biolo, Ribeiro, and Clausell 2010). Chagas disease is an important public health issue in rural and impoverished populations of Latin America due to its insect vector transmission (Hotez et al. 2008). The symptoms are often overlooked, especially in populations without reliable and affordable access to medical care, and the disease disproportionately affects people living in poverty (Hotez et al. 2012). Chagas disease is also a growing problem in the United States due to immigration from Latin American countries (Bern and Montgomery 2009). There are an estimated 238,091 US cases of Chagas disease as of 2012 (Manne-Goehler et al. 2016), also disproportionately affecting people who live below the nation's poverty line (Hotez 2008). Current treatment entails an outdated drug arsenal, the best of which is only effective during the acute form of the disease and causes side effects in a majority of patients (CDC 2017). A better understanding of the pathogenic process, epidemiology, transmission, and biological processes of *T. cruzi* will be essential for the development of better prevention and treatment protocols for

Chagas disease.

### *T. brucei* life cycle and pathogenicity

The life cycle of *T. brucei* takes place between the tsetse fly (*Glossina* spp.*)* insect vector and mammalian host (CDC 2018). Unlike *T. cruzi*, *T. brucei* remains extracellular in its mammalian host, inhabiting the bloodstream and tissue fluids (Figure 4). The extracellular fluids of an infected host contain a pleomorphic (differentiating) population of *T. brucei* parasites, which oscillate between distinct morphology types throughout the course of the infection (Barry and Turner 1991). The extremes of these morphologies are replicating slender bloodstream forms and nondividing stumpy forms, with intermediate stages between the two (Fenn and Matthews 2007). Slender bloodstream cells, which have an elongated morphology, rely entirely on glycolysis for their energy supply (Van Grinsven et al. 2009). The host immune system responds to the variant-specific surface glycoprotein (VSG) on the bloodstream form parasites, and is able to eradicate the majority of the parasite population. Antigenic variation of the VSG surface protein allows a small fraction of cells to evade the defense mechanisms of the host (Navarro and Cross 1996). Replication of these lingering cells will allow a new surge of parasitaemia to manifest within the host, dividing through binary fission and mostly comprised of replicating slender form cells (Vassella et al. 1997). As the parasitaemia reaches its peak concentration, the population of slender cells is triggered to differentiate into shorter, fatter stumpy form cells by a parasite-derived signal called the stumpy induction factor (Vassella et al. 1997, Reuner et al. 1997).

The tsetse fly becomes infected when *T. brucei* parasites from the bloodstream are taken into the digestive tract of the fly as the insect takes a bloodmeal from an

infected host (CDC 2012). Stumpy cells are able to prevail when glucose levels drop (Qiu et al. 2018), and are preadapted to survive this and other stresses associated with uptake by the tsetse fly vector (Nolan et al. 2000). Once inside the tsetse fly, the stumpy form parasites differentiate into procyclic forms in the midgut (Fenn and Matthews 2007) which rely on proline degradation and the TCA cycle for energy production (Mantilla et al. 2017), and actively multiply before migrating to the salivary gland. Throughout this journey the parasites undergo a complex differentiation into epimastigotes (Van Den Abbeele et al. 1999). Within the salivary gland, *T. brucei* epimastigotes attach to the epithelium, continue dividing, and undergo another session of differentiation into non-dividing and highly infective metacyclic trypomastigotes (Kolev, Ullu, and Tschudi 2013). Metacyclic trypomastigotes detach and enter the lumen of the salivary glands, (Kolev, Ullu, and Tschudi 2013) and from there are transmitted into the bloodstream of the next mammalian host through the bite of the tsetse fly (CDC 2018). The insect-stage differentiation process of *T. brucei* differs from the metacyclogenesis of *T. cruzi,* which has just two distinct stages (epimastigotes and metacyclic trypomastigotes) and takes place in the hindgut of the insect vector. The entire insect-stage *T. brucei* transformation process from stumpy form to metacyclic trypomastigote form within the insect takes 20-30 days (Fenn and Matthews 2007).

**African trypanosomiasis symptoms and epidemiology**

Subspecies of *T. brucei* are the causative agents of human African trypanosomiasis (HAT), also known as African sleeping sickness. HAT is a neglected tropical disease that affects an estimated 50,000-70,000 people in countries throughout sub-Saharan Africa with approximately 60 million people at risk (P. G. E. Kennedy 2004,

Brun et al. 2010). HAT is caused by two subspecies of *Trypanosoma brucei: T. b. gambiense and T. b. rhodesiense*. A third subspecies, *T. brucei brucei,* causes disease in livestock, known as nagana. *T. brucei brucei* is sensitive to immune complexes found in human blood serum, and therefore is not infective to humans under normal conditions (Vanhollebeke and Pays 2010). Both human and livestock trypanosomiasis have a great socioeconomic impact on affected villages, and have been a major reason for rural underdevelopment in sub-Saharan Africa (Brun et al. 2010). As is also the case with Chagas disease, the clinical presentation of human African trypanosomiasis is complicated, diagnosis is challenging, and the current treatments produce toxic side effects in patients (P. G. Kennedy 2013).

HAT involves two stages of disease progression: an early hemolymphatic stage, and a late meningoencephalitic stage. In the hemolymphatic stage, the parasites proceed through cycles of proliferation in the bloodstream and lymphatic system (P. G. E. Kennedy 2004; MacLean et al. 2012). If left untreated the infection will enter the meningoencephalitic stage, in which the parasites cross the blood-brain barrier and infect the central nervous system. This causes an inflammatory reaction in the brain that leads to severe neurological symptoms (seizures, sleep disturbances or coma) and death in most cases (MacLean et al. 2012).

The disease progression of HAT differs between the two causative *T. brucei* subspecies. The most common form of HAT is caused by *T. brucei gambiense*, and comprises more than 90% of reported HAT cases. This form of trypanosomiasis is more prevalent in west and central sub-Saharan Africa (Simarro, Jannin, and Cattand 2008). *T. b. gambiense* causes a chronic infection, which can at first instigate general symptoms of fatigue, anemia, weight loss, or weakness (Sternberg and Maclean 2019),

or exist in the patient for months to years before detectable neurological symptoms develop. The patient is likely in an advanced stage of central nervous system infection when these symptoms start to appear (Simarro, Jannin, and Cattand 2008). The progression of *T. brucei gambiense* HAT has an average duration of 3 years (Checchi et al. 2008). *T. b. rhodesiense* causes east African trypanosomiasis, and accounts for approximately 10% of HAT cases. East African HAT is a much more severe and quickly-progressing disease, primarily because *T. b. rhodesiense* is better able to resist lysis by normal human serum (Luc Vanhamme and Pays 2004). East African HAT can be fatal within 6 months (Odiit, Kansiime, and Enyaru 1997), and has the potential to cause epidemics in human populations (Franco et al. 2014).

**Gene expression in *Trypanosoma***

Throughout the life cycles of *T. cruzi* and *T. brucei,* the parasites encounter contrasting environments within their insect vectors and mammalian hosts. Variables that the parasites will encounter include types and abundance of nutrients available, host immune response, oxidative stress, and deviations in temperature, pH, and osmolarity (Jimenez 2014). In order to respond to these environmental changes, the parasites undergo extensive alterations in their morphologies and metabolic processes, which requires remodeling of the nuclear and mitochondrial genome throughout the organism's life cycle (Tielens and van Hellemond 2009; Jimenez 2014).

The regulation of gene expression of both the nuclear and mitochondrial genomes is carried out by unique processes in trypanosomes. Intron-less nuclear DNA is transcribed into long polycistronic non-related primary transcripts of up to 100 open reading frames by RNA polymerase II (Pol II), which are processed with the

concentrated action of *trans*-splicing and polyadenylation (Michaeli 2011; Preußer, Jaé, and Bindereif 2012). The sites and mechanism of the initiation and termination of transcription for protein-encoding genes is not well described (Kolev et al. 2010). In the process of *trans*-splicing, a spliced leader RNA (SL RNA) provides a copy of a common 39 nucleotide spliced leader sequence to the 5' end of all mRNA transcripts (Kolev et al. 2010). This addition is referred to as a cap 4 structure in trypanosomes, and allows the creation of highly stable mRNA products (Perry, Watkins, and Agabian 1987; Palenchar and Bellofatto 2006). Capping is a universal aspect of eukaryotic mRNAs, however, the 5' cap is unique and much more complex in trypanosomes in comparison to other eukaryotes (Bangs et al. 1992).

The process in which *trans*-splicing occurs is also distinct in trypanosomes in that it functions together with polyadenylation to process and separate polycistronic transcripts (Ullu, Matthews, and Tschudi 1993; Liang et al. 2003). Ullu, Matthews and Tschudi 1993 suggests that addition of a SL RNA sequence cap is a prerequisite event for 3' cleavage and polyadenylation, as the removal of *trans*-splicing ability in *T. brucei* inhibited the normal formation of the 3' end. Machinery of the spliceosome marks the 3' end splice site for cleavage, which is followed by the poly(A) addition (Liang et al. 2003; Matthews, Tschadi, and Ullu 1994). Because of polycistronic transcriptional processes in trypanosomes, the regulation of gene expression in trypanosomes operates predominantly at the post-transcriptional level (Vanhamme and Pays 1995).

**Post-transcriptional regulation**

Several processes have been described in the post-transcriptional control of trypanosome gene expression, including mRNA processing, mRNA degradation and

stability, as well as translational efficiency and protein processing (Ouellette and Papadopoulou 2009). The quantity of mRNAs available for translation are determined by the efficiency of splicing and by differences in RNA stability (Clayton 2002). Similar to the degradation processes in yeast and mammalian cells, deadenylation of the 3' untranslated region (UTR) by exonucleases was demonstrated in trypanosomes (Haile, Estévez, and Clayton 2003). Bulk degradation is carried out by cytoplasmic exonucleases in the 5' to 3' direction and in the 3' to 5' direction by a complex called the exosome. These actions are stimulated by regulatory proteins that bind to the 3' UTR and lead to rapid degradation of mRNA transcripts (Clayton 2002; Haile, Estévez, and Clayton 2003). Past studies have demonstrated that some RNA binding proteins (RBPs) affect RNA abundance by protecting the mRNA from degradation and increasing translation efficiency. These RBPs play critical roles in the life stage transitions of trypanosomes (Kolev, Ullu, and Tschudi 2014). The fate of RNA transcripts is regulated by interactions between RBPs and protein complexes responsible for translation, editing, and degradation (Clayton 2013).

Non-encoded 3' mRNA tails can enlist the actions of exoribonucleases and endoribonucleases, which facilitate RNA degradation. Ribonucleases may also have specific roles in RNA processing and turnover, such as the function of TbRND, demonstrated by (Zimmer et al. 2011) to have highly specific function in gRNA metabolism in *T. brucei*. Chapter 2 of this thesis explores the role of the EEP1 (Exonuclease-endonuclease-phosphatase domain-containing 1) protein of *T. brucei,* which we hypothesized to function as a ribonuclease with actions in RNA degradation during developmental transitions.

**The mitochondrial genome and editing**

The genome of the trypanosome single mitochondrion is organized within the kinetoplast and referred to as kDNA. kDNA is structured in a complex network of DNA rings known as maxicircles and minicircles. Maxicircles make up approximately 10% of the kinetoplast (approximately 50 copies per organelle, 20-40 kb in length) and encode small and large subunit ribosomal RNAs (rRNA) as well as a set of essential proteins of the electron transport chain on the inner mitochondrial membrane (Schneider et al. 2001; Feagin 1999). Minicircles are smaller and more abundant molecules (5,000 to 10,000 per cell, 0.56 – 2.5kb in length) which contain three or four repeated sequences encoding guide RNAs (gRNAs) (Feagin 1999). Mitochondrial gene expression is a cooperative endeavor between both maxicircles and minicircles to produce functional mRNA transcripts through the process of editing (Liu et al. 2005).

Mitochondrial mRNA (mtRNA) editing is a complex process of post-transcriptional regulation in which uridine residues (Us) are inserted in or deleted from precursor mRNA transcripts in order to develop open reading frames. Editing takes place in 12 of the 20 genes which comprise the maxicircle (Westenberger et al. 2006). Akin to nuclear-encoded genes, maxicircles and minicircles are polycistronically transcribed (Aphasizhev and Aphasizheva 2014). gRNAs encoded in minicircles govern the specificity of editing by serving as template sequences for endonucleolytic cleavage, as well as the insertion and deletion of uridine residues (L. Simpson et al. 2004; Stuart et al. 2005). Partial annealing of the 5' "anchor" of the gRNA to the initiation site (the site of pre-mRNA cleavage) of pre-edited mRNA begins the editing process. This union provides a template for the insertion and deletion of uridine by the multi-protein RNA editing core complex (RECC), also known as the "20S editosome," which interacts with

an RNA editing substrate binding complex (RESC) that functions in gRNA binding and stabilization (Aphasizheva, Zhang, and Aphasizhev 2016; Stuart et al. 2005; Zimmer, Simpson, and Read 2018). Editing progresses sequentially in a 3' to 5' direction along the mRNA, and requires the recruitment of multiple gRNA templates (Aphasizhev and Aphasizheva 2014) (Figure 5). RNA sequencing studies by Gerasimov et al. 2018 and Simpson et al. 2016 provide evidence that the RNA editing process in trypanosomes proceeds in a hectic and random manner, potentially resulting in the formation of alternative translatable transcripts.

**Variations in the mitochondrial transcriptome**

Research has shown that *T. brucei* and *T. cruzi* remodel their metabolic processes throughout the course of their life cycles, providing an adaptive mechanism that allows them to respond to changing nutrient environments (Tielens and van Hellemond 2009; Smith et al. 2017; Barisón, Nakamura, et al. 2017). Previously in the Zimmer laboratory, the *T. cruzi* mitochondrial transcriptome was examined for changes in mitochondrial rRNA and mRNA transcript abundances between two life stages: before and after the in-vitro induction of metacyclogenesis. This study by Shaw, Kalem, and Zimmer 2016 uncovered significant variations between transcript abundances in the insect life stages, particularly for transcripts encoding proteins of the electron transport chain that is responsible for cellular respiration. Chapter 3 of this thesis continues this work, focusing on variations in mitochondrial transcripts between the insect life stages and the intracellular amastigote stage of *T. cruzi.*

# Chapter 2: The Role of EEP1 in *Trypanosoma brucei*

This chapter is focused on the possible role of a protein factor during culture differentiation that mimics the transition from the *T. b. brucei* slender bloodstream form (BF) of the mammalian host, to the procyclic form (PF) parasites in the tsetse fly vector. Developmental events in *T. brucei* include modifications in morphology, metabolism, gene expression, protein synthesis, and signaling pathways (Fenn and Matthews 2007). Many of the underlying mechanisms behind these changes are not well understood, therefore, discovery of the roles that specific proteins play in *T. brucei* differentiation is important. This chapter describes our investigation of the role of EEP1, a nuclear-encoded protein that potentially functions in RNA degradation. We have examined the effects of EEP1 overexpression and silencing on the differentiation process described above.

**Preliminary investigation of EEP1 function**

As mentioned in Chapter 1, trypanosomes control the expression of protein-encoding genes by means of several posttranscriptional mechanisms, one of which is selective mRNA degradation (Clayton 2002). In general, various RBPs bind with mRNA to form messenger ribonucleoprotein (mRNP) complexes and determine the fate of the mRNA after it is exported from the nucleus to the cytoplasm, where it can be either translated, silenced, or degraded (Cassola 2011). mRNP complexes are believed to be

remodeled as soon as they enter the cytoplasm in other eukaryotes, but there is little information about how this process ensues in trypanosomes (Cassola 2011).

The EEP1 sequence in *T. brucei* is similar to human PDE12, which is a deadenylase. PDE12 has been shown to remove poly(A) tails from mitochondrial mRNAs, and serves as an important regulator of mitochondrial protein translation (Rorbach, Nicholls, and Minczuk 2011). The sequence resemblance to PDE12 points to EEP1 having a nucleolytic function in trypanosomes. Actually, analysis done by the Zimmer and Laurie Read labs (2011-present) found that EEP1 was an endoribonuclease *in vitro*. These laboratories found preferred endonuclease cleavage sites for recombinant EEP1 within a substrate RNA oligomer, and found that the enzyme is only active on RNA. In sum, the idea that EEP1 functions as a ribonuclease in *T. brucei* cells is supported.

Additional Zimmer and Read laboratories' unpublished studies provide more details about EEP1. It appears to be localized mainly in the cytosol, indicating that EEP1 must function differently in trypanosomes than PDE12 in humans, which is a mitochondrial enzyme. Processing bodies (P bodies) are conserved complexes localized in the cytosol of trypanosomes and other eukaryotes that contain enzymes known to be involved in mRNA turnover (Cassola 2011). Preliminary co-localization studies investigated the potential association of EEP1 with P bodies in *T. brucei*, and found that EEP1 did not localize in P bodies (Figure 6). The assay visualized the localization of overexpressed EEP1 and constitutively expressed mCherry-labeled SCD6, a component of all P-bodies (Buchan, Nissan, and Parker 2010). This indicated that EEP1 is not likely acting in the major canonical mRNA storage and decay pathways, and may instead target specific RNAs.

Finally, EEP1 was found to be developmentally regulated at the protein level. EEP1 mRNA is present at equal abundances in the *T. brucei* bloodstream form and procyclic form, but the protein is only present in the procyclic form (Figure 7). The life-stage dependent presence of EEP1 indicates that there is a BF stage translational block to EEP1 expression, which is a common phenomenon in trypanosomes for appropriate life-cycle stage transitions (Romaniuk, Cervini, and Cassola 2016).

**Hypothesis: We predict that EEP1 has a functional role in the *T. brucei* differentiation process because of the above preliminary results and the results of a genome wide RNAi screen.**

An RNAi screen by Alsford et al. 2011 used an RNAi plasmid library containing randomly cut genomic fragments to create an **inducible** library of bloodstream form *T. brucei.* This study aimed to uncover genes that potentially provide essential functions throughout life cycle transitions. Alsford et al. 2011 screened for the disappearance of fragments within the RNA silencing construct in populations of trypanosomes that carry the RNAi library before and after RNAi induction (Figure 8). Upon analysis of DNA isolated from induced and uninduced cell populations growing and differentiating to procyclic form *in vitro*, they reported that populations surviving post-differentiation showed a 3-fold over-representation of the presence of the silencing construct containing EEP1 sequence. This implies that a deficit of this protein potentially results in a gain of function during the differentiation process. In this study, we aimed to explore the potential effect of EEP1 silencing and overexpression on *T. brucei* differentiation rates, which would provide more insight into the function of EEP1.

# Methods

### *T. brucei* cell culture and differentiation

The *T. brucei brucei* SingleMarker (SM) bloodstream form (BF) cultures were maintained in HMI-9 medium with 10% FBS, in a humidified 5% $CO_2$ incubator at 37°C. Cultures were diluted approximately 1 to 25 every 2-3 days. Differentiation of *T. brucei* from BF to PF was accomplished by resuspending exponentially growing *T. brucei* BF cells in HMI-9 medium supplemented with 6mM citrate/cis-aconitate (CCA), adjusting the pH back to 7.5, and lowering the temperature to 27°C (Szöor et al. 2013). Numbers of cells in the differentiating cultures were counted every 24 hours. Cells were collected for analysis at indicated timepoints (Figure 9) by centrifugation of 1.5-2.5 ml of culture, which was resuspended in 1 ml flow cytometry (FACS) buffer (20 ml 0.5 M EDTA, 2.5 g BSA, 50 ml 10X PBS, 380 ml $H_20$) and 500μl 8% paraformaldehyde (PFA). At the 48 hour timepoint, the remaining culture was centrifuged and resuspended in 10ml SDM-79 base differentiation medium with 6mM CCA, 10% FBS, 1% penicillin-streptomycin, and pH adjusted back to 7.5. Cultures were counted and 1.5-2.5 ml was collected every 24 hours for the following 48 hours (total differentiation time: 72 - 96 hours). Statistical variation of cell concentration during differentiation was determined using a 2 way ANOVA (Tukey's multiple comparisons test) comparing column means, alpha = 0.05.

### Transfection and induction of EEP1-OE and EEP1-RNAi plasmids

pLEW100EEP1-LSH (denoted hereafter as EEP1-OE) and p2T7-177EEP1 (denoted hereafter as EEP1-RNAi) plasmids were generated previously by the Read lab. These plasmids were purified and digested with Not1 restriction enzyme for

electroporation into *T.b.b.* BF (SM) cells to generate stable transfectants (plasmids are integrated into the genome at specific locations). Parent plasmids are described in (Scahill, Pastar, and Cross 2008) and (Wickstead, Ersfeld, and Gull 2002). For transfection, BF(SM) cells were grown to confluence in HMI-9 and $5\times10^7$ cells were centrifuged at 1000xg for 10 minutes. Supernatant was removed completely and cells were resuspended in 100ul of TB-BSF buffer (90 mM $NaP0_4$ pH 7.3, 5 mM KCl, 50 mM HEPES pH 7.3, 0.15 mM $CaCl_2$). 10μg of linear plasmid was added, transferred to a transfection cuvette, and transfected at Nucleofector II (Lonza) setting Z-001. Cells were transferred to 125ml HMI-9 medium and left in the 37°C incubator for approximately 18 hours, after which 2.5μg/ml phleomycin was added for EEP1-RNAi cultures, and 0.1 μg/ml puromycin for EEP1-OE in order to select for cells that had incorporated the selectable marker specific to each plasmid. Control cultures were transfected according to the same protocol, but with an equal volume of water in place of the plasmid. These lacked any selectable marker and died within 2-5 days post-transfection. Transfected cell lines were verified via PCR on extracted DNA with appropriate primers for plasmid sequence detection as described in results. (EEP1-OE EEP1-LSH fwd: 5' CGA GAA CGA TCA TCA CCA TCA 3'. LSH plasmid rev: 5' TCC AAA GCA AAC ATG CAG ATT C 3'). EEP1-RNAi primer: Phleo_w_Xbal: 5' AAA TAA GCT CTA GAA TGG CCA ATG TGA CCA GTG C 3'. Phleo_w_PsH: 5' ACC AAC CTG CAG TCA GTC CTG CTC CTC GGC 3'. PCR products were evaluated on a 1% agarose gel run at 130 V.

Both EEP1-OE and EEP1-RNAi cell lines were induced for expression with 2.5μg/ml tetracycline. Tetracycline was added in advance of experiments comparing differentiation under differing amounts of EEP1: 24 hours prior for EEP1-OE and 48 hours prior for EEP1-RNAi. For experiments optimizing EEP1 cDNA expression, RNA

was isolated from cell lines in TriPure (Roche TriPure Isolation Agent). DNA was digested from RNA samples using a DNAfree kit (Life Technologies). cDNA was synthesized from total RNA with Omniscript RT kit (Quiagen), amplified by PCR with 1.5 $\mu$M forward and reverse primers (EEP1-LSH fwd: 5' CGA GAA CGA TCA TCA CCA TCA 3'. LSH plasmid rev: 5' TCC AAA GCA AAC ATG CAG ATT C 3'). PCR products were evaluated on a 1% agarose gel, run at 130 V. For quantitative RT-PCR (qRT-PCR), DNase digested RNA was used to synthesize cDNA with random hexamers and TaqMan Reverse Transcriptase (Applied Biosystems). RNA abundances were then quantified from samples through qRT-PCR, using LightCycler equipment and software (Roche LightCycler480 Version 1.5.0.39). Samples were quantified using absolute quantification/second-derivative maximum, as in Shaw, et al. 2016 fitted to a standard curve of five 4-fold serial dilutions of cDNA, and normalized to Telomerase Reverse Transcriptase (TERT). Amplified sequence was within the coding region of EEP1, near the 5' non-encoded region of the transcript. (Tb927.2.2430 for (47-164) 5' GTG CCA TTA TCA CTT TGG AC 3'; Tb927.4.2430 rev (47-164) 5' CTA AGT CGC TCA ATT GCT CT 3'). This amplification measured both endogenous and exogenous EEP1 mRNA levels.

**Antibody tag and flow cytometry**

*T. brucei* BF (SM) PFA-fixed cell samples from indicated timepoints throughout the differentiation protocol were centrifuged at 1000xg and resuspended in primary antibody at 1:20,000 dilution in FACS buffer for the EP procyclin analysis (primary antibody: rabbit-derived anti-EP procyclin, gift from Jay Bangs laboratory). For the VSG analysis, primary antibody was diluted 1:5,000 in FACS buffer (Primary antibody: rabbit

derived anti-VSG221, gift from Jay Bangs laboratory). Cells were incubated with primary antibody at RT for 45 minutes, rinsed once with 1 ml FACS buffer, centrifuged and resuspended in secondary antibody (Alexa Fluor 488 goat anti-rabbit IgG; Life Technologies) at a 1:200 dilution in FACS buffer. Cells were incubated with secondary antibody at RT for 45 minutes, and washed with 1ml FACS buffer. Sony SH800Z Cell Sorter flow cytometry instrumentation was used to detect presence of EP procyclin and VSG on cell surface by Alexa Fluor 488 fluorescence. 50,000 – 100,000 events were analyzed from each sample, and evaluated with FlowJo version X 10.0.7r2.

**Western blot analysis of EEP1 expression**

For protein collection, approximately $10^8$ cells of each sample were centrifuged at 1000 xg and resuspended in 2 parts 1X PBS + 1 part 4X SDS loading buffer (40% Glycerol, 240 mM Tric/HCl pH 6.8, 8% SDS, 0.04% bromophenol blue, 5% beta-mercaptoethanol). Samples were heated to 95°C for 5 minutes and stored at -20°C. Samples were run on 7.5% acrylamide gel at 35 mA, and transferred to nitrocellulose transfer membrane at 55 mA for 50 minutes. Membrane was covered with TBS (Tris-buffered saline (50 mM Tris-Cl, pH 7.6; 150 mM NaCl) containing 0.05% Tween + 5% milk for 1 hour at RT, and incubated with primary antibody (Antigen Purified EEP1 #81 Bleed 1 51112) at 1:300 dilution with 1% milk for 12 hours at 4°C. Primary EEP1 antibody was rinsed in fresh TBS-Tween three times for 5 minutes, 10 minutes, and 15 minutes each. Membrane was incubated with secondary antibody (800 CW-conjugated goat anti-rabbit IgG; LI-COR Biosciences) diluted 1:5000 in 1% milk for 1 hour at RT. Secondary antibody was rinsed in fresh TBS-Tween three times for 5 minutes, 10 minutes, and 15 minutes each. Gel was imaged with LI-COR instrumentation at 800CW

for 10 minutes.

**Growth assays comparing EEP1-OE and EEP1 RNAi bloodstream form cell lines**

*T.b.b.* BF cell lines containing the EEP1-OE plasmid and the EEP1-RNAi plasmid were cultured at $5\times10^3$ cells/ml. Each cell line was cultured with 3 replicates induced with tetracycline at 2.5μg/ml (+TET), and 3 replicates containing no tetracycline as a negative control (-TET). Cultures were grown in HMI-9 and kept in 37°C incubator. Parasite concentration was counted in each culture every 24 hours for 6 days, with dilution in fresh medium to original concentration every 48 hours. Statistical differences were compared using linear regression analysis, and significance was determined using alpha = 0.05.

# Results

**Creation of EEP1 silenced and overexpressed *T. brucei* cell lines**

RNA interference (RNAi) has been shown to be an exceptional tool for use in functional analysis of *T. brucei* gene products. The presence of an endogenous RNAi pathway sets *T. brucei* apart from *T. cruzi,* as the latter lacks requisite components of the pathway (Subramaniam et al. 2006). In the tetracycline-induced RNAi system we used to silence EEP1, tetracycline is used to enable double-strand RNA (dsRNA) synthesis and generate a population of heterogeneous small interfering RNAs (siRNAs) that specifically silence the corresponding mRNA (Alsford et al. 2011).

Dr. Zimmer previously created EEP1-OE (also possessing a linker-strep-histidine C-terminal tag) and EEP1-RNAi plasmid constructs for her generation of PF cell lines for

overexpression and silencing (not used in this study). Inducible EEP1-OE and EEP1-RNAi BF cell lines were required for experiments testing the impacts of EEP1 abundance on BF to PF differentiation. These were generated *in vitro* and verified for presence of the desired construct by electrophoresis of DNA isolates amplified by PCR (Figure 10). Primers were specific for the LSH segment occurring behind the EEP1 sequence in the EEP1-OE plasmid (Figure 11). For the EEP1-RNAi plasmid, primers amplified the phleomycin resistance gene. These results show that the plasmids were successfully integrated into the *T. brucei* genome for both cell lines.

As with BF *T. brucei* EEP1-RNAi cell lines, EEP1-OE cell lines require induction with tetracycline in order to overexpress EEP1. In order to proceed with experimenting on our newly-created cell lines, we needed to know when each induced cell line exhibited pronounced changes (either depletion for silencing or increases for overexpression) in EEP1 mRNA abundances. (Due to the translational block, there will be no protein expression to measure). To investigate this, we induced EEP1-OE and EEP1-RNAi cell line cultures with tetracycline for 24 and 48 hours and isolated RNA from each culture. RNA from uninduced EEP1-OE and EEP1-RNAi was also collected for comparison, as well as that of un-transfected *T. brucei* BF(SM) cells. EEP1-OE RNA was evaluated for EEP1 plasmid mRNA abundances with the same primer described in Figure 11 using RT-PCR, and products were evaluated on an agarose gel (Figure 12a). We found that the 24 hour timepoint yielded the largest product band for EEP1-OE plasmid expression. EEP1 mRNA abundances in the induced EEP1-RNAi cell line were evaluated using qRT-PCR using a primer targeting a sequence of the EEP1 mRNA transcript, and found that EEP1 was silenced most prominently at the 48 hour timepoint (Figure 12b). qPCR results for EEP1-OE using the same primer also verified our

findings that the 24 hour timepoint showed the most robust overexpression of EEP1 mRNA (Figure 12b). These data indicate that we successfully generated our requisite cell lines and verified that they produce the desired EEP1 mRNA overexpression or silencing, at least at the mRNA level, upon induction. Because there is translational repression of EEP1 at the BF stage, EEP1 protein expression in any of these cell lines is unlikely.

Following evaluation of whether our BF EEP1-OE and EEP1-RNAi cell lines showed the appropriate up- and down- regulation of EEP1 mRNA levels, we needed to verify that upon release of EEP1 translational repression in BF cells, differences in abundances at the protein levels would emulate that of the mRNA. Prior analysis in the Read laboratory suggested that release of the translational block should occur as soon as BF cells began differentiating (not shown). After inducing our cell lines with tetracycline for the amount of time determined by our optimization process, we then differentiated EEP1-OE and EEP1-RNAi BF cell lines to the procyclic form and isolated proteins 48 hours into the differentiation process. We found that the induced EEP1-OE cell line expressed a larger protein band at the appropriate EEP1 mass of 78.5 kDA, compared to the BF(SM) untransfected control (Figure 13). Our induced EEP1-RNAi cell line also showed the expected results in comparison to the untransfected cell line: there was no trace of the fuzzy, low-intensity EEP1 protein band that appears in the differentiated cells without tetracycline. These results confirmed that our desired cell-line phenotypes were created: a greater abundance of EEP1 protein was present in the induced EEP1-OE cell line and there was indication of EEP1 silencing in our EEP1-RNAi cell line when differentiated to PF.

As a final control measure in our experiment, we had to evaluate whether the addition of a plasmid and tetracycline would alter the growth phenotype of our transfected cell lines. To evaluate this, we investigated cell proliferation rate by counting parasite concentration after three consecutive dilutions in tetracycline induced (+TET) and uninduced (-TET) cultures. We found, as reported in Figure 14, that there was no significant difference between the growth rates of +TET and -TET in both the EEP1-OE and EEP1-RNAi cell lines, except for the third replicate of EEP1-RNAi. Given the fact that EEP1 mRNA is not made into protein in BF, very little change in the growth phenotype was the result we expected. The growth analysis confirmed that there are no growth effects produced by the introduction or silencing of EEP1 that would complicate our analysis.

**Evaluation of EEP1 influence on *T. brucei* differentiation**

In order to evaluate the potential effects of EEP1 on life-cycle stage changes, we differentiated our *T. brucei* BF cell lines to insect-stage PF cells. The differentiation process has been long been known to be induced *in vitro* by exposure to citrate/*cis*-aconitate (CCA) and a reduction of temperature from 37°C to 27°C (Czichos 1986). Under these conditions, several distinct changes take place. The VSG coat is released from the cell surface, and the parasites switch their energy metabolism from relying entirely on glycolysis (breaking down glucose to several products; predominantly pyruvate) to employing a fully functional electron transport chain to undergo oxidative phosphorylation (Fenn and Matthews 2007). As cells transform to the PF life stage, VSG is replaced by a completely different surface glycoprotein called procyclin.

Because the Alsford et al. 2011 RNAi screen indicated that the knockdown of EEP1 provides an advantage in differentiation, we suspected that we would see this reflected in cell numbers through BF to PF differentiation. We hypothesized that overexpressing EEP1 would produce a detrimental effect on the differentiation process. Typically, during the differentiation process, a certain number of BF cells die, while some prevail and successfully differentiate to the PF stage. To evaluate whether EEP1 expression has an influence on this, we quantified cell death between our EEP1-OE and EEP1-RNAi cell lines through the process of differentiation. Using the differentiation protocol described in Methods, we differentiated *T. brucei* BF (SM), EEP1-OE, and EEP-RNAi cell lines (transfected cell lines tetracycline induced and uninduced) to procyclic form parasites. We found that there was no significant difference between parasite numbers in these cell lines throughout the differentiation process (Figure 15). In summary, no growth phenotype or increased death rate during differentiation was observed between the EEP1-OE and EEP1-RNAi cell lines.

After finding that cell survival in the differentiation process is not altered between our EEP1-OE and EEP1-RNAi cell lines, we needed to measure whether there were differences in the ability of BF cells to transition to the PF stage. To assess this, we observed the presence or absence of life stage-defined cell surface markers (Procyclin and VSG) throughout the differentiation process. We differentiated induced and uninduced EEP1-OE and EEP1-RNAi BF cell lines to PF cells, taking culture samples at a variety of timepoints from 0 to 72 hours past the initiation of differentiation. When bloodstream form *T. brucei* transitions to the insect-stage procyclic form, procyclin replaces VSG on the cell surface. We used an AF488-conjugated antibody to detect cell-surface procyclin (detailed in Methods), and using flow cytometry, we evaluated our cell

lines for proportions of cells at each time-point that wield procyclin. Using a comparison to an untransfected *T. brucei* BF(SM) cell line as our negative control, the results of this analysis are described in Figures 16 and 17. These figures comprise two representative trials out of several differentiation experiments that were performed. Although population proportions at each time point varied between replicate experiments, there was no difference in the rate of procyclin appearance between the +TET and -TET variables in either EEP1-OE or EEP1-RNAi.

After assessing *T. brucei* differentiation rates by observing the presence of procyclin, we needed to check whether there would be any difference if we instead observed the disappearance of VSG through the differentiation process. Using our EEP1-OE and EEP1-RNAi induced and uninduced cell lines, we used an AF488 conjugated antibody for VSG to evaluate the presence or absence of VSG at various time-points (Figure 18). We found that there was no difference in the rate of disappearance of VSG between any of our cell lines, which corresponds with the results from our analysis of procyclin.

In summary, we evaluated cell numbers, the appearance of procyclin, and the disappearance of VSG throughout the *T. brucei* differentiation process. All three of these experiments showed that variances in EEP1 protein abundances have no impact on BF to PF differentiation.

# Discussion

This chapter follows up on the preliminary evidence found in a *T. brucei* genome-wide RNAi screen that showed potential involvement of EEP1 in differentiating cells.

After exploring the effects of varying levels of EEP1 on differentiating *T. brucei* cells, our results do not support our initial hypothesis.

RNAi screening can be a powerful tool for functional genomics studies. However, important cautions should be considered when interpreting the data from these screens, as false discovery can occur due to off-target effects (Mohr and Perrimon 2012). The Alsford et al. 2011 RNAi screen may have potentially run into sequence-specific off-target effects that may have produced false positive effects, such as an over-representation of cells with EEP1 silencing. RNAi methods have also been shown to contribute to false negative results, if the RNAi design does not result in an adequate knockdown of a target gene (Mohr and Perrimon 2012). Furthermore, in Alsford et al. 2011, a different strain of BF *T.brucei* was used for RNAi library implementation and differentiation (*T. brucei* MiTat 1.2, clone 221a). The differentiation process was also slightly different; cells were transferred to glucose-free DTM medium before supplementation with *cis*-aconitate (we kept ours in HMI-9 medium before switching to SDM-79 medium). These differences could have potentially uncovered some gene expression characteristics that may not develop in our *T. brucei* BF (SM) strain and differentiation protocol.

In the case of our EEP1 investigation, EEP1 was decreased 29.2% in the EEP1-RNAi cell line after a 48-hour induction with tetracycline (Figure 12). It is possible that this degree of knockdown was not robust enough to produce changes in the differentiation phenotype. In future experiments, a knockout design could be applied to eliminate the EEP1 gene and completely deplete protein abundances.

Preliminary Zimmer and Read lab studies showed that recombinant EEP1 targets RNA *in vitro*. We are not yet sure what the specific target of EEP1 is, but recent Zimmer

lab results (unpublished) have shown that specifically Asp tRNA was degraded more rapidly upon EEP1 overexpression *in vivo* in PF *T. brucei*. The effects of EEP1 silencing by RNAi were not as dramatic but seemed to show the opposite result on the same target. Future investigations may include studying the influence of cellular EEP1 abundance on differing RNA targets, such as nuclear and mitochondrial mRNAs, rRNAs, gRNAs, snRNAs and various tRNAs. Given the previous unpublished results, I would hypothesize that EEP1 function is specific to tRNA degradation.

# Chapter 3: Mitochondrial RNA Expression in *Trypanosoma cruzi*

As mentioned in Chapter 1, *T. cruzi* encounters a variety of different environments throughout the course of its life cycle. Previous research endeavors have demonstrated that the parasites remodel their metabolic processes in order to deal with these changes (Tielens and van Hellemond 2009; Barisón, Nakamura, et al. 2017). Nuclear genetic regulation and changes across the life cycle have been investigated by many research endeavors, but mitochondrial genome expression has been largely neglected by current research efforts. Because at least 15 of the 20 genes of the maxicircle encode subunits for the electron transport chain, evaluating abundances of these transcripts throughout the life cycle of *T. cruzi* will form a solid basis for understanding the regulation of mitochondrial protein formation and metabolic processes. Based on the Zimmer laboratory's previous findings of metabolic and transcriptomic modifications within the two insect life stages (Kalem et al. 2018; Shaw, Kalem, and Zimmer 2016), the focus of this chapter is the continued investigation of

mitochondrial mRNA abundances between the *T. cruzi* insect life stages (replicating and non-replicating) and the replicating intracellular life stage within the mammalian host. In addition, we assessed whether variations in the mammalian host cell type would affect mitochondrial RNA (mtRNA) transcript abundances, and compared two different *T. cruzi* strains in our experiments.

**The *T. cruzi* maxicircle**

There are 20 transcripts encoded in the maxicircle, including 2 encoding ribosomal subunits and 15 encoding components of the electron transport chain (Figure 19). Three maxicircle transcripts are classified as maxicircle unidentified reading frames (MURF) and are titled MURF1, MURF2 and MURF5. Two ribosomal RNAs are encoded, 12S and 9s rRNA, as well as small subunit ribosomal protein S12 (RPS12). C-rich region 3 and 4 open reading frames (CR3 and CR4) are also present on the maxicircle, the function of which is currently undescribed. Two duplicate conserved element sequences are located upstream of the ribosomal RNA genes. These elements may function as the sites of initiation for replication and polycistronic transcription (Westenberger et al. 2006a).

This chapter and the work done by Shaw et al. 2016 is focused on 13 maxicircle transcripts that are either the organellar rRNAs, encode proteins of the electron transport chain that have recognized function in cellular respiration, or are classified as a MURF. A complete list of the transcripts evaluated and their corresponding electron transport chain proteins are compiled in in Table 1. Five of this list are required to undergo the RNA editing process before translation is possible.

**Mitochondrial transcript abundance changes during starvation that leads to metacyclogenesis**

Previous studies by Shaw et al. 2016 quantified transcript abundance variations that occur during the requisite period of starvation between the replicating epimastigote and the non-replicating metacyclic trypomastigote stages of *T. cruzi* CL Brener (CLB). A nutrient-deprivation medium was used to prompt the process of metacyclogenesis *in vitro* and generate a mixed culture containing metacyclic trypomastigotes and infective intermediates. As presented in Figure 20a, Shaw et al. 2016 recorded a trend of increase in abundances of a majority of never-edited transcripts in the infective culture, relative to exponentially replicating cells. As depicted in Figure 20b, little to no change occurred in most pre-edited transcript levels during metacyclogenesis, and in contrast, there was a significant change in abundances of fully edited transcripts. The following hypotheses outline the aims of the continuation of this transcriptome evaluation, in the mammalian host life stage.

**Hypothesis 1: Replicating *T. cruzi* life stages will show similar patterns of mitochondrial mRNA expression.**

We expected that mtRNA transcript abundances in replicating intracellular amastigotes would be observed at levels similar to what was previously recorded in replicating epimastigotes, relative to that of the infective culture. However, we anticipated that the results would not be identical between amastigotes and epimastigotes, due to the fact that the two replicating life stages inhabit contrasting nutrient environments both *in vitro* and *in vivo,* and thus utilize different primary substrates to generate energy. Studies have shown that intracellular *T. cruzi*

amastigotes utilize glucose or triacylglycerols from their host cells (Gazos-Lopes et al. 2017; Shah-Simpson et al. 2017) and epimastigotes rely mostly on carbohydrates in their exponential growth phase within the insect digestive tract, switching to amino acids as glucose levels depreciate (Barisón, Nakamura, et al. 2017).

**Hypothesis 2: Sylvio-X10 and CL Brener strains have been shown to be metabolically different, therefore, we expect that modifications in the mitochondrial transcriptome will be strain dependent.**

Currently, six classes of *T. cruzi* groups have been described and classified into discrete typing units (DTUs TcI - TcVI) based on geographic distribution and nuclear markers. There are also three *T. cruzi* clades (A, B and C), based on maxicircle gene analysis (Westenberger et al. 2006; Ruvalcaba-Trejo and Sturm 2011; Brisse, Dujardin, and Tibayrenc 2000). CLB is a hybrid strain of Clade B and DTU TcVI and Sylvio X10 (SYL-X10) is of clade A and DTU TcI (Zingales et al. 1997; Ruvalcaba-Trejo and Sturm 2011). Comparatively, the strains have substitutions and indels in maxicircle transcripts encoding protein subunits of the electron transport chain (Ruvalcaba-Trejo and Sturm 2011). Recent studies in the Zimmer laboratory (Kalem et al. 2018). have shown that there is variability in important mitochondrial characteristics between *T. cruzi* strains, including mitochondrial membrane potential, mitochondrial morphology, acidic metabolic byproduct excretion, and maximal respiratory capacity. Strain-specific variations were also revealed using high-throughput RNA sequencing of the total genome, specifically in abundances of mRNA transcripts encoding proteins with important metabolic functions (Kalem et al. 2018). We expected that mitochondrial mRNA abundances would show

variations in life-stage transition trends between *T. cruzi* SYL-X10 and CLB strains.

**Hypothesis 3: The type of mammalian host cell infected by *T. cruzi* will impact mitochondrial mRNA expression in the amastigote life stage.**

As mentioned in Chapter 1, *T. cruzi* amastigotes in the acute stage of Chagas disease multiply profusely within host cells. In a chronic *T. cruzi* infection, repressed translation gives rise to latency of amastigotes within host cells, which can ensue asymptomatically for decades (Teixeira et al. 2011). To investigate the effect of host cell type on the *T. cruzi* mitochondrial transcriptome, we used two different forms of host cells to generate amastigotes *in vitro*. To mimic a typical cell infected during the acute infection, we used fibroblasts, and to represent the chronic stage of infection, we used cardiomyocytes. We predicted that transcript abundances would show a general trend of being reduced in the cardiomyocyte host cells in comparison to fibroblast host cells.

# Materials and Methods

### *T. cruzi* culture and mammalian cell infection

The *T. cruzi* CL Brener (generously provided by the DoCampo lab, University of Georgia) and Sylvio X10 (ATCC® 50823) strains were maintained in liver infusion tryptose (LIT) medium with 10% fetal bovine serum (FBS) and 1% penicillin-streptomycin at 27°C and 5% $CO_2$. Epimastigotes in exponential-phase growth were diluted with fresh LIT every 2-4 days. To induce metacyclogenesis, 1 ml of exponential-growth phase *T. cruzi* in LIT were added to 10 ml of Roswell Park Memorial Institute Medium (RPMI) and incubated at 27°C for 8 days. To obtain metacyclic trypomastigotes, the top

7ml fraction of 8-day RPMI culture was collected and *T. cruzi* parasite concentration was counted for use in mammalian cell infection assays.

Two mammalian cell lines were used for infectivity assays to procure *T. cruzi* amastigotes: human cardiomyocyte line AC16, maintained in Dulbecco's Modified Eagle's Medium (DMEM)/F-12 with 12.5% FBS and 1% penicillin-streptomycin, and murine fibroblast line 3T3-L1, maintained in DMEM with 10% FBS and 1% penicillin-streptomycin. Mammalian cells were cultivated by weekly passage and incubated at 37°C in 5% $CO_2$.

For infectivity assays (timeline shown in Figure 21) fibroblast cells were plated in 6-well plates at $5x10^4$ per well, in DMEM + 10% fetal bovine serum (FBS) and incubated at for 24h at 37°C, 5% $CO_2$. Cardiomyocytes were plated at 2.5 x $10^4$ per well, in DMEM/F-12 + 12.5% FBS and kept for 24 hours at 37°C in 5% $CO_2$. Medium was removed and replaced with warm DMEM + 2% FBS medium. Cells were infected with *T. cruzi* parasites from top fraction of 8 day RPMI culture at a multiplicity of infection (MOI) of 100 parasites per mammalian cell for SYL-X10 infectivity assays, and an MOI of 200 parasites per mammalian cell for CL Brener infectivity assays. Infected mammalian cells were incubated for 24 hours at 37°C, after which extracellular *T. cruzi* were removed from the mammalian cell medium by rinsing 5X with warm DMEM + 2% FBS. Remaining mammalian cells were incubated for an additional 48 hours. Mammalian cells were then rinsed with DMEM + 2% FBS medium to remove any remaining *T. cruzi* before RNA isolation and staining.

Nutrient-starved cells were generated by resuspending exponential growth phase *T. cruzi* SYL-X10 in TAU at $1\times10^7$ cells/ml and incubating at 27°C for 48 hours.

**Staining and microscopy**

At the time of RNA collection, 1-2 wells of *T. cruzi* were dried and fixed with 100% methanol, and permeabilized with 1 ml IF-PERM per well for 15 minutes at RT. At indicated timepoint, 1 ml buffer for Giemsa by Soerensen (17.5 ml 9.08g/L $KH_2PO_4$ , 82.5 ml $Na_2HPO_4$ anhydricum, pH 7.45.) and 500ul Wright Giemsa stock solution (Ricca Chemical Company, Giemsa Stain Stock Solution) were added, swirled to mix, and left for 30 minutes at RT. Stain was removed and cells were rinsed thoroughly with water. Stained cells were covered with water and photographed at 400X. *T. cruzi* intracellular amastigote quantification was determined by counting 100 mammalian cells in each of 3 replicates. Statistical analysis was performed to determine differences in number of cells infected and number of amastigotes per cell using 2 way ANOVA, alpha = 0.05.

*T. cruzi* 8 day RPMI culture used for mammalian cell infection was fixed on a microscopy slide with 100% methanol and stained with 3% Giemsa by Sorensen (as indicated above) for 20 minutes and rinsed with water. Slide was viewed at 600X and photos were taken for quantification of metacyclic trypomastigotes. Metacyclic cells were identified by the kinetoplast located completely posterior to the nucleus (Shaw, Kalem, and Zimmer 2016) (Figure 1). Cells were quantified manually using a cell counting program: NIH ImageJ64 1.47v. A minimum of 100 cells were counted for each of 3 replicate cultures, and analyzed for strain-specific differences using an unpaired *t* test, parametric, with alpha = 0.05.

**RNA isolation and semi-quantitative RT-PCR**

*T. cruzi* infected mammalian cells in 4-5 wells were lysed directly in TriPure (Roche TriPure Isolation Agent) for RNA isolation. A similar quantity of uninfected cells

from both cell lines were lysed with TriPure to be used as uninfected control RNA. DNA was digested from RNA samples using a DNAfree kit (Life Technologies). cDNA was synthesized from total RNA with random hexamers and TaqMan Reverse Transcriptase (Applied Biosystems). RNA abundances were then quantified from samples through qRT-PCR, using LightCycler equipment and software (Roche LightCycler480 Version 1.5.0.39). Samples were quantified using absolute quantification/second-derivative maximum, as in Shaw et al. 2016, and fitted to a standard curve of five 4-fold serial dilutions of cDNA. Samples were from three biological replicates, collected on different days, and measured in duplicate wells. Primer sequences are listed in Table 2. Statistical differences between life stages were quantified using a ratio paired *t* test (amastigotes vs. infective culture, amastigotes vs. exponentially growing epimastigotes); alpha = 0.05. Statistical differences between amastigotes in cardiomyocytes and fibroblasts was calculated using parametric unpaired *t* tests of relative data (amastigotes relative to infective culture or exponentially growing epimastigotes); alpha = 0.05.

# Results

**Metacyclic trypomastigotes were quantified in the mixed parasite life-stage infection culture in order to optimize the infection protocol.**

Because we used CLB and SYL-X10 parasites for infections, we needed to know the proportion of metacyclic trypomastigotes in the top 70% fraction of each 8 day RPMI metacyclogenesis culture, which would give us an idea of how many parasites are likely infective. As discovered in Shaw et al. 2016, the top 70% volume of an undisturbed 8 day RPMI *T. cruzi* culture contains the greatest percentage of metacyclic

trypomastigotes, compared to the fraction of culture beneath, which contains a greater proportion of epimastigotes and dead cells. *T. cruzi* CL Brener and Sylvio-X10 strains were incubated in RPMI differentiation for 8 days and the top fraction was sampled and stained with Wright Giemsa stain to quantify metacyclic trypomastigotes (details in Methods).

CLB and SYL-X10 differentiation cultures yielded 14.78% ± 6.871 and 57.32% ± 20.79 metacyclic trypomastigotes, respectively (Figure 22; an example photograph of CLB and SYL-X10 infective culture is shown in Figure 23), which indicated that we would likely need to use a higher MOI in CLB infections than in infections with SYL-X10. The reported percentage of cells have completed metacyclogenesis with the kinetoplast completely posterior to the nucleus. Some parasites are present in the culture as intermediate forms with the kinetoplast in the process of migrating to the posterior portion of the cell, and some cells remain as epimastigotes showing signs of starvation, which are elongated morphology, shrinkage of the cell body and conical shape at posterior end (Gonçalves et al. 2018) (Figure 1, Figure 23). Proportions of intermediate-stage parasites and starving epimastigotes were not quantified in our analysis, because we currently do not know at which point in metacyclogenesis that the parasites become infectious.

**Establishment and optimization of a mammalian cell infection protocol was required to generate intracellular amastigotes for RNA analysis**

In order to generate intracellular amastigotes in quantities sufficient for RNA analysis, we developed *T. cruzi* strain-specific protocols for mammalian cell infections. We optimized infection protocols to generate a maximum number of intracellular

amastigotes, while minimizing material from mammalian cells and other trypanosome life stages (trypomastigotes and epimastigotes). Wells from infection assays were stained and photographed in order to quantify the number of intracellular amastigotes present within mammalian cells under different conditions. Accurate counts required being able to easily designate cell boundaries, so the mammalian cells had to be plated in a way that they would not become crowded or overlap. We performed initial experiments to determine the cell plating ranges that would be appropriate for amastigote collection and quantification. We found that cardiomyocytes plated at an initial number of $2.5 \times 10^4$ cells per well would mitigate crowding (Figure 24), and fibroblasts plated at $5 \times 10^4$ were sufficient to accurately quantify an infection. Enrichment of mammalian cell medium was also adjusted to DMEM+2% FBS (from 10% FBS normal culture medium) in order to reduce proliferation of the mammalian cells.

Multiplicity of infection (MOI) describes the number of parasites (potentially including metacyclic trypomastigotes, epimastigotes, and intermediates) that are added per one mammalian cell. Infections were conducted at a variety of MOI to evaluate the optimum for each *T. cruzi* cell line that would yield the highest percentage of infected cells while still maintaining host cell integrity. For infections performed for RNA collection, we chose to use 50-100 parasites per mammalian cell for SYL-X10 infectivity assays, and 200 parasites per mammalian cell for assays using CLB because these numbers generated consistent percentages of cells infected with amastigotes, as shown in Figure 25.

After the initial addition of parasites to mammalian cells and subsequent wash, the mammalian cells were incubated for an additional 48 hours (72 hours of total exposure to the parasites and intracellular parasite growth, as shown in Figure 21). We

observed that if the cells were left for a longer duration than approximately 72-80 hours, the *T. cruzi* parasites would begin to differentiate from amastigotes to bloodstream trypomastigotes and burst the mammalian cells. Numerous extracellular amastigotes and flagellated parasites was an indication of this occurrence, as well as the presence of mammalian cells with intracellular amastigotes in very large numbers (Figure 26). These high amastigote numbers are not ideal for RNA collection, because the populations may have exceeded the replicative amastigote stage and started to transition to the non-replicative bloodstream trypomastigote stage.

To quantify the number of amastigotes per cell in our *T. cruzi* infections, we had to develop an effective staining protocol. After attempting with Wright Giemsa and hematoxylin protocols, we found that incubation of methanol-fixed cells with IF-Perm before the addition of Giemsa stain was successful in staining the nuclei of mammalian cells, as well as the DNA of trypanosomes within the cells.

**Variations in intracellular amastigote quantification were found between host cell types, but these differences should not create discrepancies in transcriptomic data.**

Because we utilized two different strains of *T. cruzi* to infect two different mammalian cell types, it was important to determine whether the variable of mammalian cell type had the potential to create a difference in the number of cells that would be infected. To test this, cells infected with *T. cruzi* were stained and the number of infected cells was quantified. Figure 3 shows photographs of typical amastigote infections in fibroblasts and cardiomyocytes. From a total of three biological replicate infection assays, the proportion of infected mammalian cells was calculated, and the average

number of amastigotes per infected mammalian cell was determined. Quantifications of infectivity assays are reported in Figure 27. The percent of cells with amastigotes was not different between CLB and SYL-X10 in fibroblasts, but was calculated to have a significant difference between cardiomyocyte infections (P = 0.0455) (Figure 27a). There was no significant difference between the number of amastigotes per cell between both *T. cruzi* strains and host cell lines, which provides evidence that all infections were in a similar phase of replication (Figure 27b). We do not expect that differences in MOI or number of cells infected have an effect on our RNA analysis, because at the time of RNA collection, all existing amastigotes should be in a replicating phase regardless of how efficiently the *T. cruzi* strain infects host cells.

**Specific never-edited and completely-edited mitochondrial RNA transcripts are lower in abundance in the *T. cruzi* CL Brener intracellular life stage *in vitro,* relative to cells incubated in RPMI differentiation medium.**

We hypothesized that never-edited mitochondrial transcript abundances would be lower in the replicating amastigote stage relative to the non-replicating metacyclic trypomastigote stage present in 8 day RPMI culture, as they were previously shown to be elevated in the infective stage relative to the replicating epimastigote stage (Shaw, Kalem, and Zimmer 2016) (Figure 20). To test this in the CL Brener strain, qRT-PCR methods were used to quantify the abundance of specific mitochondrial mRNA transcripts from *T. cruzi* intracellular amastigotes and 8 day RPMI infective culture containing metacyclic trypomastigotes (hereafter referred to as “infective culture”). Quantification of metacyclic trypomastigote percentage of this culture is reported in Figure 22. We examined abundances of two ribosomal mRNA transcripts (9S and 12S)

as well as 6 never-edited maxicircle transcripts. Relative to infective culture, several of these transcripts were significantly lower in abundance in the amastigote stage as compared with day 8 RPMI nutrient-starved cells, and most showed a trend of reduced transcript abundances (Figure 28a). The striking exception to this is the MURF5 transcript. In previous work comparing mtRNA abundances in epimastigotes to infective culture, MURF5 transcript abundance differed very little, if at all (Figure 20). MURF5 abundances in CLB were shown to be significantly higher in abundance in amastigotes infecting fibroblasts – an unexpected anomaly from the rest of the qPCR data (Figure 28a). In general, these data support our hypothesis; never-edited maxicircle transcript abundances were generally found to be lower in amastigotes than in the infective culture.

We predicted that there would be significantly reduced transcript abundances in CLB maxicircle completely edited transcripts in the amastigote life stage, relative to those of the infective culture. To test this, we examined qRT-PCR data that utilized primers for the pre-edited and edited sequences of four different maxicircle transcripts (8 primers total). In general, little to no change in abundance was observed in pre-edited CLB transcripts, the exception being that of the ATPase-6 (A6) pre-edited transcript, which was significantly higher in the amastigote stage (Figure 28b). Edited transcript abundances were generally reduced in the four that were tested (CO3-E and MURF2-E were significantly different, $P < 0.05$), the most striking change being the *maxicircle unidentified reading frame 2* (MURF2) edited transcript. Our hypothesis was supported by these results.

**CL Brener and Sylvio X10 strain showed similar trends in abundances, with some exceptions.**

Kalem et al. 2018 uncovered notable differences in metabolism and gene expression between *T. cruzi* strains. In order to investigate whether strain specific variation exists in maxicircle transcript abundances, we performed a mitochondrial transcriptome analysis on the SYL-X10 strain that was similar to our analysis of the CLB mitochondrial transcriptome. We found that never-edited transcript abundances showed similar trends in SYL-X10 as in CLB: the abundances were generally decreased in the amastigote stage relative to the infective culture (Figure 28a, Figure 28c). Another odd exception to the trend was the inconsistent MURF5 transcript, which points to the notion that MURF5 may not be a viable protein-encoding sequence. Pre-edited and edited sequences showed similar trends: there was little to no change in most pre-edited transcript abundances between life stages measured, and a significant downregulation of edited transcripts in the amastigote stage (Figure 28b, Figure 28d). An exception to this in the SYL-X10 strain is the CO3 pre-edited transcript, which was found to be in significantly higher abundances in amastigotes infecting cardiomyocytes (Figure 28d).

In Shaw et al. 2016, *T. cruzi* CLB strain cells were exposed to nutrient deprivation in TAU medium, and abundances of several never-edited and edited mitochondrial RNA transcripts were shown to increase in abundance, relative to exponentially replicating parasites maintained in LIT. We performed a similar analysis in SYL-X10 in order to explore whether mtRNA transcript abundances would behave consistently in a different *T. cruzi* strain. Because transcript abundances within the two strains behaved similarly in our previous transcriptome analyses, we hypothesized that trends in SYL-X10 would be similar to what was observed in CLB. In Shaw et al. 2016,

cells were exposed to TAU starvation medium for 72 hours and analyzed at 8 different time-points. These multiple time-points were unnecessary to duplicate, and in order to make our comparison quickly, we exposed our cells to TAU for 48 hours (one time-point only). Transcript abundances were significantly higher in starved cells for all never-edited transcripts, with several (9S, 12S, MURF5, CO1) at 5 to 10-fold the levels of the exponentially replicating cells (Figure 29a). This was shown to be similar in the 12S and CO1 levels of CLB. Interestingly, MURF5 abundance levels were shown to be about 7-fold higher in SYL-X10 after the 48-hour TAU starvation, while only about 2-fold higher in CLB after the same treatment.

Because we noticed a potentially more pronounced change of mtRNA abundances in SYL-X10 life stage changes compared with CLB, we directly compared mtRNA abundances from the same life stages in these two strains. In comparisons of infective culture in SYL-X10 relative to CLB, we noticed that there was a general trend in elevated abundances of never-edited, pre-edited and completely edited transcripts in the SYL-X10 strain, but only one of these data points was found to be statistically significant (Figure 30a,c). In this strain comparison in the intracellular amastigote life stage, there were no significant trends indicated in the never-edited transcripts (Figure 30b). However, there was a general pattern of higher abundances in the amastigote edited transcripts in SYL-X10 relative to CLB, while pre-edited transcripts showed no difference between the strains (Figure 30d).

mtRNA abundances showed generally similar trends in pre- and completely edited transcripts in CLB and SYL-X10 *T. cruzi* strains, 48-hour TAU starved cells relative to exponentially growing cells. An exception to this is the CO3-P transcript, which was shown to be at a much higher in abundance in CLB (48-hour TAU relative to

LIT), and was nearly unchanged in SYL-X10 (Figure 29b). Overall, the general trends in the never-edited and completely edited transcripts further support our prediction that mitochondrial transcript abundances in CLB and SYL-X10 will be altered similarly when the parasites are exposed to nutrient deficiency.

**mtRNA transcripts in intracellular amastigotes were lower in abundance relative to epimastigotes.**

Previous evaluations compared mitochondrial mRNA transcript abundances in replicating life stages (intracellular-stage amastigotes and insect-stage epimastigotes) to non-replicating infective culture transcript abundances. We were curious to evaluate whether there were any differences in the mitochondrial transcriptome between the two replicating life stages. RNA isolated from exponentially growing *T. cruzi* SYL-X10 epimastigotes (three biological replicates) was evaluated using qRT-PCR and compared with that of SYL-X10 replicating intracellular amastigotes from cardiomyocyte and fibroblast infectivity assays. Never-edited maxicircle transcript levels were measured, as well as pre-edited and completely edited transcript levels. Relative to exponentially growing cells, most mRNA never edited transcripts were lower in abundance in amastigotes (Figure 31a). Similar to our comparisons of amastigotes to D8 RPMI, fully edited transcripts in amastigotes were shown to be at dramatically lower abundances in some transcripts (completely edited CO3, CYB, and MURF2) (Figure 31b). Abundances of several transcripts, however, remained unchanged in the pre-edited and fully edited mRNA sequence, and in CO3, there were significantly higher abundances of the pre-edited transcript. Overall, these results show that there is a general trend of lower translatable mtRNA transcript abundances in SYL-X10 amastigotes when compared to

insect-stage epimastigotes, revealing a difference in the mitochondrial transcriptome between these two replicating life stages. Based on the previously shown similarities, we would expect that CLB transcript abundances would show similar results, but this was not tested in this analysis.

**Little to no difference in transcript abundance was found between AC16 and 3T3-L1 cell lines, for both SYL-X10 and CLB amastigotes.** As detailed in the introduction, 3T3-L1 fibroblasts and AC16 cardiomyocytes were chosen in this experiment to represent the acute and chronic stages of *T. cruzi* infection, respectively. Because these trypanosomiasis stages manifest so differently in vivo, we wanted to determine whether transcript abundance would contrast between *T. cruzi* parasites infecting these different cell types. After analysis of relative transcript abundance data from SYL-X10 infections, we concluded that transcript levels behaved similarly overall in these mammalian cell lines, with a few exceptions. As pointed out previously, MURF5 abundances of SYL-X10 amastigotes in AC16 cells were shown to be in significantly higher abundance than in 3T3-L1 cells. This was seen both in abundances relative to infective culture (Figure 28c) and relative to exponentially growing epimastigotes (Figure 31a). ND2 also showed significantly reduced abundances in fibroblasts compared to cardiomyocytes, relative to infective culture (Figure 28c). Pre-edited and edited CYB abundances relative to infective culture were significantly higher in cardiomyocytes (Figure 28d). Other differences between mammalian cell types were found in the pre-edited CO3, pre-edited MURF2 and completely edited CYB transcripts, all of which showed significantly higher abundances in the cardiomyocyte infection than in the fibroblast infection, relative to exponentially growing epimastigotes (Figure 31b). No significant differences between

relative transcript abundances in mammalian cell lines were calculated in the CLB strain.

# Discussion

This chapter provides evidence for mitochondrial transcriptome alterations through the *T. cruzi* life cycle transition from insect life stages to the intracellular life stage within the mammalian host. To address specific questions we investigated, this discussion will be organized by the three hypotheses described previously in Chapter 3 Introduction.

**Hypothesis 1: Replicating *T. cruzi* life stages will show similar patterns of mitochondrial mRNA expression.**

This study provides evidence that expression of most never-edited and fully edited mtRNA transcripts are similar in replicating epimastigotes and replicating intracellular amastigotes. However, results indicate that there was an even more dramatic downregulation trend in the intracellular amastigote life stage relative to the non-replicating insect life stage present in the infective culture (Figure 28, Figure 31). Mitochondrial mRNA abundances have been shown previously (Shaw, Kalem, and Zimmer 2016) to be correlated with the immediate nutrient environment, which may include types and levels of nutrients present. *T. cruzi* epimastigotes replicate exponentially in vitro at an approximate concentration of $3.0\times10^7$ to $8.75\times10^7$ cells/ml, according to (Barisón, Rapado, et al. 2017). This is a greatly higher concentration of parasites utilizing nutrients than the typical number of amastigotes per mammalian cell that we measured, which was less than five amastigotes per cell (Figure 27b Avg.

amastigotes per cell). This variance in parasite concentration may potentially offer explanation as to why amastigote mRNA abundances were found to be generally lower than those of epimastigotes. Results from Shaw et al. 2016 showed that when *T. cruzi* had less nutrients available, mtRNA transcript abundances were elevated. However, it is important to note that it would be tremendously difficult to compare the actual nutrient levels available to the epimastigotes in LIT to the amastigotes replicating in host cells. Overall, the similar patterns we observed in mRNA expression between replicating stage *T. cruzi* provide support for our hypothesis.

As pointed out in Results, abundance levels of the never-edited MURF5 (maxicircle unidentified reading frame) transcript showed divergent alterations through life cycle changes relative to patterns shown in other transcripts. Previously in the Zimmer laboratory, the MURF5 DNA sequence was analyzed for start and stop codons in the SYL-X10 strain. Neither of these important elements were found, which suggests that MURF5 does not encode a translatable protein product. The MURF5 sequence was found by Ruvalcaba-Trejo and Strum 2011 to have a relatively large number of insertion/deletion mutations throughout the gene, and also to overlap 7 nucleotides on the 3' end with the next adjacent maxicircle gene. Because of these abnormalities, and the indications we have found in transcript abundance levels, we can infer that MURF5 likely does not yield a biologically relevant reading frame.

Our transcriptomic analysis provides a quantification of mRNA transcript abundances at the very beginning and end of the editing process; we measured pre-edited mRNA transcript abundances and their corresponding fully-edited transcripts. Although this study yields valuable information about editing patterns in different life stages, these experiments do not provide any quantification of the intermediate stages of

editing. Experiments in the future may build upon this basis of knowledge with an RNA-Seq analysis that would delineate the progress of editing at various timepoints in the *T. cruzi* life cycle.

**Hypothesis 2: Sylvio-X10 and CL Brener strains have been shown to be metabolically different, therefore, we expect that modifications in the mitochondrial transcriptome will be strain dependent.**

Kalem et al. 2018 revealed variations between CLB and SYL-X10 strains in extracellular acidification, ATP-coupled respiration, spare respiratory capacity, mitochondrial membrane potential, and mitochondrial morphology. Our study revealed that the life cycle-dependent responses of mitochondrial gene expression to life stage or environmental stimuli were not divergent from one another, but very comparable. This finding does not support our initial prediction. Potentially, there could be overall differences in the quantity of all transcribed products between these strains, but this would not be revealed in our data because it was reported as normalized ratios. When we tested SYL-X10 to CLB directly, we found it generally to not be the case. A single exception is the edited mtRNA abundances in amastigotes, which were shown to be generally elevated in SYL-X10 relative to CLB (Figure 30d). Kalem et al. 2018 experimentally addressed whether there are differences in the number of total electron transport chain complexes between *T. cruzi* strains (analysis of nuclear-encoded proteins) and discovered no significant variations. The differences we found in edited mtRNA abundances could point to an explanation as to why Kalem et al. 2018 noticed distinctions in metabolism between the two strains. Overall, this investigation of mitochondrial transcript abundances reveals potential reasons for metabolic differences

between CLB and SYL-X10, leaving questions for future research in this area.

**Hypothesis 3: The type of mammalian host cell infected by *T. cruzi* will impact mitochondrial mRNA expression in the amastigote life stage.**

Very little variation was observed in mtRNA transcript abundances between amastigotes in fibroblasts and in cardiomyocytes; therefore, this hypothesis was not supported. A potential limitation to this study is the infection of the host cell lines *in vitro,* within the exact same cell culture medium. With these circumstances, host cells did not experience the typical *in vivo* environment, stressors, and signaling that might provide typical divergent characteristics for these cell types in a living mammalian host. Dumoulin and Burleigh 2018 published that the ability of *T. cruzi* amastigotes to alter proliferation rate is an important characteristic of the parasite's adaptation to environmental stressors within the host cell. This growth plasticity allows the parasites to either continue replication in the acute stage of infection (typically within superficial cells such as fibroblasts) or slow down their proliferation rate and enter into a latent phase in deep organellar cells such as cardiomyocytes. As revealed in the discussion of Hypothesis 1, there is an association between *T. cruzi* replication status and mitochondrial transcript abundance levels. It is possible that our *in vitro* experiment did not provide amastigotes with the appropriate intracellular stressors that would prompt them to alter their mitochondrial transcriptome or change their growth rate in these different host cell types. It is also possible that our hypothesis is incorrect; host cell type could have very little influence on the induction of gene expression alterations and amastigote latency. The intracellular-stage processes could be governed by different factors entirely.

**Summary**

The experiments in this chapter provide important pieces of evidence in the puzzle of *T. cruzi* mitochondrial transcriptome regulation within specific insect and mammalian life stages. We divulged that regardless of *T. cruzi* strain or the type of host cell infected, the mitochondrial transcriptome follows an established pattern of expression across the stages of the life cycle that we investigated. The final *T. cruzi* life stage remaining to be analyzed for transcriptomic data is the flagellated form that is released from the cell to the interstitial fluid or bloodstream of the host: the bloodstream trypomastigote. We predict that because this is an infective and non-replicating life stage, it will exhibit mitochondrial transcriptome alterations that are similar to the metacyclic trypomastigote infective insect stage. Overall, the data that we have collected may be used as a basis for the continued exploration of the post-transcriptional regulatory processes that govern mitochondrial proteins, metabolic function, and host-parasite interactions within the *T. cruzi* life cycle.

# Chapter 4: Conclusion

This body of work details our investigation of some genetic factors involved in life-cycle transitions of two important trypanosome parasites: *T. brucei* and *T. cruzi*. These studies are separate, but related in their focus on the differentiation that occurs when the parasites are relocated to a new environment of contrasting temperature, nutrient availability, cell density, and other variables. Environmental factors prompt both species of parasites to undergo morphological and metabolic changes, which require the remodeling of gene expression. While my studies each focused on a different

mechanism in separate differentiation processes, both examined aspects of post-transcriptional regulation. Specifically, we focused on life cycle-specific mature RNA abundance and degradation. As detailed in Chapter 1, stability, maturation, and degradation are factors that contribute to the fluctuating changes in gene product abundance in trypanosomes.

In Chapter 2, we examined the potential influence of a putative endoribonuclease, EEP1, on the transition from the mammalian stage *T. brucei* to the insect stage and concluded that it has no influence on the differentiation process. The work described in Chapter 3 measured *T. cruzi* mitochondrial mRNA abundance changes in the differentiation process from insect to mammalian host life stages. We found that in replicating mammalian life stages, mRNA abundances of most mitochondrial transcripts are dramatically reduced relative to non-replicating infective insect stage parasites. Furthermore, the *T. cruzi* mammalian stage mitochondrial mRNA levels were comparable to those of the insect replicating life stage, indicating that changes in nutrient availability and replication status have a strong influence on the expression of electron transport chain components.

As in any scientific study, the context of the experiment plays an enormous role in the quality of outcome. The control and acknowledgment of the context of the experiment is very important, especially when drawing conclusions. Our trypanosome studies were performed *in vitro,* using cell lines cultivated in culture flasks for an unknown number of previous replication cycles. In our *T. cruzi* experiments, a potential limitation to our results could be the fact that we are infecting mammalian cells *in vitro*, rather than infecting cells that are part of a live organism. Follow-up work may include

an *in vivo* investigation of mitochondrial RNA expression in various *T. cruzi* infected cells and tissues, perhaps utilizing a mouse model to generate acute stage infections.

The *T. brucei* BF (SM) cell line we utilized for cultured experiments has a growth and differentiation pattern that differs from typical wild type cells but was selected because its culture differentiation protocol was well established. When BF (SM) cells proliferate to a high density, they remain in a replicating slender bloodstream form rather than differentiating into stumpy cells, as wildtype parasites would do in the bloodstream. This anomaly creates a potential limitation to differentiation studies in culture. If we wanted to completely rule out the possibility of EEP1 playing a role in mammalian to insect stage differentiation, studies in a cell line that more closely emulates wild type behavior may be used to investigate the role of EEP1 and other enzymatic factors involved in post-transcriptional regulation. Because we found no evidence of EEP1 function in BF to PF differentiation, future directions are likely to proceed to exploration of specific EEP1 targets.

Much is still unknown about the array of components involved in post-transcriptional regulation and regulation of the editing process in trypanosomes. The work described in this thesis extends the base of knowledge of post-transcriptional processes in both *T. cruzi* and *T. brucei.* These studies give rise to new research directions to explore, so that more pieces of information can come together to contribute to the overall understanding of genetic processes that are required for the differentiation, and thus, the pathogenicity of trypanosome parasites. When these important genetic processes are further exposed, they will be crucial in the development of drug targets that may help overcome the enormous public health burdens of African Trypanosomiasis and Chagas disease.

| Maxicircle sequence name | Editing required for translatable mRNA? | Description |
|---|---|---|
| 9S | No | 9S ribosomal RNA |
| 12S | No | 12S ribosomal RNA |
| ND1 | No | NADH dehydrogenase subunit 1 (Complex I) |
| ND2 | No | NADH dehydrogenase subunit 2 (Complex I) |
| ND4 | No | NADH dehydrogenase subunit 4 (Complex I) |
| ND5 | No | NADH dehydrogenase subunit 5 (Complex I) |
| CO1 | No | Cytochrome c oxidase subunit 1 (Complex IV) |
| MURF5 | No | Maxicircle unidentified reading frame 5 |
| CO2 | Yes | Cytochrome c oxidase subunit 2 (Complex IV) |
| CO3 | Yes | Cytochrome c oxidase subunit 3 (Complex IV) |
| MURF2 | Yes | Maxicircle unidentified reading frame 2 |
| A6 | Yes | ATPase-6 |
| CYB | Yes | Cytochrome b (Complex III) |

**Table 1** Maxicircle primers used for mitochondrial rRNA and mRNA analysis through *T. cruzi* life stages.

| Name | Forward Primer | Reverse Primer | TriTrypDB or Source |
|---|---|---|---|
| ***TERT*** | SAME AS CLB | SAME AS CLB | Shaw et al. 2016 |
| ***PFR2*** | SAME AS CLB | SAME AS CLB | Shaw et al. 2016 |
| **9S** | SAME AS CLB | SAME AS CLB | FJ203996.1 |
| **12S** | SAME AS CLB | SAME AS CLB | FJ203996.1 |
| **ND1** | SAME AS CLB | AGCTGGCCCGACTCTAAG | FJ203996.1 |
| **ND2** | SAME AS CLB | SAME AS CLB | FJ203996.1 |
| **ND4** | CACGTGTGATTACCGGAAATGC | TGCTAATACTACACTCATTTCGG | FJ203996.1 |
| **ND5** | TCTGTTTGGTTTAATATCCGGA | GTCAAAAACTTATAAAATGCCTACCTAATA | FJ203996.1 |
| **CO1** | AAGCCTAGTCACGTCTGCG | TAACACCCCCAGCTAGAACT | FJ203996.1 |
| **MURF5** | GATGTATACAATATGACATTTTTTTG | AATGATATTAATGTGTATAGTATTC | FJ203996.1 |
| **A6-p** | CATTTTGCCAAGCTTAGAAGAAA | AAAAAATCTCTCCCTTTTACAAAAAGCC | FJ203996.1 |
| **A6-e** | SAME AS CLB | ATTTTTTTTTTGTGATTTATTTTGGTTGCG | Figure S1: Ruvalcaba-Trejo and Strum 2011 |
| **CO2-p** | ATTACAGTGTAACCATGTACTCACATT | TTCATTACACCTCCCCGGTTCT | FJ203996.1 |
| **CO2-e** | ATTACAGTGTAACCATGTACTCACATT | ATTACACCTCCCCGGTATACAA | Figure S1: Ruvalcaba-Trejo and Strum 2011 |
| **CO3-P** | SAME AS CLB | SAME AS CLB | Shaw et al. 2016 |
| **CO3-e** | TGTTGTTTATTACTGTGTTGTCCAATATTG | SAME AS CLB | Figure S1: Ruvalcaba-Trejo and Strum 2011 |
| **CYb-p** | TAATAAAAAGCGGAGAAAAGAGGAA | TCCATATATCCTATATAAACAACCTGACA | FJ203996.1 |
| **CYb-e** | SAME AS CLB | TCCATATATCCTATATAAACAACCTGACA | Figure S1: Ruvalcaba-Trejo and Strum 2011 |
| **MURF2-p** | SAME AS CLB | CATATAATATATAATCTAAATCAAATCATCAT | FJ203996.1 |
| **MURF2-e** | TAATGTTTTGGTTGTTTTAATTTAGTTTTATT | CATATAATATATAATCTAAATCAAATCATCAT | Figure S1: Ruvalcaba-Trejo and Strum 2011 |

**Table 2** Primers designed for SYL-X10 qRT-PCR cDNA amplification. Primers denoted "SAME AS CLB" are the same as those used for the CL Brener strain, were designed by Dr. Aubie Shaw and are listed in Shaw et al. 2016 supplementary material.

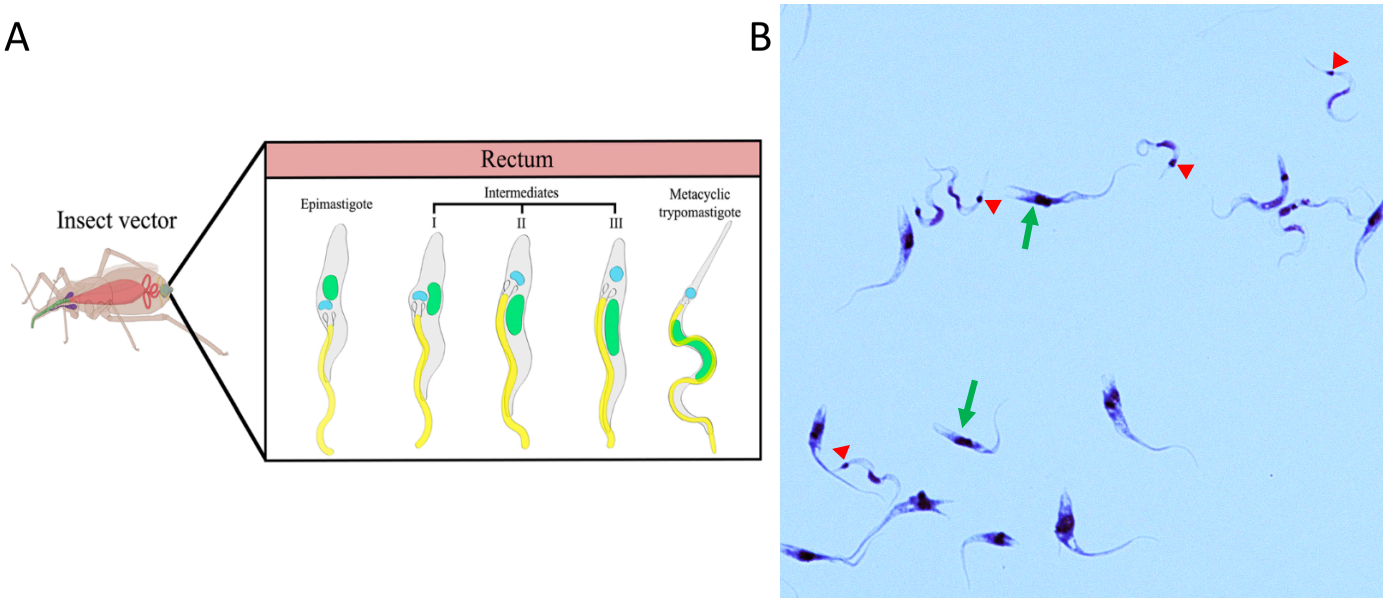


**Figure 1** Infective cultures stained with Wright Giemsa. Exponentially growing cells were placed in nutrient restrictive medium for 8 days to induce metacyclogenesis. (A) Diagram showing morphological changes during the process of metacyclogenesis, the transition from epimastigote to metacyclic trypoastigote. The kinetoplast (blue) transitions to the posterior portion of the cell, relative to the nucleus (green). B) Representative photograph taken at 1000X, showing metacyclic trypomastigotes and epimastigotes. Red arrowheads indicate the kinetoplast of metacyclic trypomastigotes.

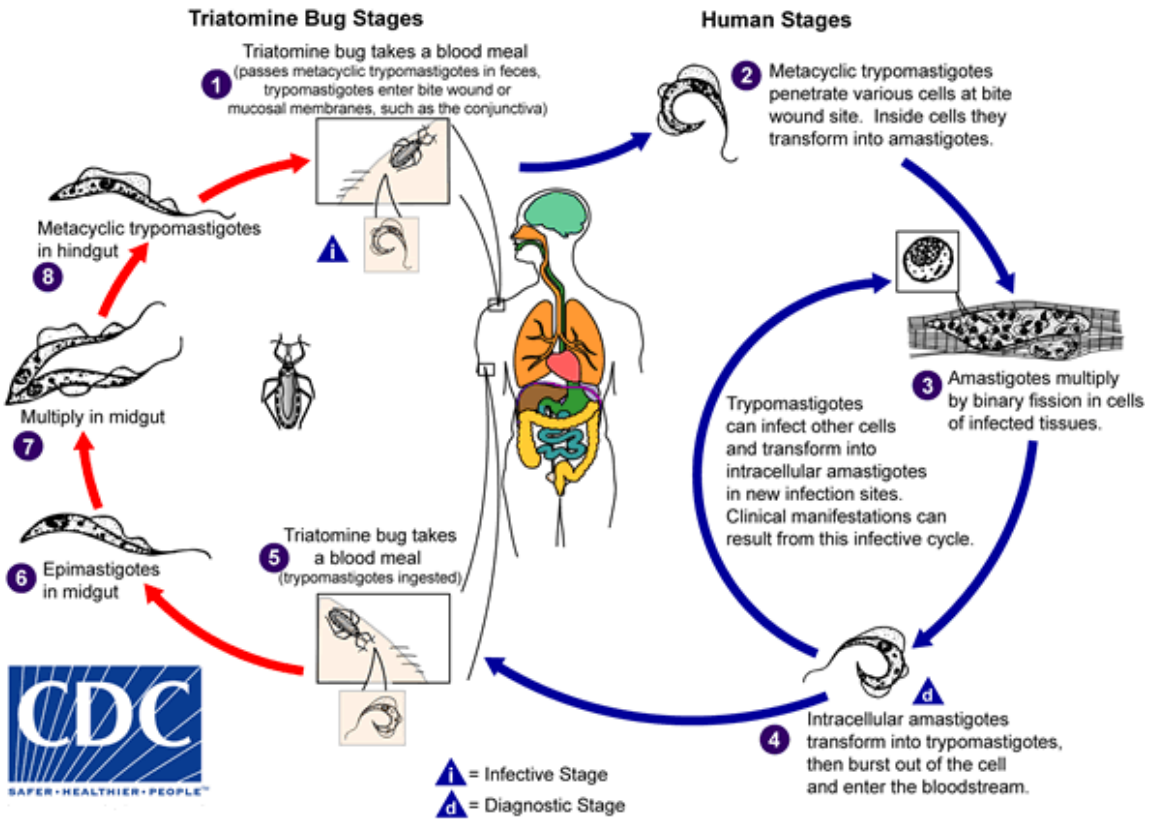


**Figure 2** The life cycle of *Trypanosoma cruzi* has stages within a triatomine insect vector and mammalian host. Taken from CDC Public Health Image Library https://phil.cdc.gov ID#3384.

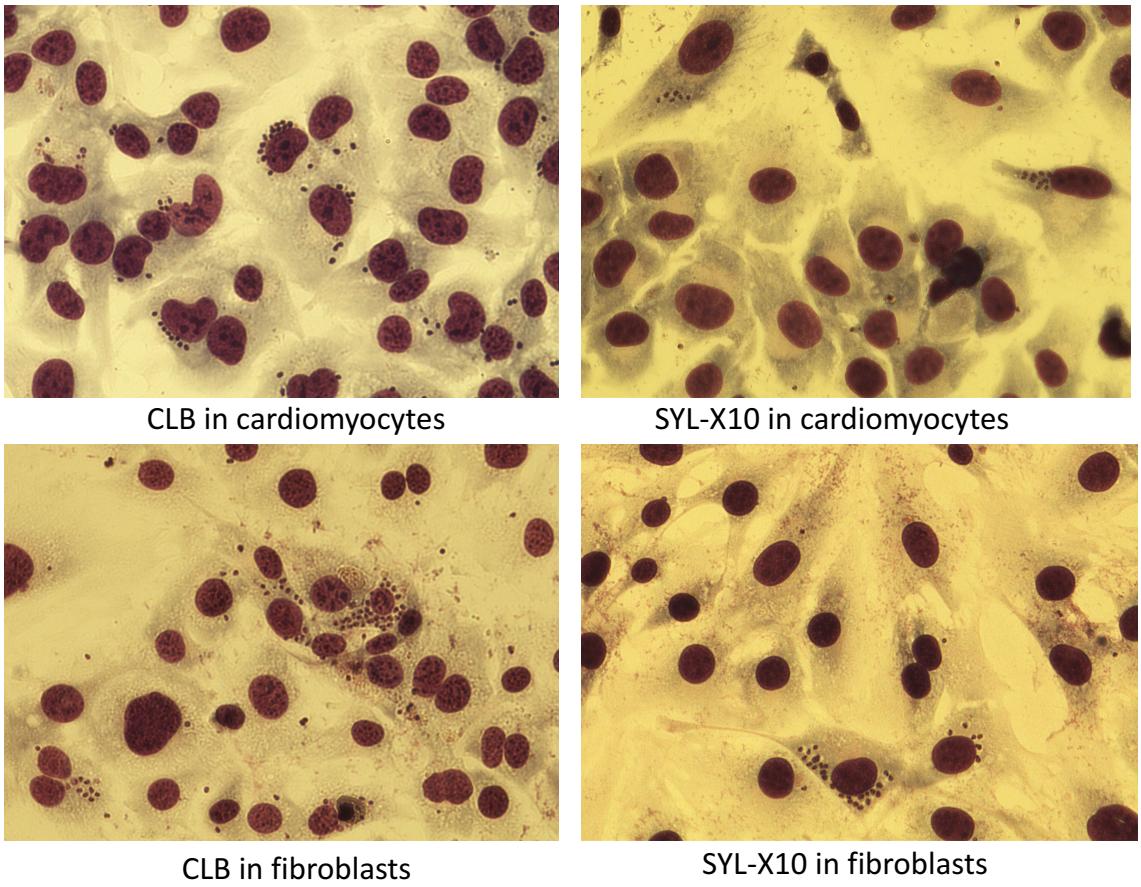


**Figure 3** *T. cruzi* amastigotes in 3T3-L1 fibroblasts and AC16 cardiomyocytes, stained with Wright Giemsa. Small dark spots represent amastigotes, large dark spots indicate the mammalian cell nucleus. Photographs were taken at 400X. Two strains of *T. cruzi* are represented: Sylvio X10 (SYL-X10, left column) and CL Brener (CLB, right column).

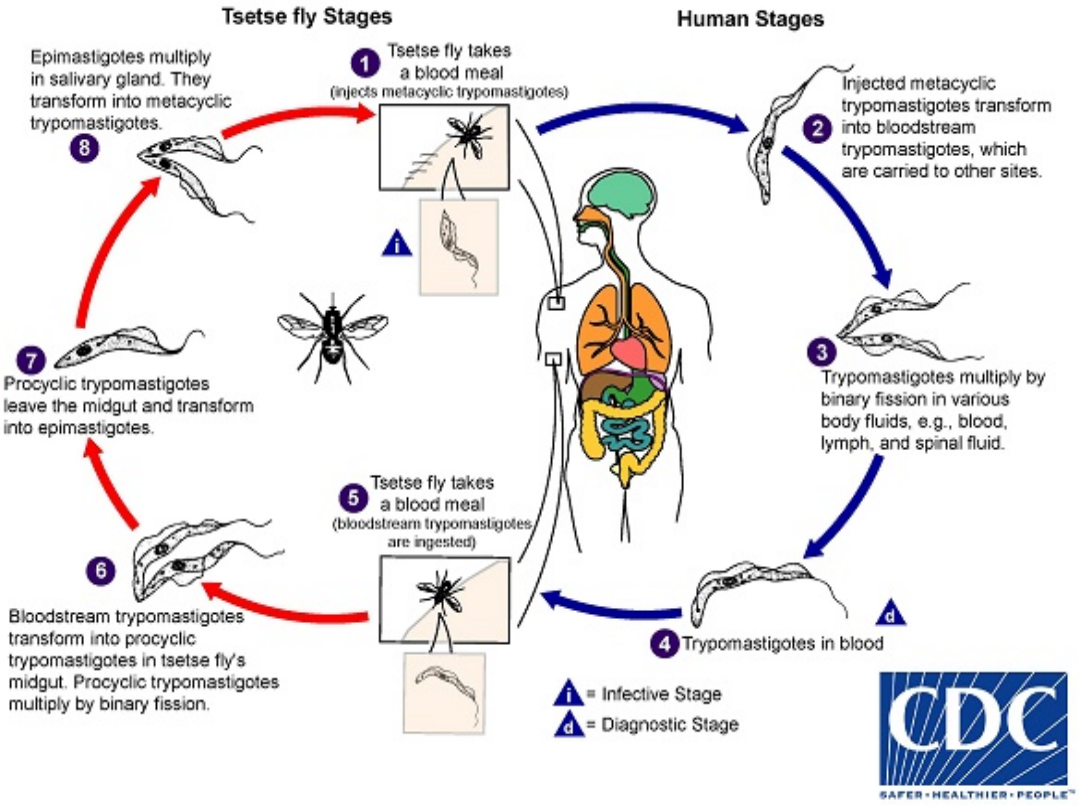


**Figure 4** The life cycle of *Trypanosoma brucei* is divided between the tsetse fly vector and a mammalian host. Taken from CDC Public Health Image Library https://phil.cdc.gov.

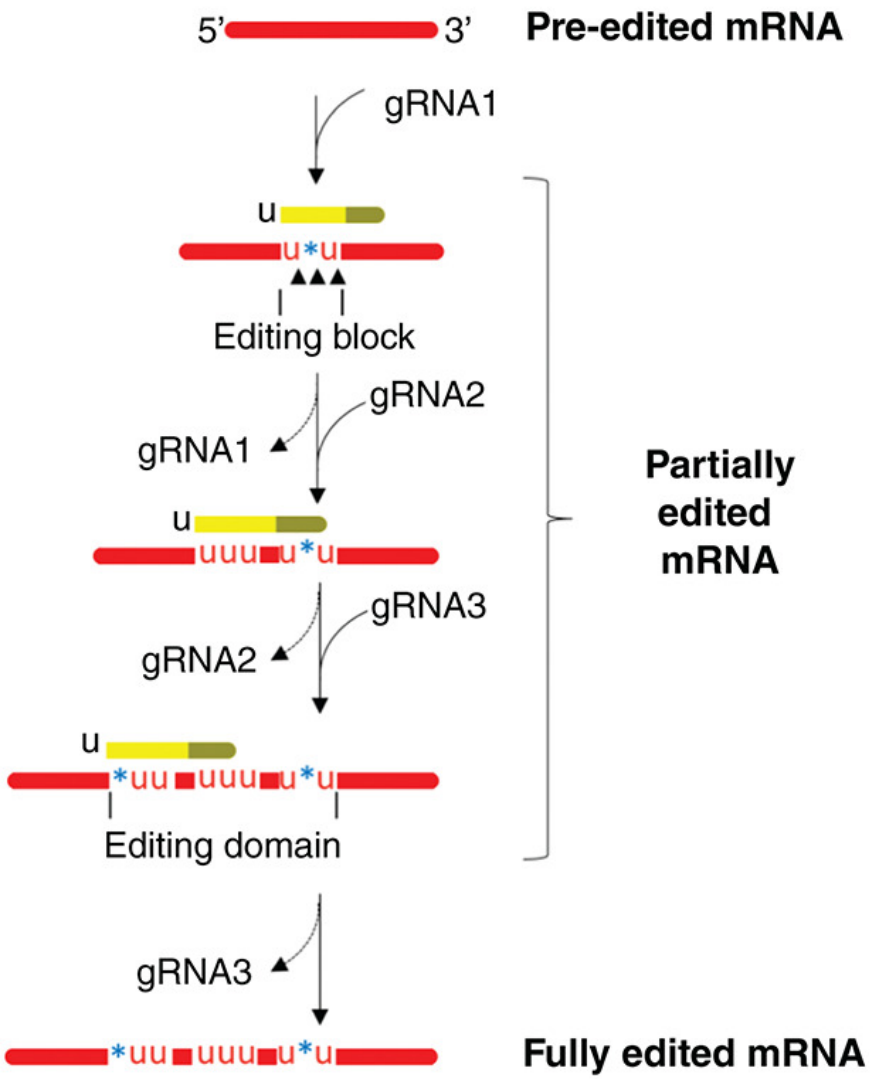


**Figure 5** Features of the mRNA editing process in trypanosomes. A gRNA template anchors its 5' anchor region to the mRNA, and guides the insertion and deletion of uridine residues, catalyzed by the RNA editing core complex. Editing proceeds with subsequent gRNA templates in a 3' to 5' direction. Reprinted from Read et al. 2016. Copyright 2016 Wiley Periodicals, Inc.

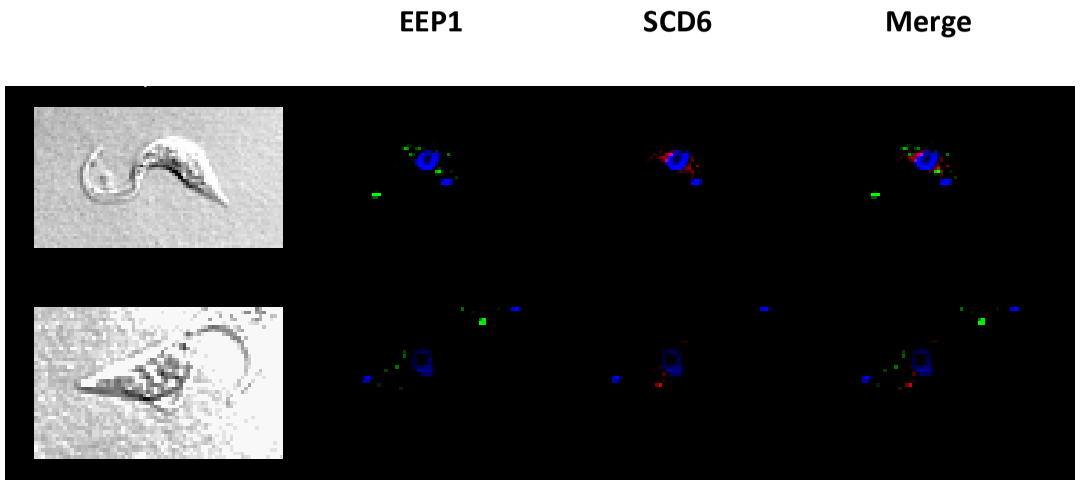


**Figure 6** EEP1 and SCD6 localization in the cytoplasm of *T. brucei,* shown by indirect immunofluorescence microscopy. Cell line used was procyclic form *T. brucei* over-expressing EEP1. Results are qualitatively similar in wild-type cells but EEP1 foci are less abundant and fainter. SCD6 is a component of all processing bodies (Buchan, Nissan and Parker 2010). Blue fluorescence depicts the DAPI stained kinetoplast and nucleus. An extra copy of SCD6 was C-terminally tagged with mCherry and inserted into an intergenic rRNA locus. SCD6 is represented by red fluorescence. EEP was detected by a specific rabbit antibody and visualized with an anti-rabbit Alexa488-conjugated secondary antibody. EEP1 is represented by green fluorescence. Microscopy and figure compilation by Pamela Vu.

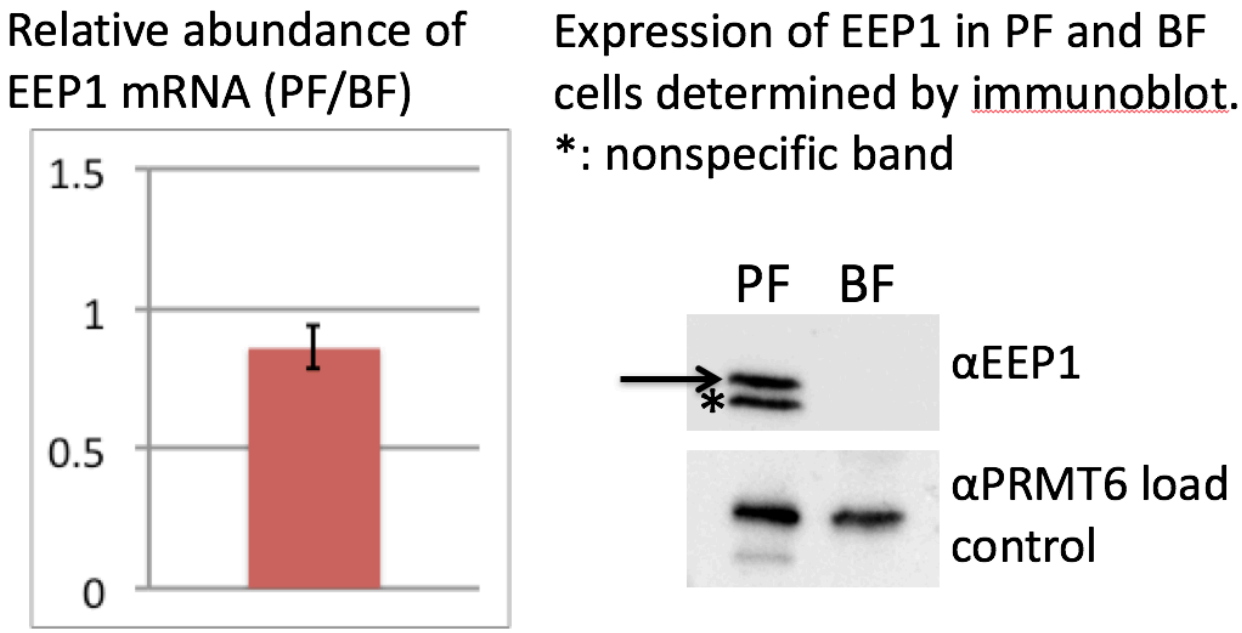


**Figure 7** EEP1 expression is developmentally-regulated at the protein level. (A) Relative abundance of EEP1 mRNA. mRNA abundances do not change between the procyclic form (PF) and bloodstream form (BF) life stages. (B) EEP1 expression between life cycle stages. Arrow denotes EEP1 protein band that is only visible in the PF. Data generated and compiled by Dr. Sara Zimmer.

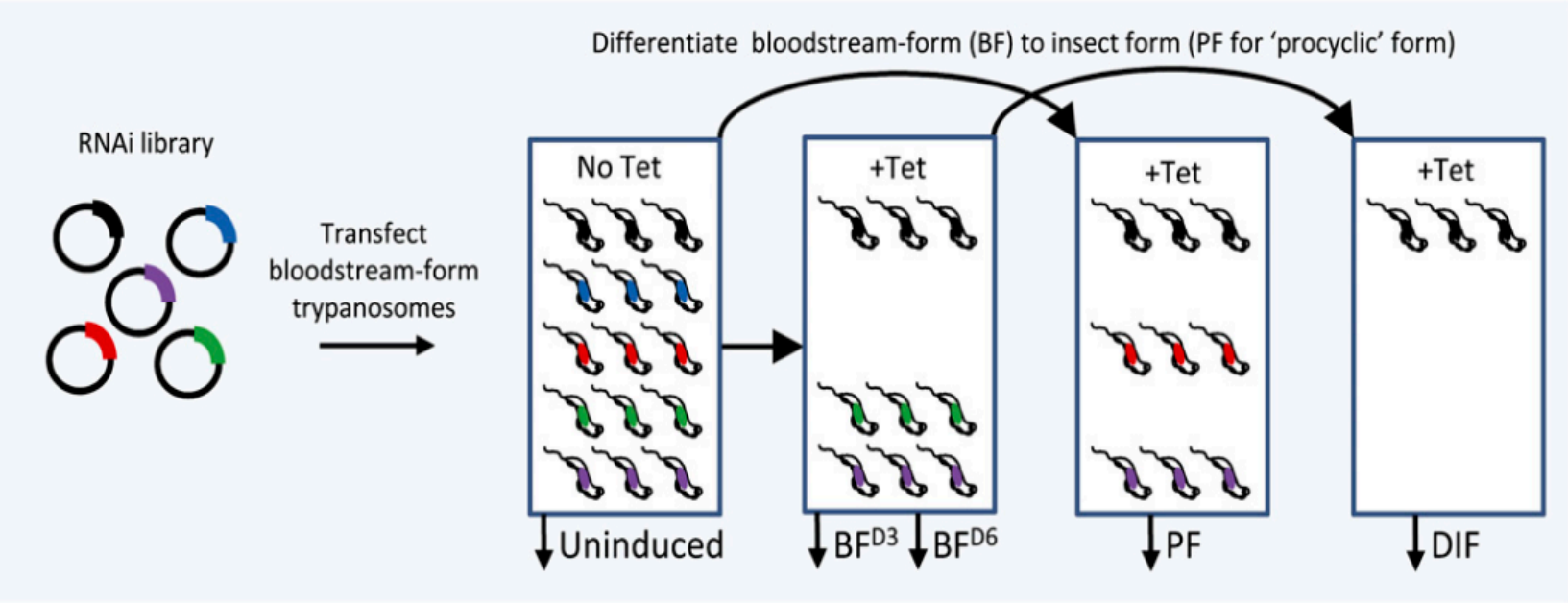


**Figure 8** Diagram of the RNAi library and growth conditions analyzed by Alsford et al. 2011. +Tet indicates RNAi silencing induced with tetracycline. No Tet indicates that RNAi was uninduced. DIF refers to a differentiating population.

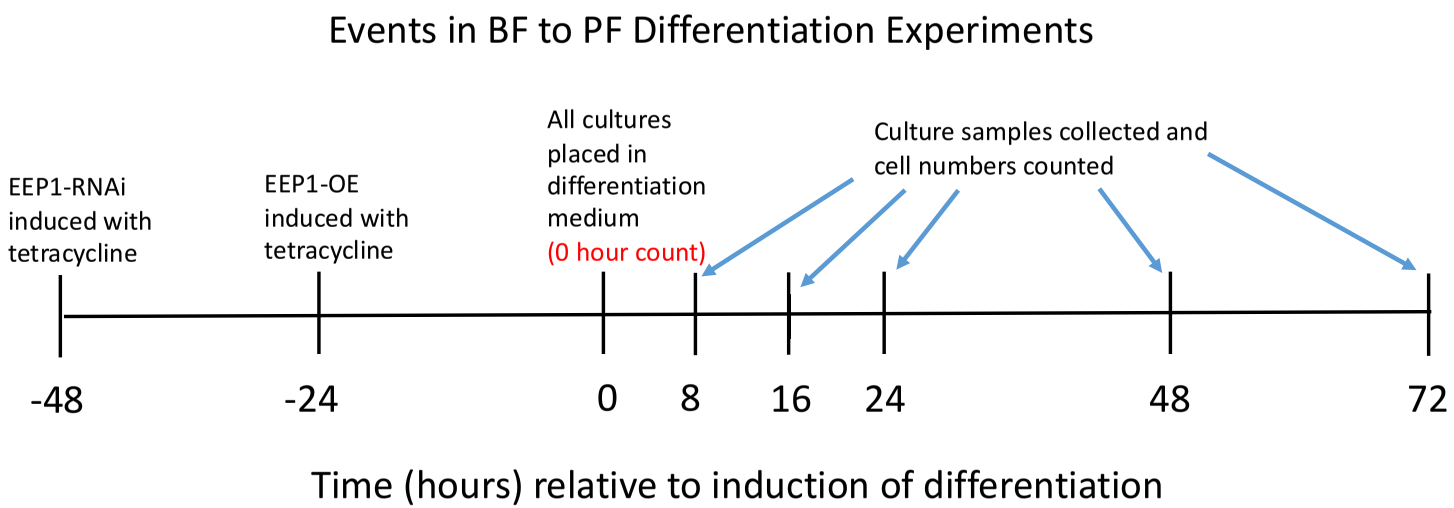


**Figure 9** Timeline of *T. brucei* BF to PF differentiation protocol with EEP1-OE and EEP1-RNAi inducible cell lines.

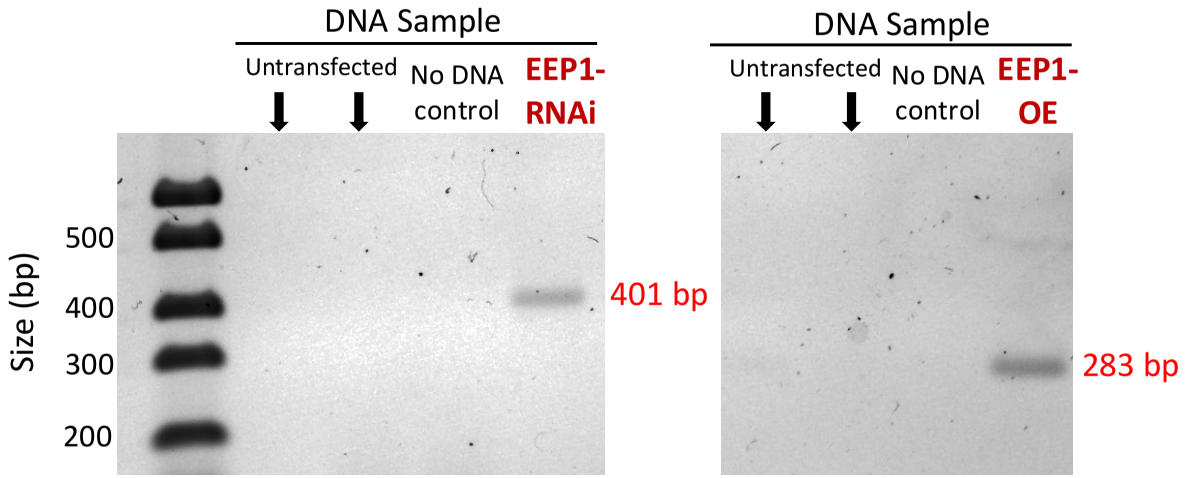


**Figure 10** Expression constructs are detected by PCR in DNA from cell lines transfected with EEP1-OE and EEP1-RNAi plasmids. EEP1-RNAi was amplified using a primer for the phleomycin resistance gene that is part of the P2T7-177 RNAi plasmid. EEP1-OE plasmid was amplified using a primer for the LSH portion of the plasmid sequence, a tag on the C-terminal end of the exogenous EEP1 copy. DNA isolated from untransfected *T. brucei* cells was used as a negative control, as well as a sample with no DNA in the reaction.

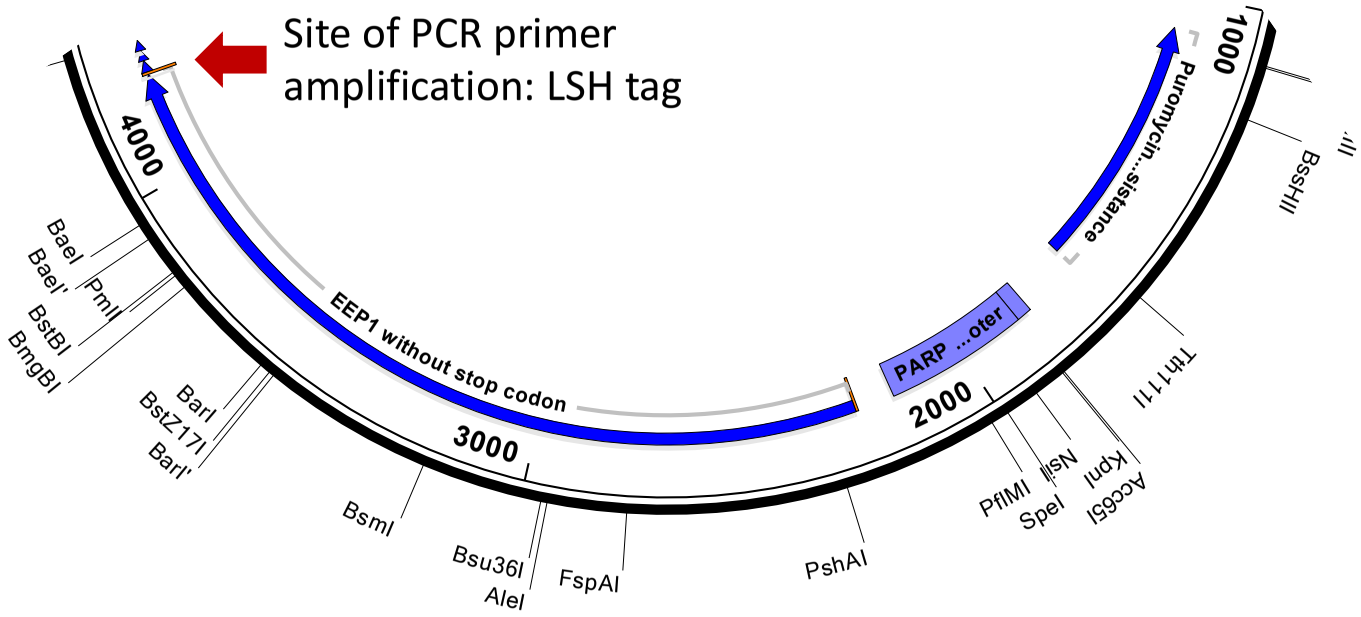


**Figure 11** Diagram of EEP1-encoded region of the pEEP1(WT)-LSH(PURO) plasmid used to transfect *T. brucei* BF (SM) with tetracycline inducible EEP1 overexpression. Red arrow indicates the site amplified by PCR: the linker-strep-his (LSH) tag. Amplification of this region is used to determine plasmid integration and overexpression at the mRNA level.

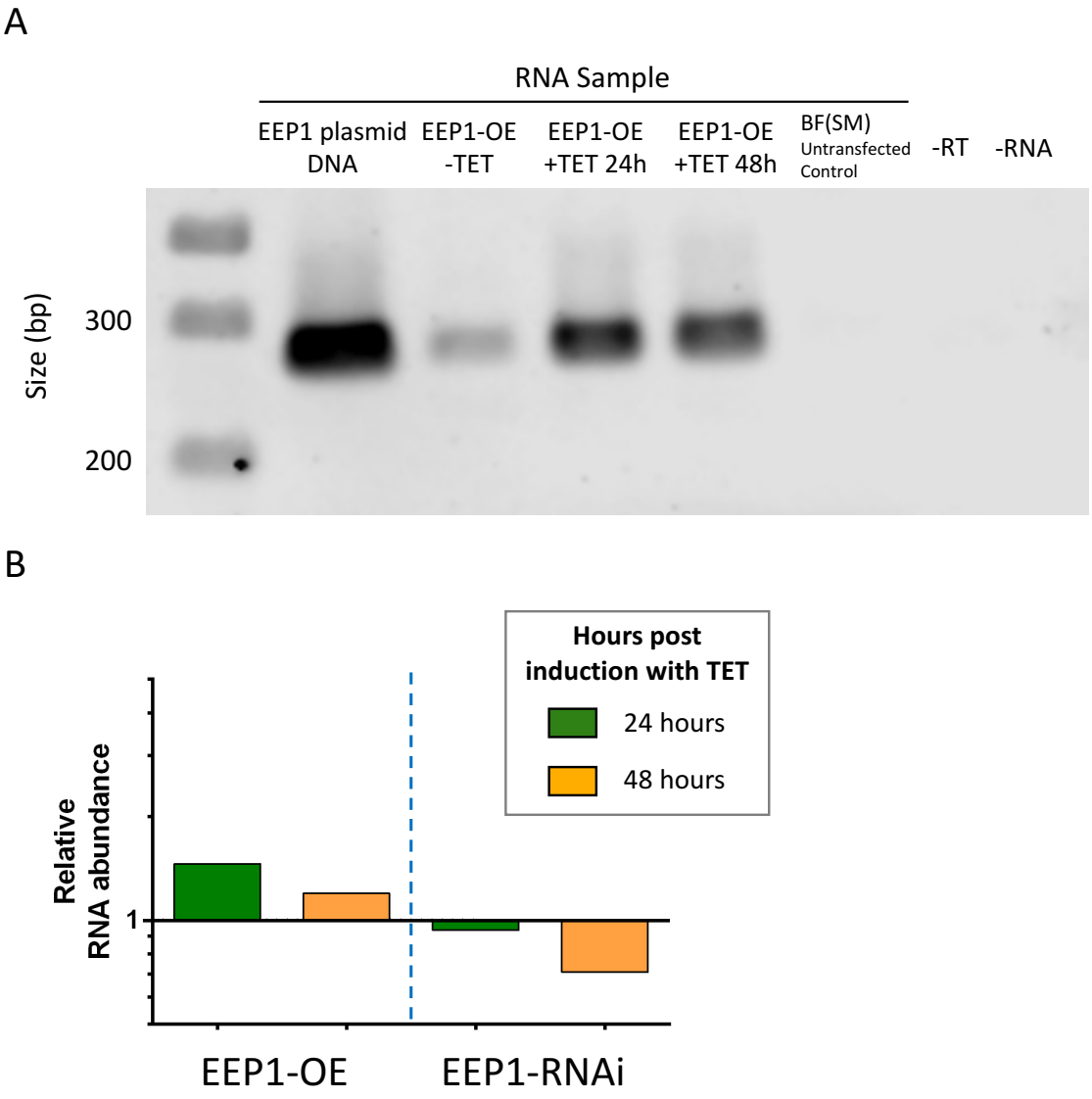


**Figure 12** (A) PCR products of *T. brucei* cDNA with EEP1-LSH amplification from transfected cell line. DNA from transfected cells was used as a positive control. This experiment verifies that there is greater expression of EEP1 mRNA in 24 and 48 hour tetracycline induced EEP1-OE cells (+TET 24h, +TET 48h) than uninduced (-TET) EEP1-OE cells. Negative controls were untransfected cells (BF (SM) ), no reverse transcriptase (-RT) and no RNA (-RNA). Amplicon is 283 bp. (B) Reverse transcription qPCR results quantifying EEP1 mRNA abundances of tetracycline induced EEP1-OE and EEP1-RNAi cell lines relative to uninduced cells. 24 hours and 48 hours post tetracycline induction are represented. Primers are selected from within the EEP1 coding region. One biological replicate and two technical replicates were performed. These data provides insight as to the timeframe of tetracycline exposure that yields the most dramatic overexpression and knockdown of EEP1 mRNA.

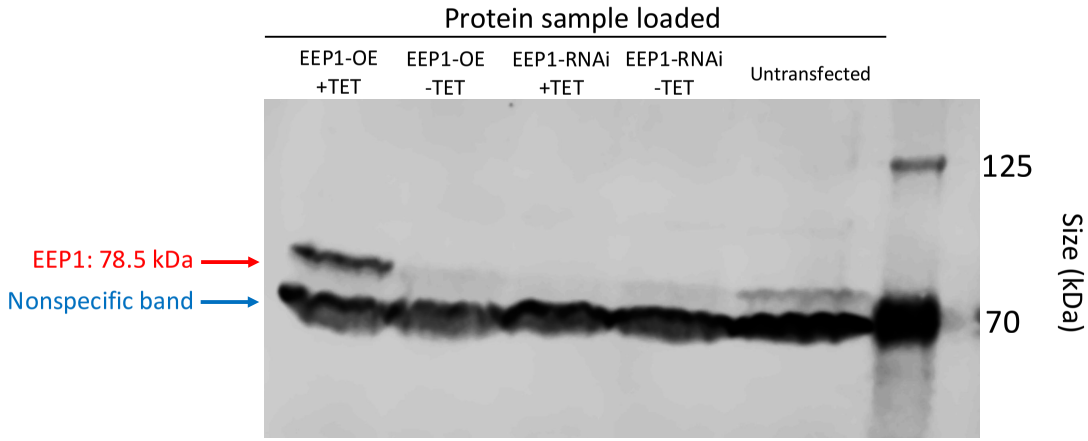


**Figure 13** Western blot showing EEP1 protein expression in procyclic form cells. Primary antibody: Antigen Purified EEP1 #81 Bleed 1 51112. Two transfected cell lines were tested: EEP1-OE (OE) and EEP1-RNAi (RNAi), tetracycline induced (+TET) and uninduced (-TET). Transfected and untransfected BF cell lines were differentiated to procyclic forms for 48 hours before protein isolation was performed. Control is untransfected BF(SM) cells, which we expected to show a band of endogenous EEP1 protein. The nonspecific band, indicated by the blue label, was utilized as a loading control.

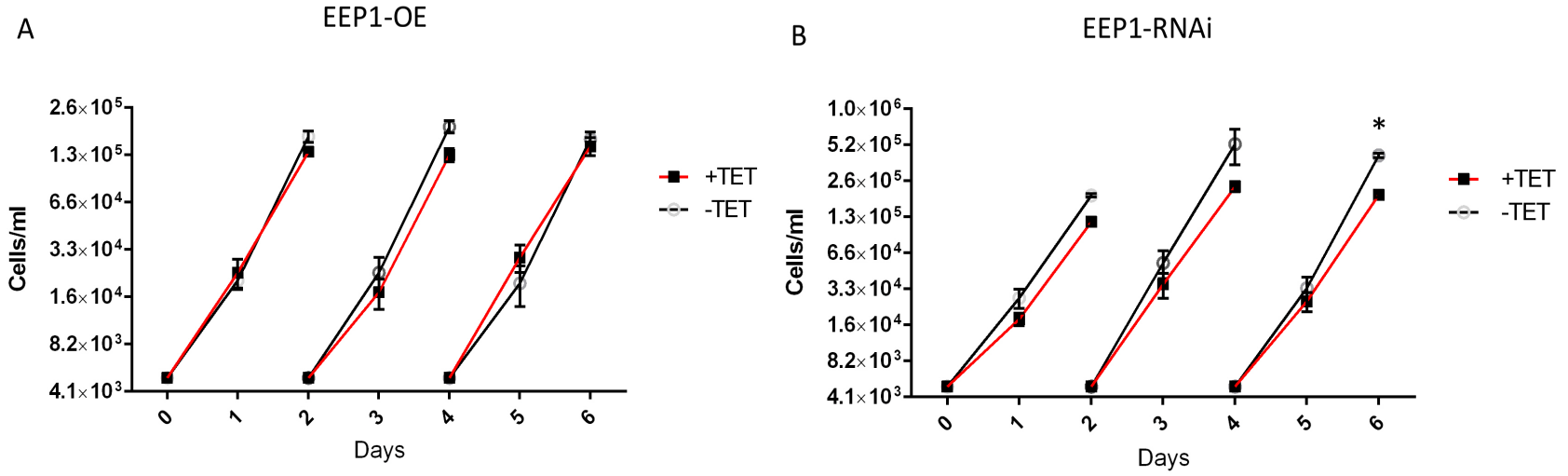


**Figure 14** Growth curves of EEP1-OE and EEP1-RNAi tetracycline induced and uninduced cell lines (+TET and –TET, respectively). Cultures were diluted every 2 days to the original concentration of $5\times10^3$ cells/ml, for three consecutive growth phases. Three technical replicates were counted for each data point. (A) EEP1-OE +TET and -TET cultures had no statistically significant variations in slope or overall elevations, as indicated by linear regression analysis, alpha = 0.05. (B) EEP1-RNAi +TET and -TET cultures were shown to have statistically significant variation in slope in the 4-6 day growth points, as indicated by linear regression analysis and indicated by asterisk (*). No significant variations in slope and overall elevations were detected in growth days 0-4. alpha=0.05.

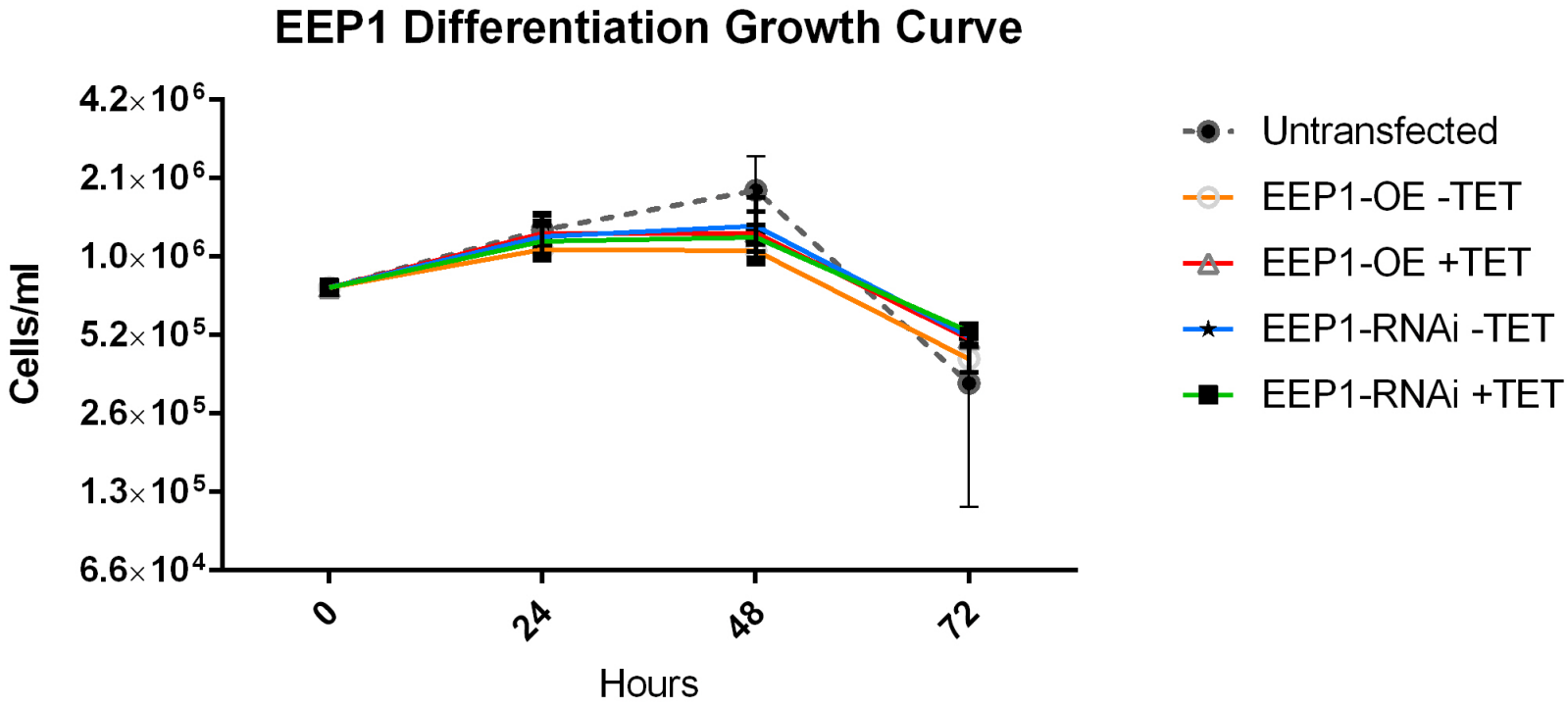


**Figure 15** *T. brucei* parasite concentration counts through a 72 hour BF to PF differentiation. Cultures were counted at 0 hours and every 24 hours following. Three replicates were performed for tetracycline induced and uninduced (+TET and -TET, respectively) EEP1-OE and EEP1-RNAi cell lines. Two replicates were performed for the untransfected cell line, *T. brucei* BF (SM) cells. A 2 way ANOVA indicated that cell concentrations were not statistically different from one another: $P > 0.05$ at all timepoints.

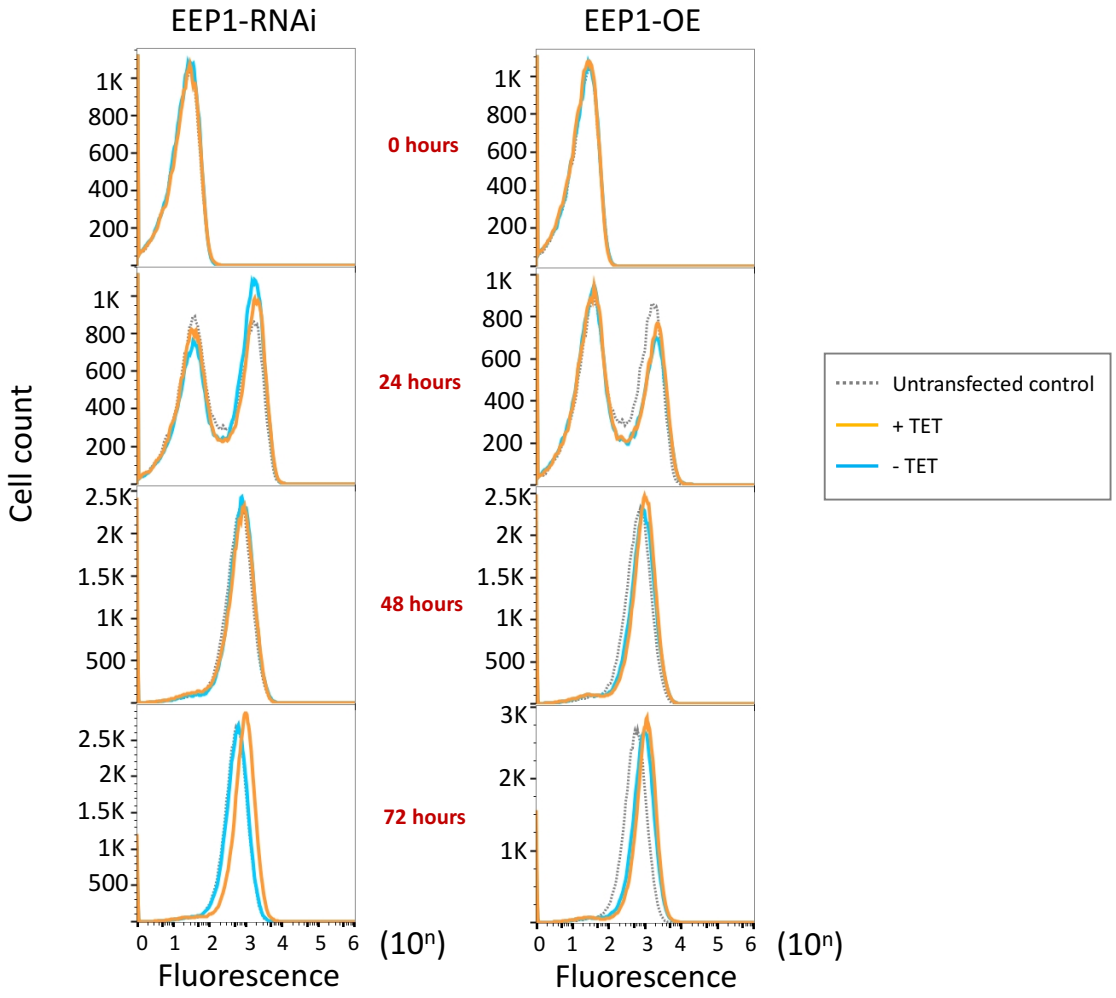


**Figure 16** (1st experiment) Histograms representing flow cytometry analysis of *T. brucei* BF to PF differentiation under TET induced (+TET) and uninduced (-TET) treatments in the cell line indicated at the top of the column. Primary antibody detected the presence of cell-surface EP-Procyclin, a PF expressed cell surface marker. Anti-rabbit Alexa488-conjugated antibody was the secondary antibody. *T.b.b.* BF (SM) was differentiated as the untransfected control and is shown in comparison to both EEP1-RNAi and EEP1-OE results. One experimental replicate is represented, with 100,000 events analyzed per data point.

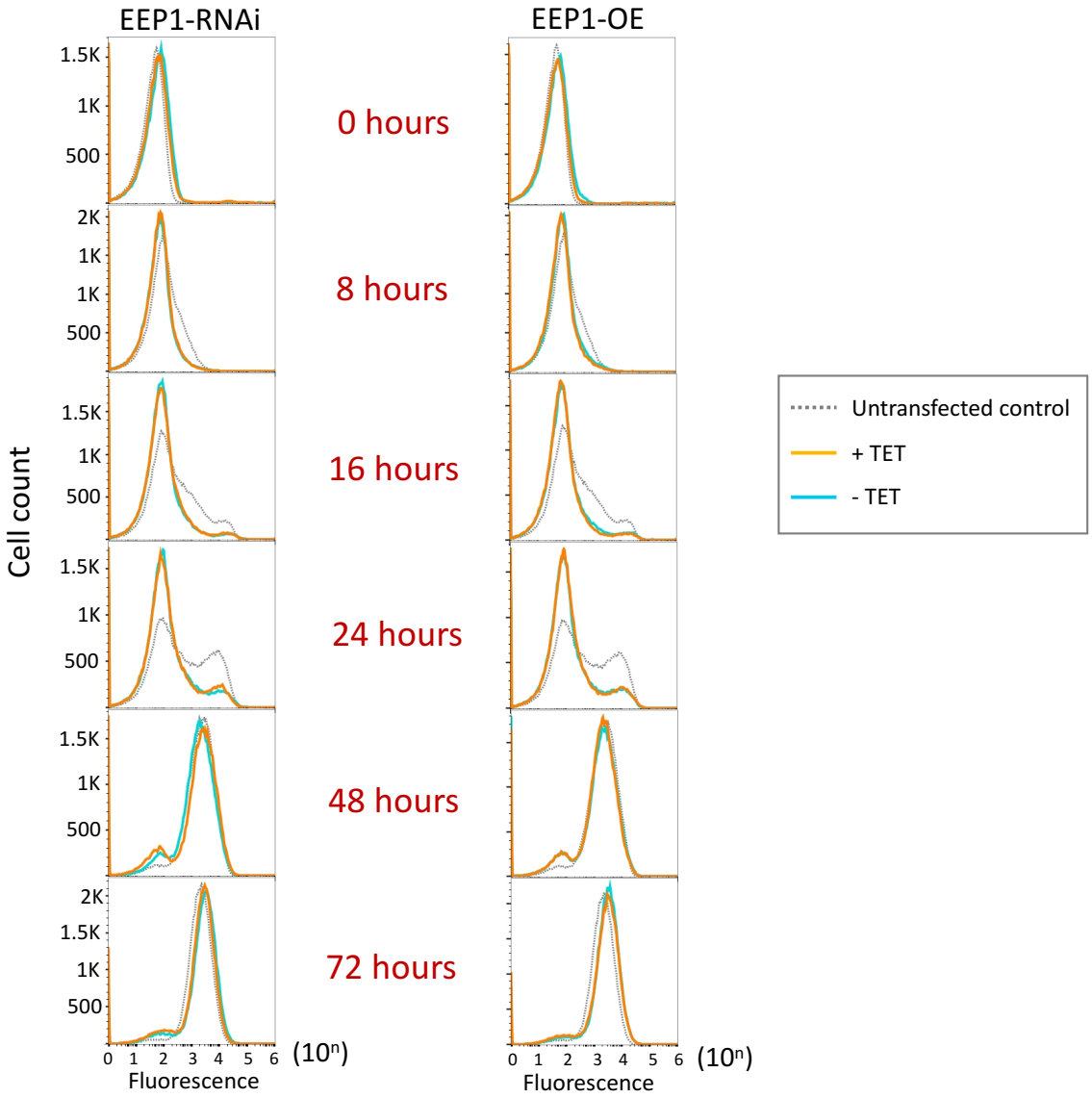


**Figure 17** (2nd experiment) Histograms representing flow cytometry analysis of *T. brucei* BF to PF differentiation under TET induced (+TET) and uninduced (-TET) treatments in the cell line indicated at the top of the column. Primary antibody detected the presence of cell-surface EP-Procyclin, a PF cell surface marker. Anti-rabbit Alexa488-conjugated antibody was the secondary antibody. *T.b.b.* BF (SM) was differentiated as the untransfected control and is shown in comparison to both EEP1-RNAi and EEP1-OE results. One experimental replicate is represented, with 100,000 events analyzed per data point.

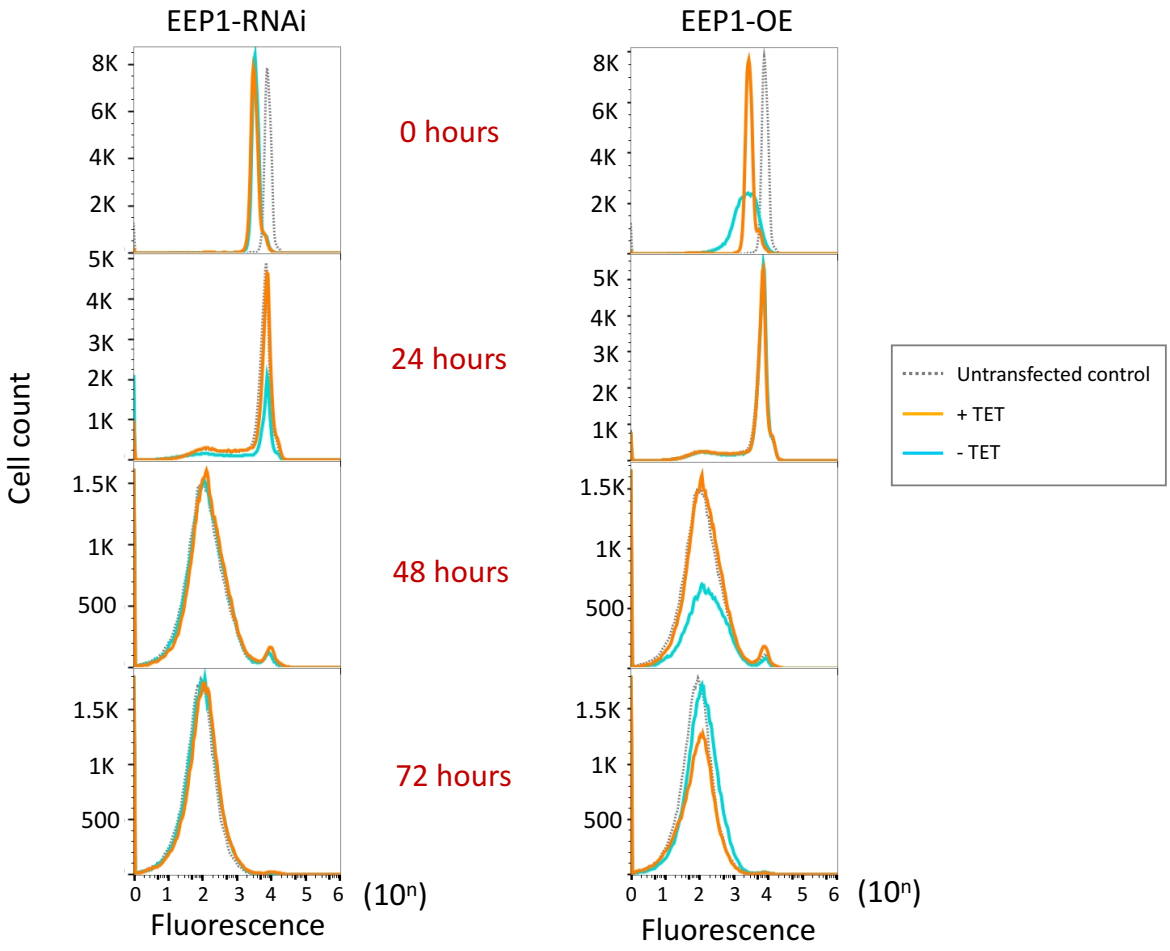


**Figure 18** Histograms representing flow cytometry analysis of *T. brucei* BF to PF differentiation under TET induced (+TET) and uninduced (-TET) treatments. Primary antibody detected the presence of BF-expressed cell-surface VSG. Alexa488-conjugated antibody was the secondary antibody. *T.b.b.* BF (SM) was differentiated as the untransfected control and is shown in comparison to both EEP1-RNAi and EEP1-OE results. One experimental replicate is represented, with 50,000 to 100,000 events analyzed per data point.

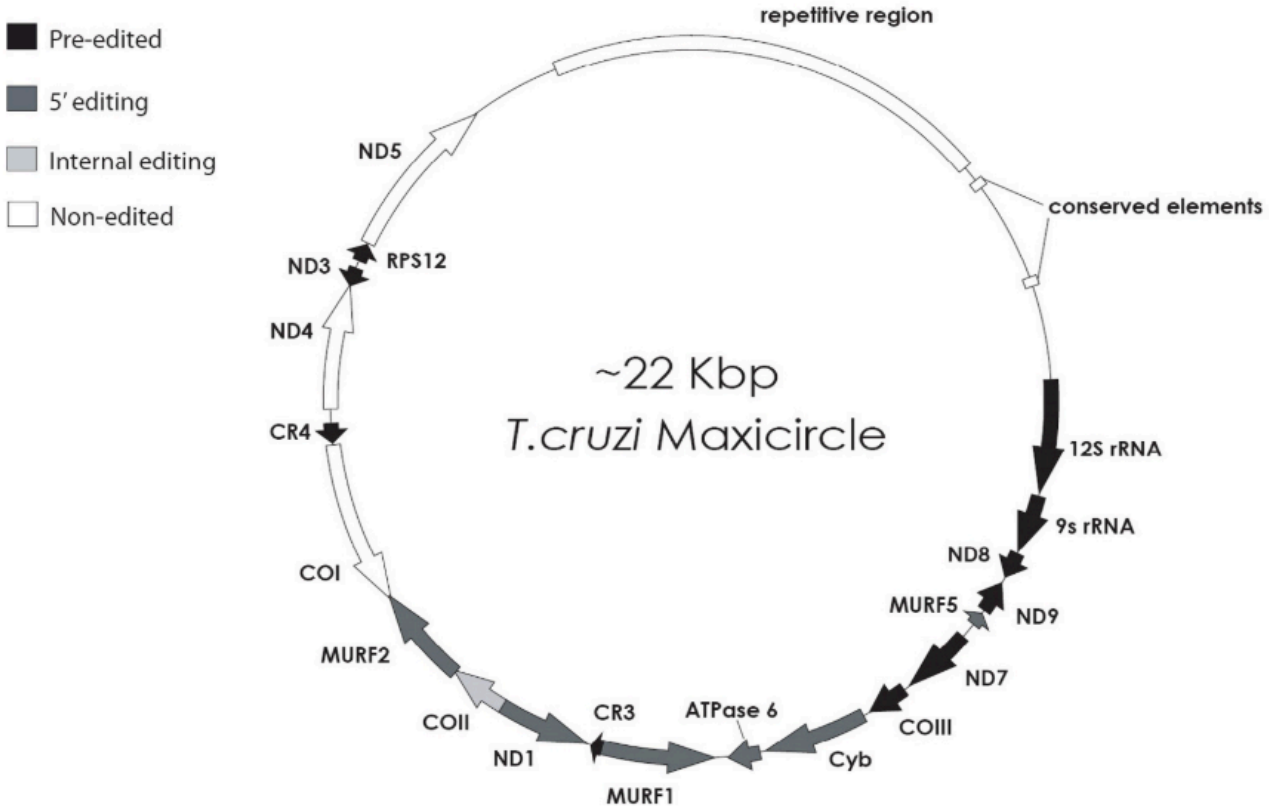


**Figure 19** The *T. cruzi* maxicircle. Genes are represented as arrows pointing in the direction of coding. Taken from Westenberger et al. 2006, Figure 1.

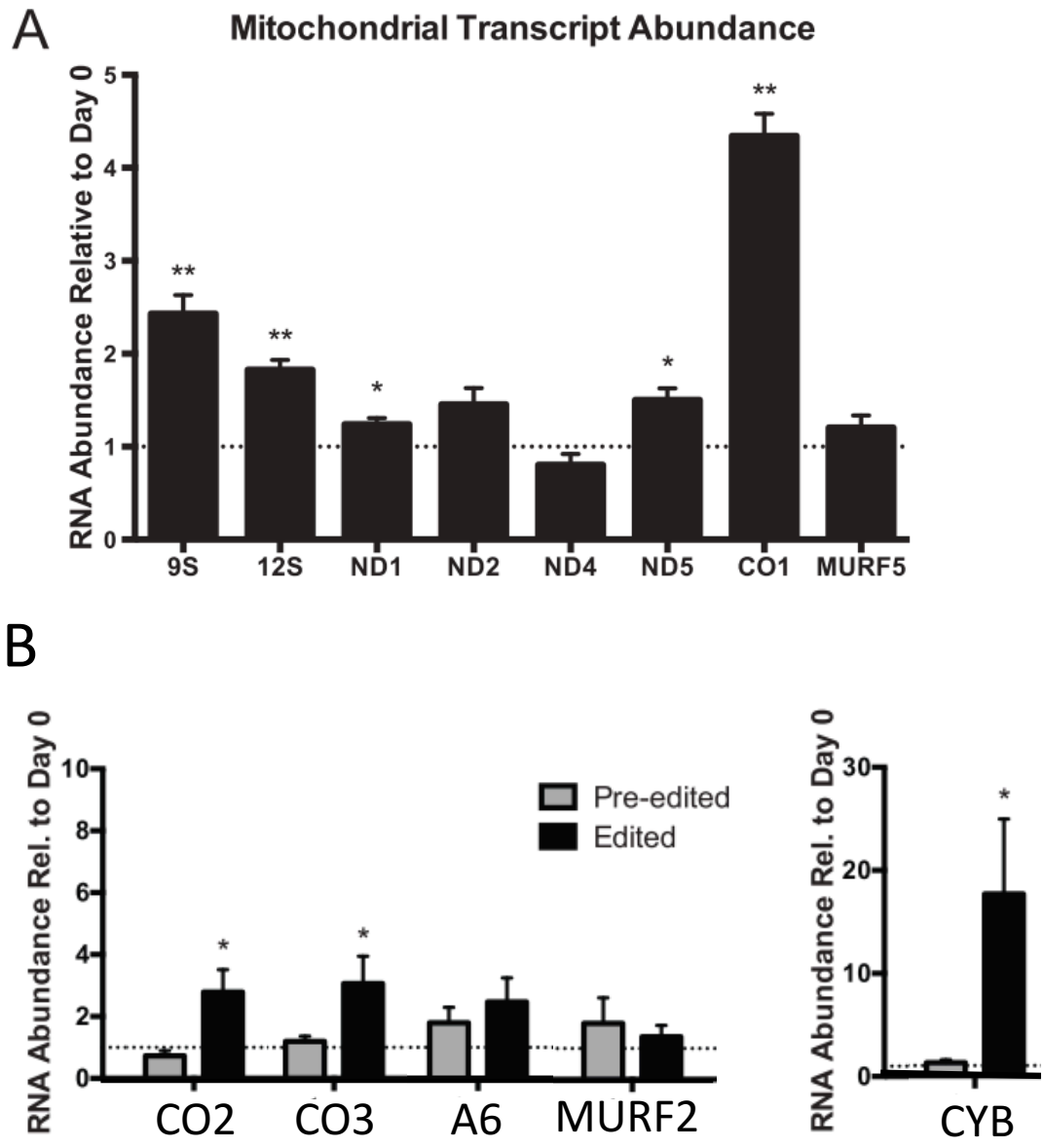


**Figure 20** Previously published mitochondrial transcript abundance changes in insect-stage *T. cruzi* parasites. Transcript abundances measured by qRT-PCR from *T. cruzi* infective culture containing metacyclic trypomastigotes (nutrient stressed in RPMI for 8 days) is shown relative to exponentially growing epimastigotes (Day 0). Data points represent mean and SEM, and asterisks (*, $P < 0.05$; **, $P < 0.001$) represent the results of unpaired *t* test comparisons. Taken from Shaw, Kalem and Zimmer 2016. (A) Never-edited mitochondrial transcript abundances. (B) Pre-edited and completely edited mitochondrial transcript abundances.

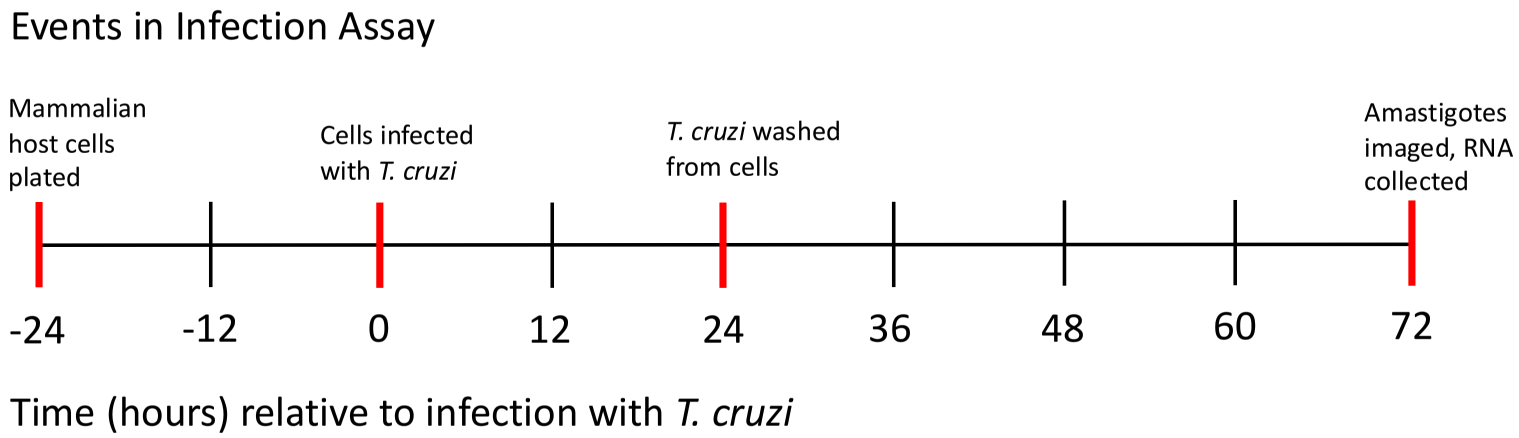


**Figure 21** Timeline of *T. cruzi* infection of mammalian cells protocol. Modified from protocol created by Dr. Aubie Shaw.

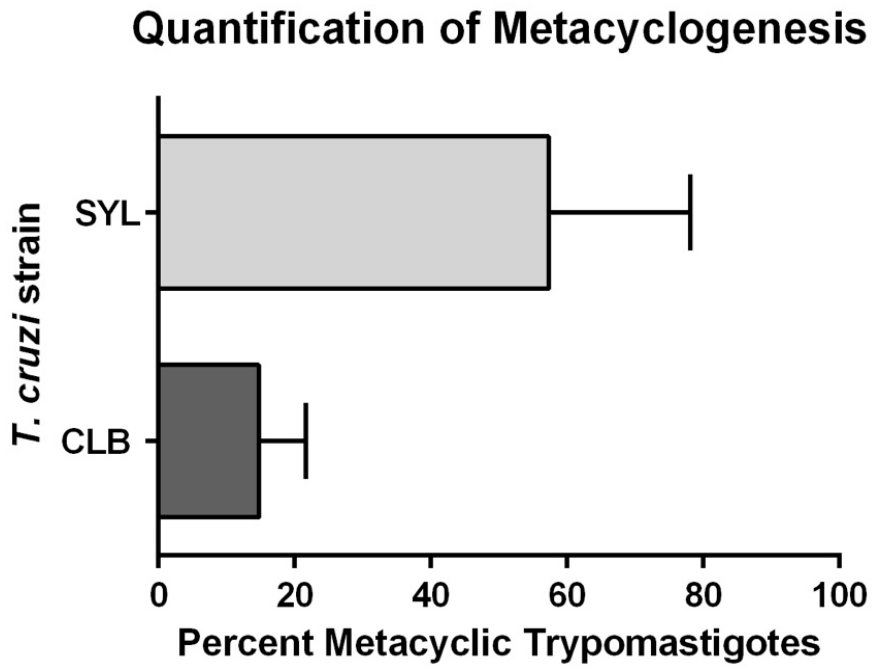


**Figure 22** Quantification of *T. cruzi* metacyclogenesis in the differentiated cultures of parasites used to infect mammalian cultured cells. Percentage of the total cells in the culture found to be metacyclic trypomastigotes are shown for Sylvio-X10 (SYL) and CL Brener (CLB) strains. Error bars represent with SEM. Data point differences are not significant, as indicated by an unpaired t test with alpha = 0.05. P = 0.1239.

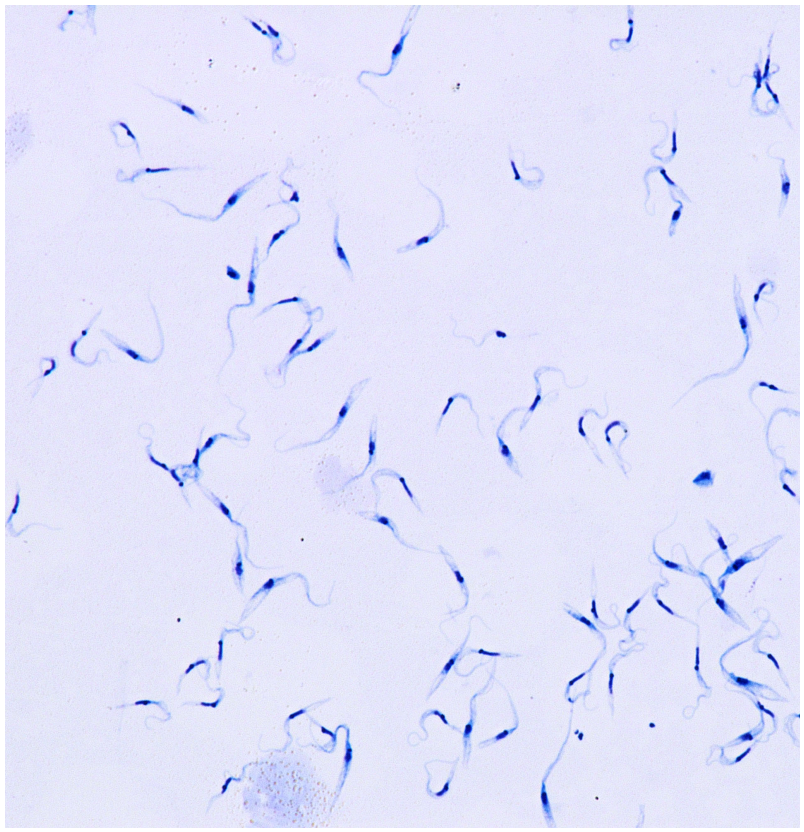

CL Brener

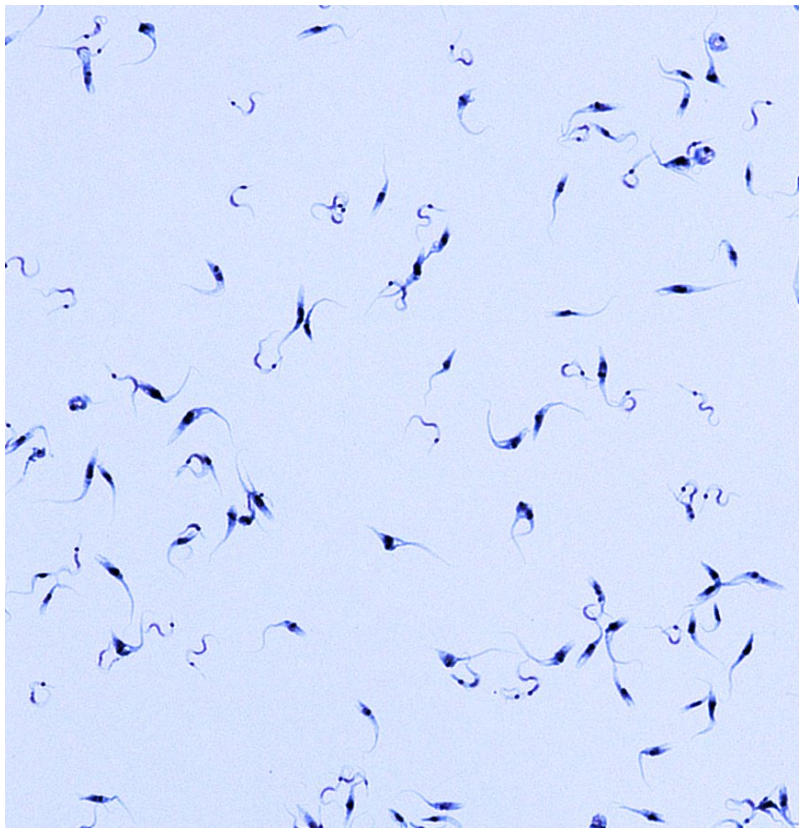

Sylvio X10

**Figure 23** Photographs of CL Brener and Sylvio X10 infective culture from 8 day nutrient deprivation in RPMI. Stained with Wright Giemsa stain.

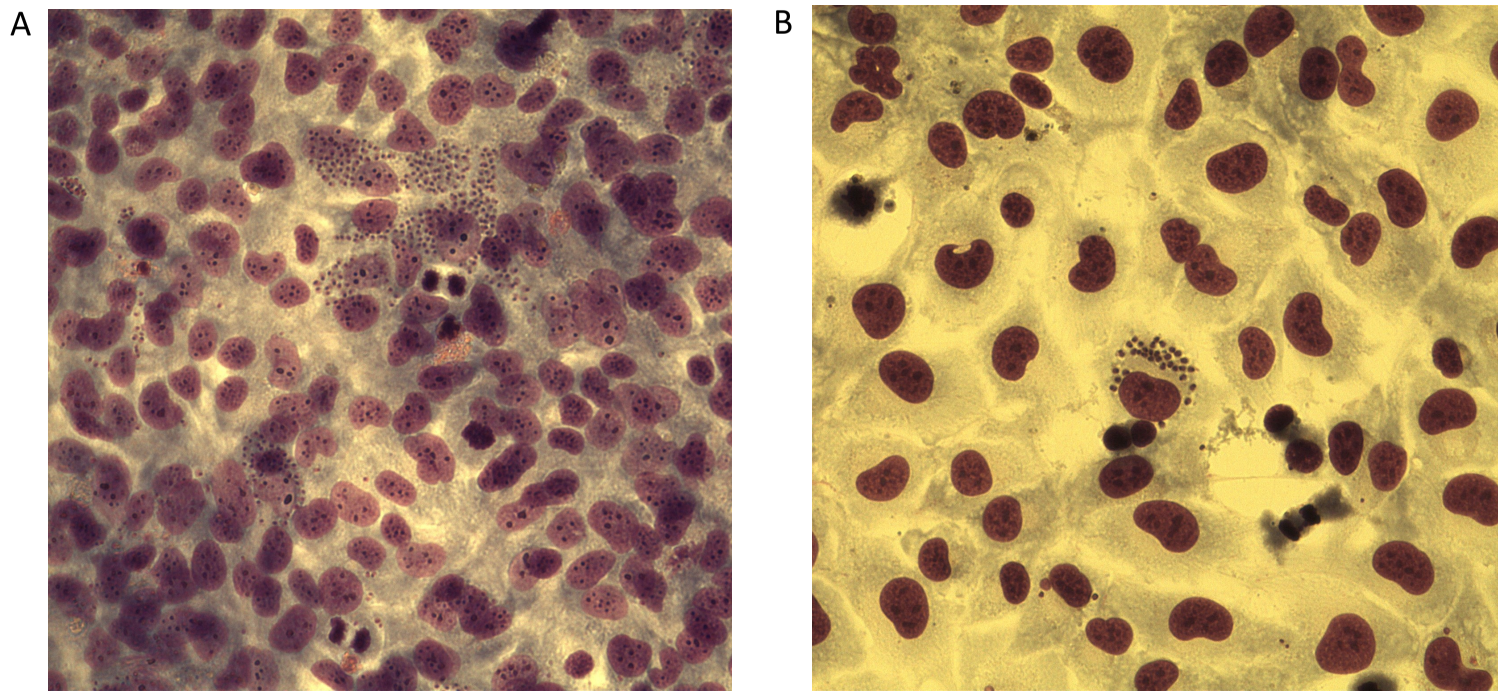


**Figure 24** CL Brener intracellular amastigotes in AC16 cardiomyocytes, stained with Wright Giemsa stain. (A) Cardiomyocytes plated at $5x10^4$ cells per well. Wells are very crowded in some places and amastigotes are very difficult to stain and count. (B) Cardiomyocytes plated at $2.5x10^4$ cells per well. We are able to reasonably see the borders of most of the cells and easily see amastigotes (small dark spots), providing an accurate quantification of infection.

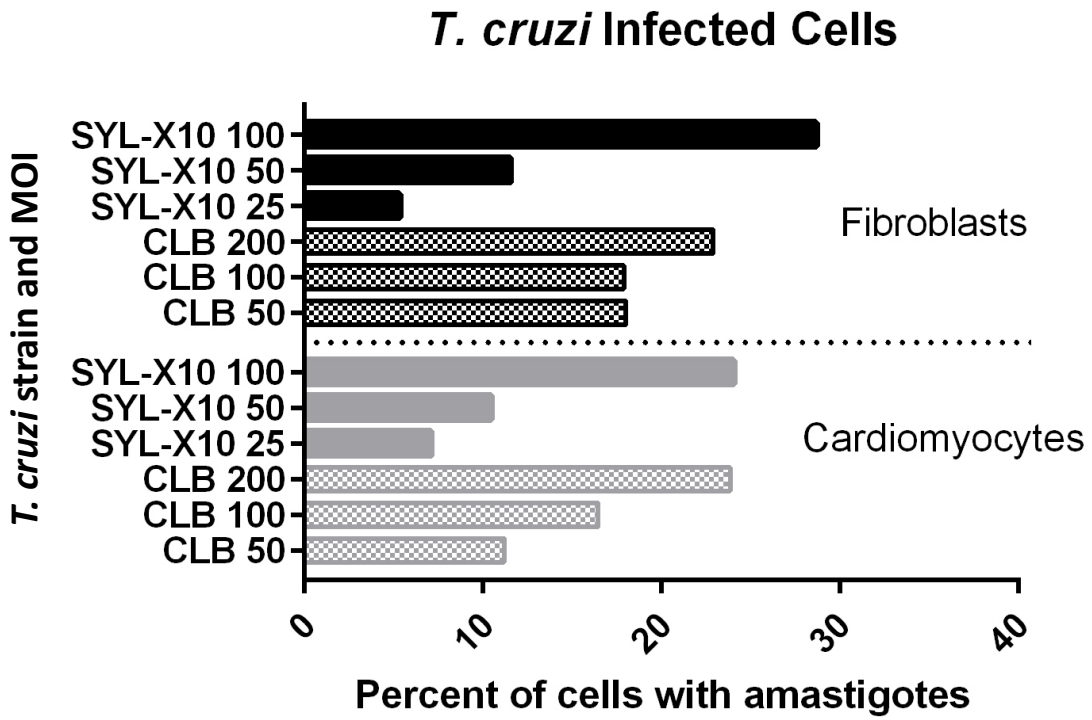


**Figure 25** Preliminary quantification of intracellular amastigotes in two mammalian cell types (fibroblasts and cardiomyocytes) after infection with infective *T. cruzi* culture at various multiplicity of infection (MOI), the number of parasites added per mammalian cell. Data points represent one replicate of each infection; at least 100 mammalian cells were quantified for each. Y-axis represents *T. cruzi* strain (SYL-X10 or CLB) and MOI. Data was used to determine the MOI necessary to produce the most robust *T. cruzi* infections for RNA isolation.

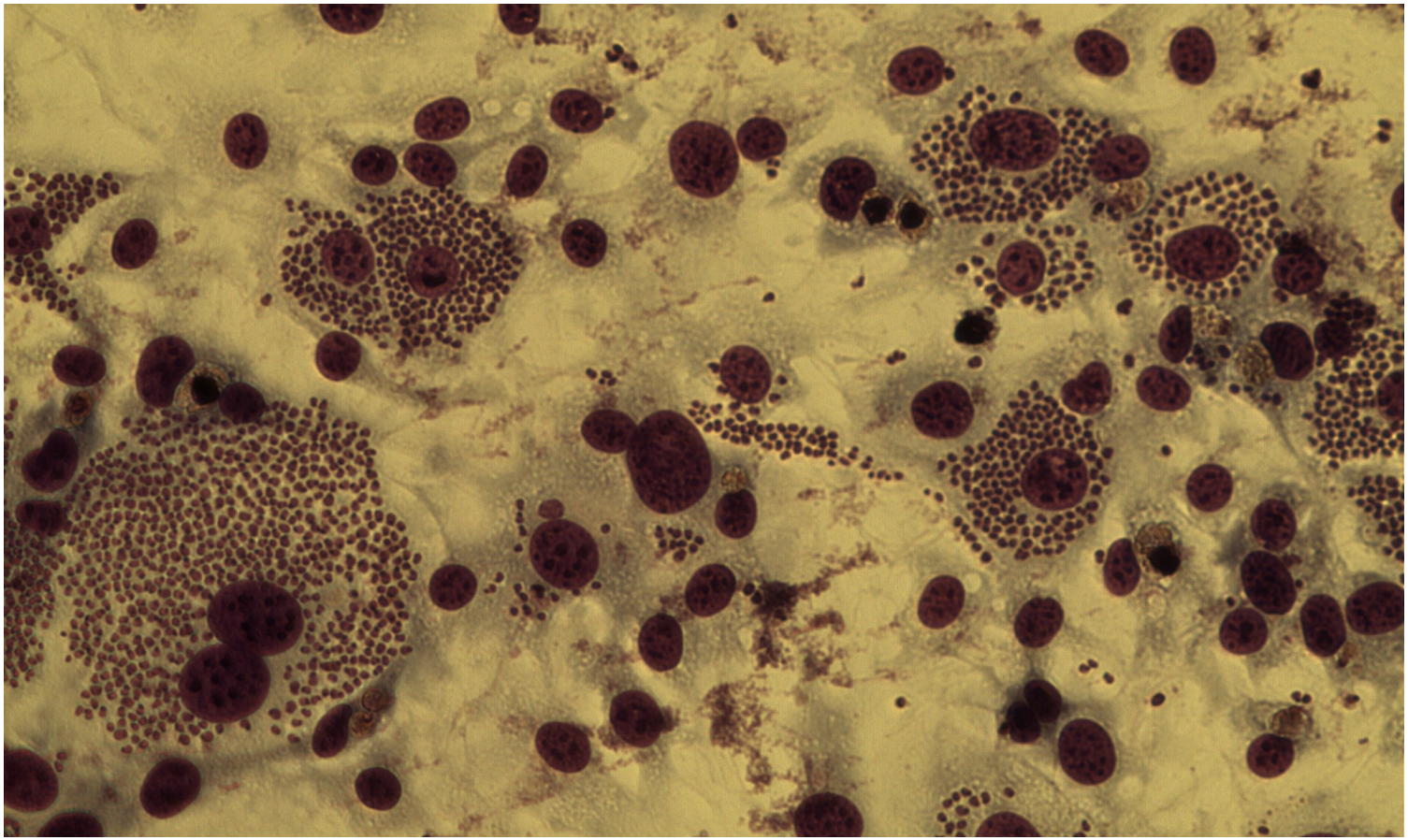

**Figure 26** 3T3-L1 fibroblasts infected with *T. cruzi* CL Brener and stained with Wright Giemsa stain. Photographs demonstrate an infection 110 hours post infection with *T. cruzi.*

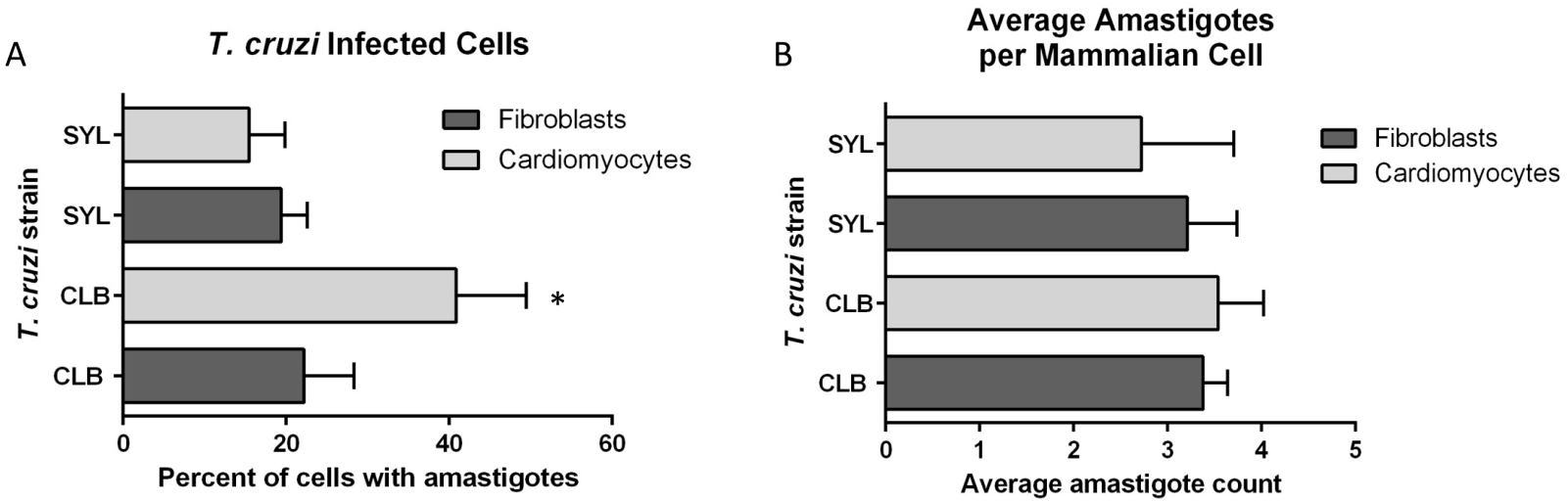


**Figure 27** Quantification of *T. cruzi* infectivity assays in two mammalian cell lines. Infectivity assays utilized *T. cruzi* strains CL Brener or Sylvio-X10 (y-axis) which were used to infect 3T3-L1 murine fibroblasts (dark gray) and AC16 human cardiomyocytes (light gray). Assays performed in triplicate, with at least 100 mammalian cells counted for each replicate. Data points represent mean, and error bars represent SEM. (A) Percentage of total mammalian cells that contain one or more *T. cruzi* amastigote within the cytoplasm. Statistically significant variations denoted by asterisk (*) for $P < 0.05$ in a 2 way ANOVA (CLB cardiomyocytes: $P = 0.0455$). (B) Average number of amastigotes in cytoplasm per infected mammalian cell. Results of a 2 way ANOVA indicate that these results are not statistically different ($P > 0.05$).

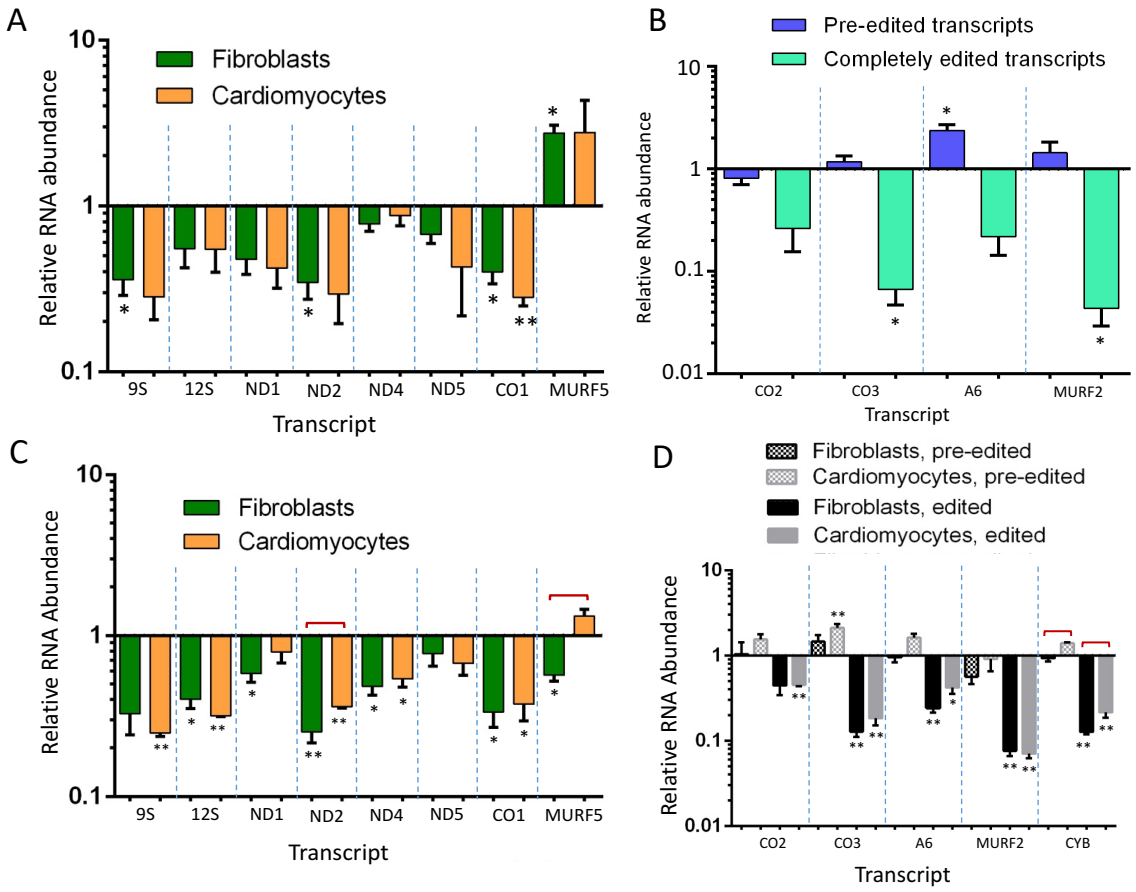


**Figure 28** Mitochondrial RNA abundances in *T. cruzi* CLB amastigotes, relative to infective culture abundances. Data points represent mean of three replicate infection assays, and error bars represent SEM. Relative measurements quantified by qRT-PCR and normalized to normalization genes, TERT and PFR. Asterisks (**, $P < 0.01$; *, $P < 0.05$) indicate results of a ratio paired *t* test in comparison to 8 day nutrient deprivation culture. Red brackets represent significant differences ($P < 0.05$) between transcript abundances of amastigotes in fibroblasts and cardiomyocytes, as indicated by an unpaired *t* test. (A) Relative abundances of never-edited mtRNA transcripts in CLB infections of two mammalian cell lines, fibroblasts and cardiomyocytes. (B) Relative abundances of CLB pre-edited and completely edited mtRNA transcripts. Infections were performed in fibroblasts only. (C) Relative abundances of SYL-X10 never-edited mtRNA transcripts in fibroblast and cardiomyocyte infections. (D) Relative abundances of SYL-X10 pre-edited and completely edited mtRNA transcripts in fibroblast and cardiomyocyte infections.

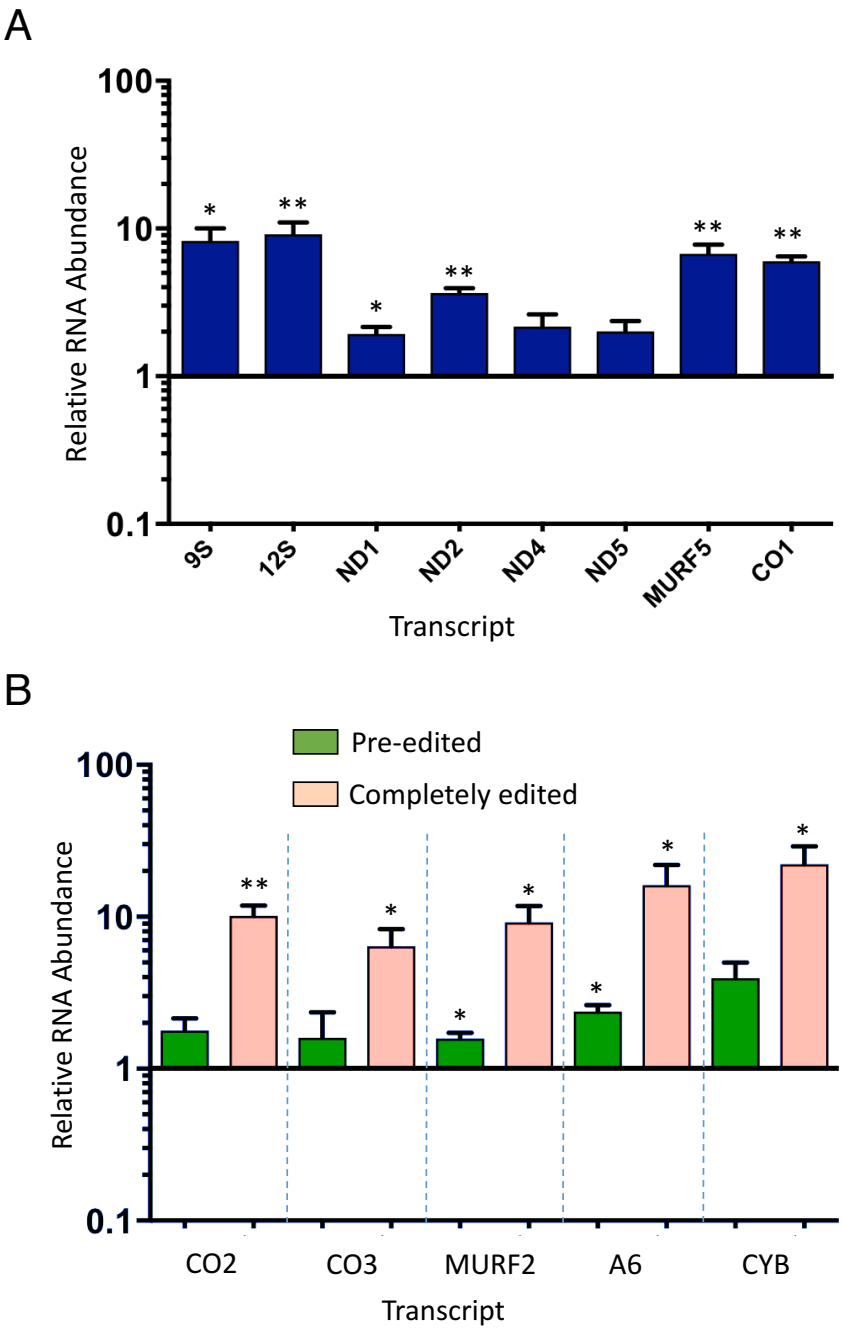


**Figure 29** Mitochondrial RNA abundances in *T. cruzi* SYL-X10 TAU starved cells, relative to exponentially growing cells. Data points represent mean of three replicate samples. Error bars represent SEM. Relative measurements quantified by qRT-PCR and normalized to normalization genes, TERT and PFR. Asterisks (**, $P < 0.01$; *, $P < 0.05$) indicate results of a ratio paired *t* test in comparison to exponentially growing cells. (A) Relative abundances of never-edited mtRNA transcripts. (B) Relative abundances of pre-edited and completely edited mtRNA transcripts. Quantitative RT-PCR performed by Sean Faacks, under E. Susa supervision.

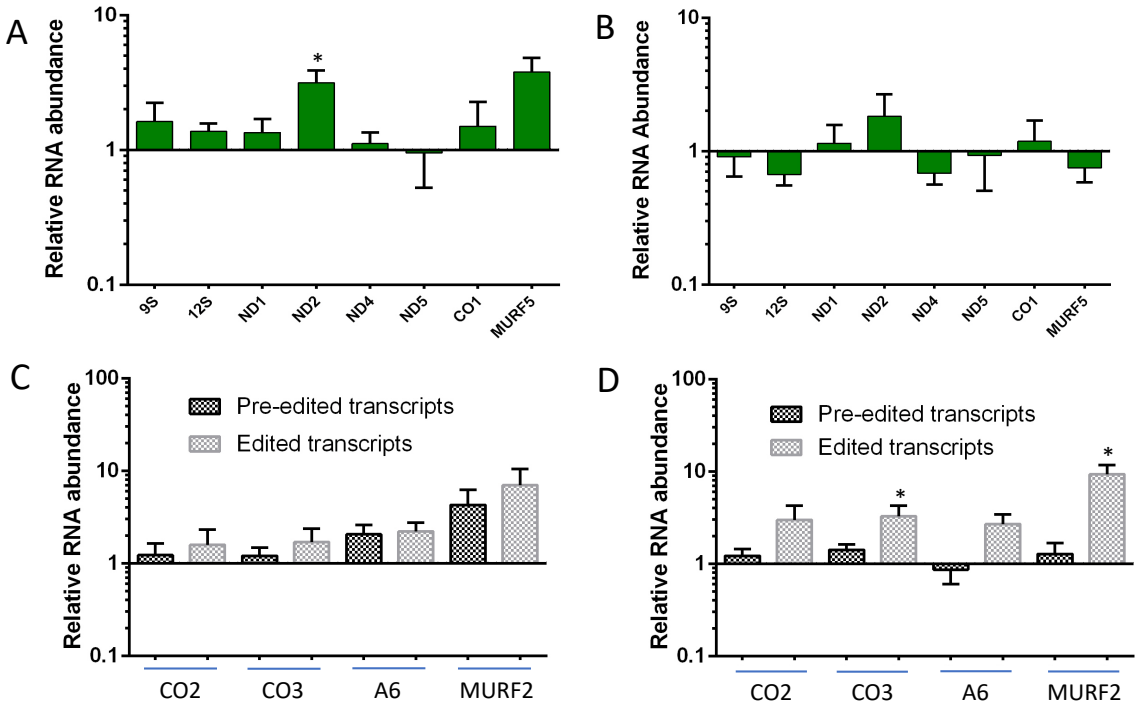


**Figure 30** Mitochondrial RNA abundances in *T. cruzi* SYL-X10 infective culture and amastigotes in fibroblasts, relative to the same CLB life stages. Data points represent the mean of three replicates, and error bars represent SEM. Relative measurements quantified by qRT-PCR and normalized to normalization genes, TERT and PFR. Asterisks (*, $P < 0.05$) indicate results of a multiple *t* tests corrected for multiple comparisons by the Holm-Sidak method. (A) SYL-X10 never-edited mtRNA transcripts in infective culture relative to that of CLB infective culture. (B) SYL-X10 never-edited mtRNA transcript abundances in amastigotes, relative to that of CLB amastigotes. Infections were performed in fibroblasts only. (C) SYL-X10 pre-edited and completely edited mtRNA transcripts in infective culture, relative to that of CLB infective culture. (D) SYL-X10 pre-edited and completely edited mtRNA transcript abundances in amastigotes, relative to that of CLB amastigotes. Infections were performed in fibroblasts.

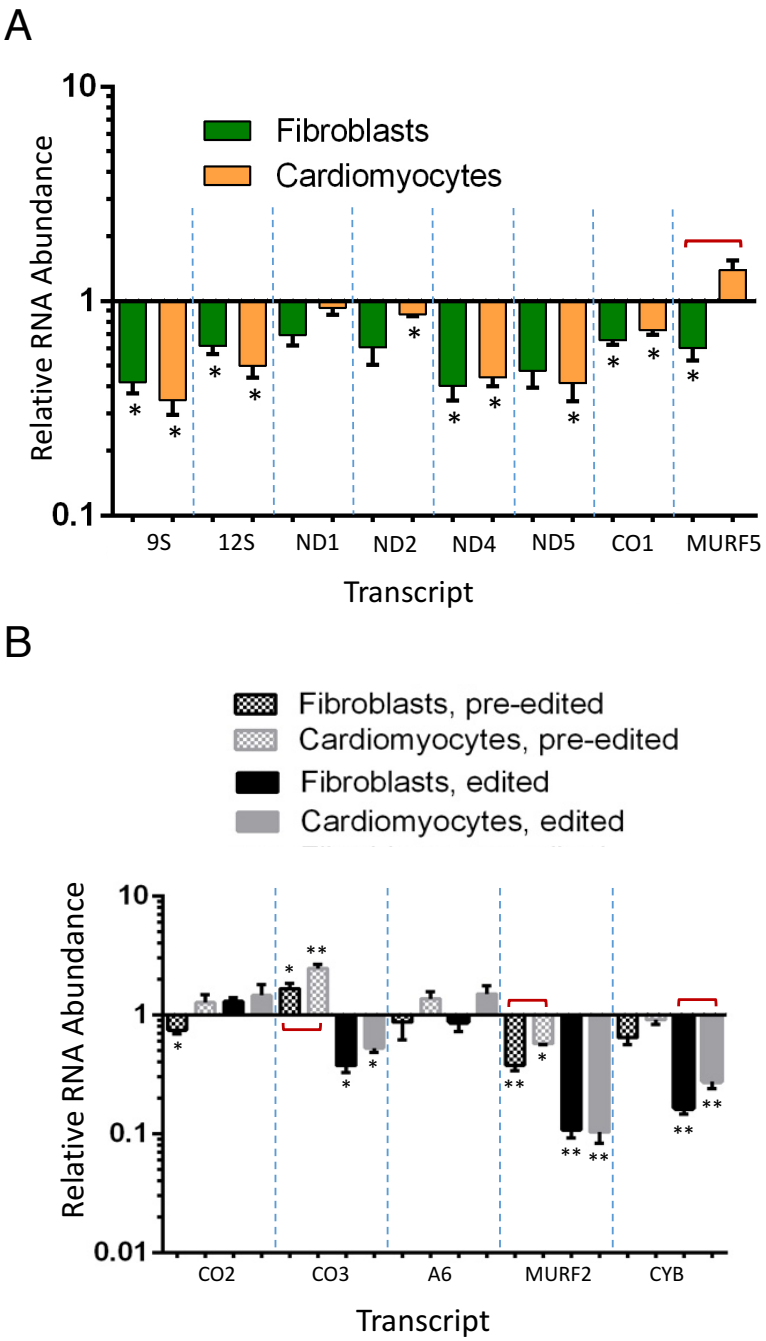


**Figure 31** Mitochondrial RNA abundances in *T. cruzi* SYL-X10 amastigotes, relative to exponentially growing SYL-X10 culture. Data points represent mean of three replicate infection assays in two mammalian cell lines, fibroblasts and cardiomyocytes. Error bars represent SEM. Relative measurements quantified by qRT-PCR and normalized to normalization genes, TERT and PFR. Asterisks (**, $P < 0.01$; *, $P < 0.05$) indicate results of a ratio paired *t* test in comparison to exponentially growing cells. Red brackets indicate results of an unpaired *t* test comparing relative abundances in cardiomyocytes and fibroblasts ($P < 0.05$). (A) Relative abundances of never-edited mtRNA transcripts. (B) Relative abundances of pre-edited and completely edited mtRNA transcripts.

# Bibliography

Abbeele, J Van Den, Y Claes, D van Bockstaele, D Le Ray, and M Coosemans. 1999. "*Trypanosoma brucei spp*. Development in the Tsetse Fly: Characterization of the Post-Mesocyclic Stages in the Foregut and Proboscis." *Parasitology* 118 ( Pt 5) (May): 469–78. http://www.ncbi.nlm.nih.gov/pubmed/10363280.

Alsford, Sam, Daniel J Turner, Samson O Obado, Alejandro Sanchez-Flores, Lucy Glover, Matthew Berriman, Christiane Hertz-Fowler, and David Horn. 2011. "High-Throughput Phenotyping Using Parallel Sequencing of RNA Interference Targets in the African Trypanosome." *Genome Research* 21 (6): 915–24. https://doi.org/10.1101/gr.115089.110.

Andrews, N W. 1993. "Living Dangerously: How *Trypanosoma cruzi* Uses Lysosomes to Get inside Host Cells, and Then Escapes into the Cytoplasm." *Biological Research* 26 (1–2): 65–67. http://www.ncbi.nlm.nih.gov/pubmed/7670547.

Aphasizhev, Ruslan, and Inna Aphasizheva. 2014. "Mitochondrial RNA Editing in Trypanosomes: Small RNAs in Control HHS Public Access." *Biochimie* 100: 125–31. https://doi.org/10.1016/j.biochi.2014.01.003.

Aphasizheva, Inna, Liye Zhang, and Ruslan Aphasizhev. 2016. "Investigating RNA Editing Factors from Trypanosome Mitochondria." *Methods*. https://doi.org/10.1016/j.ymeth.2016.03.020.

Bangs, James D, Pamela F Crainll, Takeshi Hashizumell, James A Mccloskeyllii, and John C Boothroyd. 1992. "The Journal Of Biological Chemistry Mass Spectrometry of mRNA Cap 4 from Trypanosomatids Reveals Two Novel Nucleosides." Vol. 267. http://www.jbc.org.ezp3.lib.umn.edu/content/267/14/9805.full.pdf.

Barisón, María Julia, Ludmila Nakamura, Rapado ‡1, Emilio F Merino, Elizabeth Mieko, Furusho Pral, Brian Suarez Mantilla, et al. 2017. “Metabolomic Profiling Reveals a Finely Tuned, Starvation-Induced Metabolic Switch in *Trypanosoma cruzi* Epimastigotes.” https://doi.org/10.1074/jbc.M117.778522.

Barisón, María Julia, Ludmila Nakamura Rapado, Emilio F Merino, Elizabeth Mieko Furusho Pral, Brian Suarez Mantilla, Letícia Marchese, Cristina Nowicki, Ariel Mariano Silber, and Maria Belen Cassera. 2017. “Metabolomic Profiling Reveals a Finely Tuned, Starvation-Induced Metabolic Switch in *Trypanosoma Cruzi* Epimastigotes.” *The Journal of Biological Chemistry* 292 (21): 8964–77. https://doi.org/10.1074/jbc.M117.778522.

Barrias, Emile Santos, Tecia Maria Ulisses de Carvalho, and Wanderley De Souza. 2013. “*Trypanosoma Cruzi:* Entry into Mammalian Host Cells and Parasitophorous Vacuole Formation.” *Frontiers in Immunology* 4: 186. https://doi.org/10.3389/fimmu.2013.00186.

Barry, J.D., and C.M.R. Turner. 1991. “The Dynamics of Antigenic Variation and Growth of African Trypanosomes.” *Parasitology Today* 7 (8): 207–11. https://doi.org/10.1016/0169-4758(91)90143-C.

Bern, Caryn, and Susan P. Montgomery. 2009. “An Estimate of the Burden of Chagas Disease in the United States.” *Clinical Infectious Diseases* 49 (5): e52–54. https://doi.org/10.1086/605091.

Berná, Luisa, Maria Laura Chiribao, Gonzalo Greif, Matias Rodriguez, Fernando Alvarez-Valin, and Carlos Robello. 2017. “Transcriptomic Analysis Reveals Metabolic Switches and Surface Remodeling as Key Processes for Stage Transition in *Trypanosoma Cruzi*.” *PeerJ* 5: e3017.

https://doi.org/10.7717/peerj.3017.

Biolo, Andréia, Antonio L. Ribeiro, and Nadine Clausell. 2010. “Chagas Cardiomyopathy—Where Do We Stand After a Hundred Years?” *Progress in Cardiovascular Diseases* 52 (4): 300–316. https://doi.org/10.1016/J.PCAD.2009.11.008.

Brisse, Sylvain, Jean-Claude Dujardin, and Michel Tibayrenc. 2000. “Identification of Six *Trypanosoma Cruzi* Lineages by Sequence-Characterised Amplified Region Markers.” *Molecular and Biochemical Parasitology*. Vol. 111. www.parasitology-online.com.

Brun, Reto, Johannes Blum, Francois Chappuis, and Christian Burri. 2010. “Human African Trypanosomiasis.” *The Lancet* 375 (9709): 148–59. https://doi.org/10.1016/S0140-6736(09)60829-1.

Buchan, J Ross, Tracy Nissan, and Roy Parker. n.d. “Analyzing P-Bodies and Stress Granules in *Saccharomyces Cerevisiae*.” *Guide to Yeast Genetics: Functional Genomics, Proteomics, and Other Systems Analysis* 470: 619–40. Accessed March 1, 2019. https://doi.org/10.1016/S0076-6879(10)70025-2.

Cardoso, Mariana S, João Luís Reis-Cunha, and Daniella C Bartholomeu. 2015. “Evasion of the Immune Response by *Trypanosoma Cruzi* during Acute Infection.” *Frontiers in Immunology* 6: 659. https://doi.org/10.3389/fimmu.2015.00659.

Cassola, Alejandro. 2011. “RNA Granules Living a Post-Transcriptional Life: The Trypanosomes’ Case.” *Current Chemical Biology* 5 (2): 108–17. http://www.ncbi.nlm.nih.gov/pubmed/21949551.

CDC. 2017. “Parasites - American Trypanosomiasis,” September. https://www.cdc.gov/parasites/chagas/index.html.

CDC - African Trypanosomiasis. 2018. Accessed March 4, 2019. https://www.cdc.gov/parasites/sleepingsickness/.

Checchi, Francesco, João A N Filipe, Daniel T Haydon, Daniel Chandramohan, and François Chappuis. 2008. “Estimates of the Duration of the Early and Late Stage of Gambiense Sleeping Sickness.” *BMC Infectious Diseases* 8 (February): 16. https://doi.org/10.1186/1471-2334-8-16.

Clayton, Christine. 2013. “The Regulation of Trypanosome Gene Expression by RNA-Binding Proteins Trypanosomes Depend on Post-Transcriptional Mechanisms to Regulate Gene Expression.” https://doi.org/10.1371/journal.

Clayton, Christine E. 2002. “Life without Transcriptional Control? From Fly to Man and Back Again.” *The EMBO Journal* 21 (8): 1881–88. https://doi.org/10.1093/emboj/21.8.1881.

Czichos, Joachim. 1986. “*Trypanosoma Brucei*: Cis-Aconitate and Temperature Reduction as Triggers of Synchronous Transformation of Bloodstream to Procyclic Trypomastigotes in Vitro Glands . The Fourth Developmental Step Yields Metacyclic Forms in the Insect Sali- Parasites Have E” 291: 283–91.

Feagin, Jean E. 1999. “Mitochondrial Genome Diversity in Parasites.” www.elsevier.nl/locate/ijpara.

Fenn, Katelyn, and Keith R Matthews. 2007. “The Cell Biology of *Trypanosoma Brucei* Differentiation.” *Current Opinion in Microbiology* 10 (6): 539–46. https://doi.org/10.1016/j.mib.2007.09.014.

Fernandes, Maria Cecilia, and Norma W Andrews. 2012. “Host Cell Invasion by *Trypanosoma Cruzi*: A Unique Strategy That Promotes Persistence.” *FEMS Microbiology Reviews* 36 (3): 734–47. https://doi.org/10.1111/j.1574-

6976.2012.00333.x.

Ferreira, Ludmila R.P., Fernando de M. Dossin, Thiago C. Ramos, Edna Freymüller, and Sergio Schenkman. 2008. “Active Transcription and Ultrastructural Changes during *Trypanosoma Cruzi* Metacyclogenesis.” *Anais Da Academia Brasileira de Ciências* 80 (1): 157–66. https://doi.org/10.1590/S0001-37652008000100011.

Franco, Jose R, Pere P Simarro, Abdoulaye Diarra, and Jean G Jannin. 2014. “Epidemiology of Human African Trypanosomiasis.” *Clinical Epidemiology* 6: 257–75. https://doi.org/10.2147/CLEP.S39728.

Gazos-Lopes, Felipe, Jessica L Martin, Peter C Dumoulin, and Barbara A Burleigh. 2017. “Host Triacylglycerols Shape the Lipidome of Intracellular Trypanosomes and Modulate Their Growth.” https://doi.org/10.1371/journal.ppat.1006800.

Gerasimov, Evgeny S., Anna A. Gasparyan, Iosif Kaurov, Boris Tichý, Maria D. Logacheva, Alexander A. Kolesnikov, Julius Lukeš, Vyacheslav Yurchenko, Sara L. Zimmer, and Pavel Flegontov. 2018. “Trypanosomatid Mitochondrial RNA Editing: Dramatically Complex Transcript Repertoires Revealed with a Dedicated Mapping Tool.” *Nucleic Acids Research* 46 (2): 765–81. https://doi.org/10.1093/nar/gkx1202.

Gonçalves, Camila Silva, Andrea Rodrigues Ávila, Wanderley De Souza, Maria Cristina M. Motta, and Danielle Pereira Cavalcanti. 2018. “Revisiting the *Trypanosoma Cruzi* Metacyclogenesis: Morphological and Ultrastructural Analyses during Cell Differentiation.” *Parasites and Vectors* 11 (1): 1–14. https://doi.org/10.1186/s13071-018-2664-4.

Gonzales-Perdomo, Magaly, Pedro Romero, and Samuel Goldenberg. 1988. “Cyclic AMP and Adenylate Cyclase Activators Stimulate *Trypanosoma Cruzi* Differentiation.” *Experimental Parasitology* 66 (2): 205–12.

https://doi.org/10.1016/0014-4894(88)90092-6.

Grinsven, Koen W A van, Jan Van Den Abbeele, Peter Van den Bossche, Jaap J van Hellemond, and Aloysius G M Tielens. 2009. “Adaptations in the Glucose Metabolism of Procyclic *Trypanosoma Brucei* Isolates from Tsetse Flies and during Differentiation of Bloodstream Forms.” *Eukaryotic Cell* 8 (8): 1307–11. https://doi.org/10.1128/EC.00091-09.

Haile, Simon, Antonio M Estévez, and Christine Clayton. 2003. “A Role for the Exosome in the in Vivo Degradation of Unstable MRNAs.” https://doi.org/10.1261/rna.5940703.

Hemmige, Vagish, Herbert Tanowitz, and Aisha Sethi. 2012. *“Trypanosoma Cruzi* Infection: A Review with Emphasis on Cutaneous Manifestations.” *International Journal of Dermatology* 51 (5): 501–8. https://doi.org/10.1111/j.1365-4632.2011.05380.x.

Hotez, Peter J. 2008. “Neglected Infections of Poverty in the United States of America.” Edited by Simon Brooker. *PLoS Neglected Tropical Diseases* 2 (6): e256. https://doi.org/10.1371/journal.pntd.0000256.

Hotez, Peter J., Eric Dumonteil, Laila Woc-Colburn, Jose A. Serpa, Sarah Bezek, Morven S. Edwards, Camden J. Hallmark, Laura W. Musselwhite, Benjamin J. Flink, and Maria Elena Bottazzi. 2012. “Chagas Disease: ‘The New HIV/AIDS of the Americas.’” *PLoS Neglected Tropical Diseases* 6 (5): e1498. https://doi.org/10.1371/journal.pntd.0001498.

Hotez, Peter J, Maria Elena Bottazzi, Carlos Franco-Paredes, Steven K Ault, and Mirta Roses Periago. 2008. “The Neglected Tropical Diseases of Latin America and the Caribbean: A Review of Disease Burden and Distribution and a Roadmap for

Control and Elimination." *PLoS Neglected Tropical Diseases* 2 (9): e300. https://doi.org/10.1371/journal.pntd.0000300.

Jimenez, Veronica. 2014. "Dealing with Environmental Challenges: Mechanisms of Adaptation in *Trypanosoma Cruzi.*" *Research in Microbiology* 165 (3): 155–65. https://doi.org/10.1016/j.resmic.2014.01.006.

Kalem, Murat C., Evgeny S. Gerasimov, Pamela K. Vu, and Sara L. Zimmer. 2018. "Gene Expression to Mitochondrial Metabolism: Variability among Cultured *Trypanosoma Cruzi* Strains." Edited by Vyacheslav Yurchenko. *PLOS ONE* 13 (5): e0197983. https://doi.org/10.1371/journal.pone.0197983.

Kennedy, Peter G E. 2004. "Human African Trypanosomiasis of the CNS: Current Issues and Challenges." *The Journal of Clinical Investigation* 113 (4): 496–504. https://doi.org/10.1172/JCI21052.

Kennedy, Peter GE. 2013. "Clinical Features, Diagnosis, and Treatment of Human African Trypanosomiasis (Sleeping Sickness)." *The Lancet Neurology* 12 (2): 186–94. https://doi.org/10.1016/S1474-4422(12)70296-X.

Kolev, Nikolay G., Joseph B. Franklin, Shai Carmi, Huafang Shi, Shulamit Michaeli, and Christian Tschudi. 2010. "The Transcriptome of the Human Pathogen *Trypanosoma Brucei* at Single-Nucleotide Resolution." Edited by Stephen M. Beverley. *PLoS Pathogens* 6 (9): e1001090. https://doi.org/10.1371/journal.ppat.1001090.

Kolev, Nikolay G, Ramey-Butler K, Cross GA, Ullu E, and Christian Tschudi. 2012. "Developmental Progression to Infectivity in *Trypanosoma brucei* Triggered by an RNA-Binding Protein" 1352 (2012): 8–10. https://doi.org/10.1126/science.1229641.

Kolev, Nikolay G, Elisabetta Ullu, and Christian Tschudi. 2014. "The Emerging Role of RNA-Binding Proteins in the Life Cycle of *Trypanosoma Brucei*."

https://doi.org/10.1111/cmi.12268.

Kollien, Astrid, and Günter Schaub. 2000. “The Development of *Trypanosoma Cruzi* in Triatominae.” *Parasitology Today* 16 (9): 381–87. https://doi.org/10.1016/S0169-4758(00)01724-5.

Lentini, Gaelle, Nicolas Dos Santos Pacheco, and Barbara A. Burleigh. 2018. “Targeting Host Mitochondria: A Role for the *Trypanosoma Cruzi* Amastigote Flagellum.” *Cellular Microbiology* 20 (2): 1–8. https://doi.org/10.1111/cmi.12807.

Ley, V, N W Andrews, E S Robbins, and V Nussenzweig. 1988. “Amastigotes of *Trypanosoma Cruzi* Sustain an Infective Cycle in Mammalian Cells.” *The Journal of Experimental Medicine* 168 (2): 649–59. https://doi.org/10.1084/JEM.168.2.649.

Li, Yuan, Sheena Shah-Simpson, Kwame Okrah, A. Trey Belew, Jungmin Choi, Kacey L. Caradonna, Prasad Padmanabhan, et al. 2016. “Transcriptome Remodeling in *Trypanosoma Cruzi* and Human Cells during Intracellular Infection.” *PLoS Pathogens* 12 (4): 1–30. https://doi.org/10.1371/journal.ppat.1005511.

Liang, Xue-Hai, Asaf Haritan, Shai Uliel, and Shulamit Michaeli. 2003. “Trans and Cis Splicing in Trypanosomatids: Mechanism, Factors, and Regulation Downloaded From.” *Eukaryotic Cell* 2 (5): 830–40. https://doi.org/10.1128/EC.2.5.830-840.2003.

Liu, Beiyu, Yanan Liu, Shawn A. Motyka, Eddy E C Agbo, and Paul T. Englund. 2005. “Fellowship of the Rings: The Replication of Kinetoplast DNA.” *Trends in Parasitology* 21 (8): 363–69. https://doi.org/10.1016/j.pt.2005.06.008.

MacLean, Lorna, Hansotto Reiber, Peter G. E. Kennedy, and Jeremy M. Sternberg. 2012. “Stage Progression and Neurological Symptoms in *Trypanosoma Brucei* Rhodesiense Sleeping Sickness: Role of the CNS Inflammatory Response.” Edited by Joseph Mathu Ndung’u. *PLoS Neglected Tropical Diseases* 6 (10): e1857.

https://doi.org/10.1371/journal.pntd.0001857.

Manne-Goehler, Jennifer, Chukwuemeka A. Umeh, Susan P. Montgomery, and Veronika J. Wirtz. 2016. “Estimating the Burden of Chagas Disease in the United States.” Edited by Eric Dumonteil. *PLOS Neglected Tropical Diseases* 10 (11): e0005033. https://doi.org/10.1371/journal.pntd.0005033.

Mantilla, Brian S., Letícia Marchese, Aitor Casas-Sánchez, Naomi A. Dyer, Nicholas Ejeh, Marc Biran, Frédéric Bringaud, Michael J. Lehane, Alvaro Acosta-Serrano, and Ariel M. Silber. 2017. “Proline Metabolism Is Essential for *Trypanosoma Brucei* Brucei Survival in the Tsetse Vector.” Edited by David Horn. *PLOS Pathogens* 13 (1): e1006158. https://doi.org/10.1371/journal.ppat.1006158.

Matsuda, Nilce Mitiko, Steven M Miller, and Paulo R Barbosa Evora. 2009. “The Chronic Gastrointestinal Manifestations of Chagas Disease.” *Clinics (Sao Paulo, Brazil)* 64 (12): 1219–24. https://doi.org/10.1590/S1807-59322009001200013.

Matthews, Keith R., Christian Tschadi, and Elisabetta Ullu. 1994. “A Common Pyrimidine-Rich Motif Governs Trans-Splicing and Polyadenylation of Tubulin Polycistronic Pre-MRNA in Trypanosomes.” *Genes and Development* 8 (4): 491–501. https://doi.org/10.1101/gad.8.4.491.

Michaeli, Shulamit. 2011. “Trans-Splicing in Trypanosomes: Machinery and Its Impact on the Parasite Transcriptome.” *Future Microbiology* 6 (4): 459–74. https://doi.org/10.2217/fmb.11.20.

Mohr, Stephanie E, and Norbert Perrimon. 2012. “RNAi Screening: New Approaches, Understandings, and Organisms.” *Wiley Interdisciplinary Reviews. RNA* 3 (2): 145–58. https://doi.org/10.1002/wrna.110.

Navarro, Miguel, and George A M Cross. 1996. “DNA Rearrangements Associated with

Multiple Consecutive Directed Antigenic Switches in *Trypanosoma Brucei*." *Molecular And Cellular Biology*. Vol. 16. https://www.ncbi.nlm.nih.gov/pmc/articles/PMC231357/pdf/163615.pdf.

Nolan, Derek P, Sylvie Rolin, Jesus R. Rodriguez, Jan Van Den Abbeele, and Etienne Pays. 2000. "Slender and Stumpy Bloodstream Forms of *Trypanosoma Brucei* Display a Differential Response to Extracellular Acidic and Proteolytic Stress." *European Journal of Biochemistry* 267 (1): 18–27. https://doi.org/10.1046/j.1432-1327.2000.00935.x.

Odiit, M, F Kansiime, and J C Enyaru. 1997. "Duration of Symptoms and Case Fatality of Sleeping Sickness Caused by *Trypanosoma Brucei Rhodesiense* in Tororo, Uganda." *East African Medical Journal* 74 (12): 792–95. http://www.ncbi.nlm.nih.gov/pubmed/9557424.

Ouellette, Marc and Papadopoulou, Barbara. 2009. "Coordinated Gene Expression by Post-Transcriptional Regulons in African Trypanosomes." Accessed January 10, 2019. http://jbiol.com/content/8/11/100http://www.biomedcentral.com/1471-2164/10/427,http://www.biomedcentral.com/1471-2164/10/482andhttp://www.biomedcentral.com/1471-2164/10/495.

Overtvelt, L Van, N Vanderheyde, V Verhasselt, J Ismaili, L De Vos, M Goldman, F Willems, and B Vray. 1999. "*Trypanosoma Cruzi* Infects Human Dendritic Cells and Prevents Their Maturation: Inhibition of Cytokines, HLA-DR, and Costimulatory Molecules." *Infection and Immunity* 67 (8): 4033–40. http://www.ncbi.nlm.nih.gov/pubmed/10417171.

Palenchar, Jennifer B., and Vivian Bellofatto. 2006. "Gene Transcription in Trypanosomes." *Molecular and Biochemical Parasitology* 146 (2): 135–41.

https://doi.org/10.1016/j.molbiopara.2005.12.008.

Pastro, Lucía, Pablo Smircich, Andrés Di Paolo, Lorena Becco, María A Duhagon, José Sotelo-Silveira, and Beatriz Garat. 2017. “Nuclear Compartmentalization Contributes to Stage-Specific Gene Expression Control in *Trypanosoma Cruzi*.” *Frontiers in Cell and Developmental Biology* 5: 8. https://doi.org/10.3389/fcell.2017.00008.

Perry, K L, K P Watkins, and N Agabian. 1987. “Trypanosome MRNAs Have Unusual Cap 4 Structures Acquired by Addition of a Spliced Leader.” *Proceedings of the National Academy of Sciences of the United States of America* 84 (23): 8190–94. http://www.ncbi.nlm.nih.gov/pubmed/3120186.

Preußer, Christian, Nicolas Jaé, and Albrecht Bindereif. 2012. “MRNA Splicing in Trypanosomes.” *International Journal of Medical Microbiology* 302: 221–24. https://doi.org/10.1016/j.ijmm.2012.07.004.

Qiu, Yijian, Jillian E. Milanes, Jessica A. Jones, Rooksana E. Noorai, Vijay Shankar, and James C. Morris. 2018. “Glucose Signaling Is Important for Nutrient Adaptation during Differentiation of Pleomorphic African Trypanosomes.” *MSphere* 3 (5): 1–18. https://doi.org/10.1128/mSphere.00366-18.

Regina C. B Q., R C Figueiredo, D S Rosa, and M J Soares. 2000. “Differentiation of *Trypanosoma Cruzi* Epimastigotes: Metacyclogenesis and Adhesion to Substrate Are Triggered by Nutritional Stress.” *The Journal of Parasitology* 86 (6): 1213–18. https://doi.org/10.1645/0022-3395(2000)086[1213:DOTCEM]2.0.CO;2.

Reuner, Birgit, Erik Vassella, Barbara Yutzy, and Michael Boshart. 1997. “Cell Density Triggers Slender to Stumpy Differentiation of *Trypanosoma Brucei* Bloodstream Forms in Culture.” *Molecular and Biochemical Parasitology* 90 (1): 269–80.

https://doi.org/10.1016/S0166-6851(97)00160-6.

Romaniuk, María Albertina, Gabriela Cervini, and Alejandro Cassola. 2016. “Regulation of RNA Binding Proteins in Trypanosomatid Protozoan Parasites.” *World Journal of Biological Chemistry* 7 (1): 146–57. https://doi.org/10.4331/wjbc.v7.i1.146.

Rorbach, Joanna, Thomas J J Nicholls, and Michal Minczuk. 2011. “PDE12 Removes Mitochondrial RNA Poly(A) Tails and Controls Translation in Human Mitochondria.” Accessed February 11, 2019. https://doi.org/10.1093/nar/gkr470.

Ruvalcaba-Trejo, Laura I, and Nancy R Sturm. 2011. “The *Trypanosoma Cruzi* Sylvio X10 Strain Maxicircle Sequence: The Third Musketeer.” https://doi.org/10.1186/1471-2164-12-58.

Sabino, Ester C, Antonio L Ribeiro, Vera M C Salemi, Claudia Di Lorenzo Oliveira, Andre P Antunes, Marcia M Menezes, Barbara M Ianni, et al. 2013. “Ten-Year Incidence of Chagas Cardiomyopathy among Asymptomatic *Trypanosoma Cruzi*-Seropositive Former Blood Donors.” *Circulation* 127 (10): 1105–15. https://doi.org/10.1161/CIRCULATIONAHA.112.123612.

Scahill, Michael D, Irena Pastar, and George A M Cross. 2008. “CRE Recombinase-Based Positive-Negative Selection Systems for Genetic Manipulation in *Trypanosoma Brucei*.” *Molecular and Biochemical Parasitology* 157 (1): 73–82. https://doi.org/10.1016/j.molbiopara.2007.10.003.

Schneider, André. n.d. “Unique Aspects of Mitochondrial Biogenesis in Trypanosomatids.” Accessed January 8, 2019. www.parasitology-online.com.

Shah-Simpson, Sheena, Gaelle Lentini, Peter C Dumoulin, and Barbara A Burleigh. 2017. “Modulation of Host Central Carbon Metabolism and in Situ Glucose Uptake by Intracellular *Trypanosoma Cruzi* Amastigotes.”

https://doi.org/10.1371/journal.ppat.1006747.

Shaw, Aubie K., Murat C. Kalem, and Sara L. Zimmer. 2016. “Mitochondrial Gene Expression Is Responsive to Starvation Stress and Developmental Transition in *Trypanosoma Cruzi*.” *MSphere* 1 (2): e00051-16. https://doi.org/10.1128/mSphere.00051-16.

Simarro, Pere P, Jean Jannin, and Pierre Cattand. 2008. “Eliminating Human African Trypanosomiasis: Where Do We Stand and What Comes Next?” *PLoS Medicine* 5 (2): e55. https://doi.org/10.1371/journal.pmed.0050055.

Simpson, Larry, Ruslan Aphasizhev, Guanghan Gao, and Xuedong Kang. 2004. “Mitochondrial Proteins and Complexes in *Leishmania* and *Trypanosoma* Involved in U-Insertion/Deletion RNA Editing.” https://doi.org/10.1261/rna.5170704.

Simpson, Rachel M, Andrew E Bruno, Jonathan E Bard, Michael J Buck, and Laurie K Read. 2016. “High-Throughput Sequencing of Partially Edited Trypanosome mRNAs Reveals Barriers to Editing Progression and Evidence for Alternative Editing.” https://doi.org/10.1261/rna.055160.115.

Smith, Terry K, Frédéric Bringaud, Derek P Nolan, and Luisa M Figueiredo. 2017. “Metabolic Reprogramming during the *Trypanosoma Brucei* Life Cycle.” *F1000Research* 6. https://doi.org/10.12688/f1000research.10342.2.

Sternberg, Jeremy M, and Lorna Maclean. 2019. “A Spectrum of Disease in Human African Trypanosomiasis: The Host and Parasite Genetics of Virulence.” https://doi.org/10.1017/S0031182010000946.

Stijlemans, Benoît, Guy Caljon, Jan Van Den Abbeele, Jo A Van Ginderachter, Stefan Magez, and Carl De Trez. 2016. “Immune Evasion Strategies of *Trypanosoma Brucei* within the Mammalian Host: Progression to Pathogenicity.” *Frontiers in*

*Immunology* 7: 233. https://doi.org/10.3389/fimmu.2016.00233.

Stuart, Kenneth D, Achim Schnaufer, Nancy Lewis Ernst, and Aswini K Panigrahi. 2005. "Complex Management: RNA Editing in Trypanosomes." *TRENDS in Biomedical Sciences*. https://doi.org/10.1016/j.tibs.2004.12.006.

Subramaniam, Chandra, Paul Veazey, Seth Redmond, Jamie Hayes-Sinclair, Emma Chambers, Mark Carrington, Keith Gull, Keith Matthews, David Horn, and Mark C Field. 2006. "Chromosome-Wide Analysis of Gene Function by RNA Interference in the African Trypanosome." *Eukaryotic Cell* 5 (9): 1539–49. https://doi.org/10.1128/EC.00141-06.

Szöor, Balazs, Naomi A. Dyer, Irene Ruberto, Alvaro Acosta-Serrano, and Keith R. Matthews. 2013. "Independent Pathways Can Transduce the Life-Cycle Differentiation Signal in *Trypanosoma Brucei*." *PLoS Pathogens* 9 (10). https://doi.org/10.1371/journal.ppat.1003689.

Teixeira, Antonio R L, Mariana M Hecht, Maria C Guimaro, Alessandro O Sousa, and Nadjar Nitz. 2011. "Pathogenesis of Chagas' Disease: Parasite Persistence and Autoimmunity." *Clinical Microbiology Reviews* 24 (3): 592–630. https://doi.org/10.1128/CMR.00063-10.

Tielens, Aloysius G.M., and Jaap J. van Hellemond. 2009. "Surprising Variety in Energy Metabolism within Trypanosomatidae." *Trends in Parasitology* 25 (10): 482–90. https://doi.org/10.1016/j.pt.2009.07.007.

Tomlinson, S, F Vandekerckhove, U Frevert, and V Nussenzweig. 1995. "The Induction of *Trypanosoma Cruzi* Trypomastigote to Amastigote Transformation by Low PH." *Parasitology* 110 ( Pt 5) (June): 547–54. http://www.ncbi.nlm.nih.gov/pubmed/7541124.

Tyler, K.M., and D.M. Engman. 2001. “The Life Cycle of *Trypanosoma Cruzi* Revisited.” *International Journal for Parasitology* 31 (5–6): 472–81. https://doi.org/10.1016/S0020-7519(01)00153-9.

Ullu, E, K R Matthews, and C Tschudi. 1993. “Temporal Order of RNA-Processing Reactions in Trypanosomes: Rapid Trans Splicing Precedes Polyadenylation of Newly Synthesized Tubulin Transcripts.” *Molecular and Cellular Biology* 13 (1): 720–25. http://www.ncbi.nlm.nih.gov/pubmed/8417363.

Vanhamme, L, and E Pays. 1995. “Control of Gene Expression in Trypanosomes.” *Microbiology and Molecular Biology Reviews* 59 (2).

Vanhamme, Luc, and Etienne Pays. 2004. “The Trypanosome Lytic Factor of Human Serum and the Molecular Basis of Sleeping Sickness.” *International Journal for Parasitology* 34 (8): 887–98. https://doi.org/10.1016/J.IJPARA.2004.04.008.

Vanhollebeke, Benoit, and Etienne Pays. 2010. “The Trypanolytic Factor of Human Serum: Many Ways to Enter the Parasite, a Single Way to Kill.” *Molecular Microbiology* 76 (4): 806–14. https://doi.org/10.1111/j.1365-2958.2010.07156.x.

Vassella, E., B. Reuner, B. Yutzy, and M. Boshart. 1997. “Differentiation of African Trypanosomes Is Controlled by a Density Sensing Mechanism Which Signals Cell Cycle Arrest via the CAMP Pathway.” *Journal of Cell Science* 110 (21).

Walker, Dawn M, Steve Oghumu, Gaurav Gupta, Bradford S McGwire, Mark E Drew, and Abhay R Satoskar. 2014. “Mechanisms of Cellular Invasion by Intracellular Parasites.” *Cellular and Molecular Life Sciences : CMLS* 71 (7): 1245–63. https://doi.org/10.1007/s00018-013-1491-1.

Westenberger, Scott J, Gustavo C Cerqueira, Najib M El-Sayed, Bianca Zingales, David A Campbell, and Nancy R Sturm. 2006a. “*Trypanosoma Cruzi* Mitochondrial

Maxicircles Display Species-and Strain-Specific Variation and a Conserved Element in the Non-Coding Region." https://doi.org/10.1186/1471-2164-7-60.

Westenberger SJ, Cerqueira GC, El-Sayed NM, Zingales B, Campbell DA, and Sturm NR. 2006. "*Trypanosoma Cruzi* Mitochondrial Maxicircles Display Species-and Strain-Specific Variation and a Conserved Element in the Non-Coding Region." https://doi.org/10.1186/1471-2164-7-60.

"WHO | The Parasite." 2016. *WHO*. https://www.who.int/trypanosomiasis_african/disease/parasite/en/.

Wickstead, Bill, Klaus Ersfeld, and Keith Gull. 2002. "Targeting of a Tetracycline-Inducible Expression System to the Transcriptionally Silent Minichromosomes of *Trypanosoma Brucei*." *Molecular and Biochemical Parasitology* 125 (1–2): 211–16. https://doi.org/10.1016/S0166-6851(02)00238-4.

Zimmer, Sara L., Sarah M. McEvoy, Jun Li, Jun Qu, and Laurie K. Read. 2011. "A Novel Member of the RNase D Exoribonuclease Family Functions in Mitochondrial Guide RNA Metabolism in *Trypanosoma Brucei*." *Journal of Biological Chemistry* 286 (12): 10329–40. https://doi.org/10.1074/jbc.M110.152439.

Zimmer, Sara L., Rachel M. Simpson, and Laurie K. Read. 2018. "High Throughput Sequencing Revolution Reveals Conserved Fundamentals of U-Indel Editing." *Wiley Interdisciplinary Reviews: RNA* 9 (5): 1–16. https://doi.org/10.1002/wrna.1487.

Zingales, Bianca, Maria S Elizabeth Pereira, Kátia A Almeida, Eufrosina S Umezawa, Nédia S Nehme, Riva P Oliveira, Andrea Macedo, et al. 1997. "Biological Parameters and Molecular Markers of Clone CL Brener - The Reference Organism of the *Trypanosoma Cruzi* Genome Project." *Rio de Janeiro*. Vol. 92.

http://www.scielo.br/pdf/mioc/v92n6/3427.pdf.